IMPROVING BIODIESEL THROUGH PYROLYSIS: DIRECT DYNAMICS INVESTIGATIONS INTO THERMAL DECOMPOSITION OF METHYL LINOLEATE

A Master's Thesis

Presented to

The Graduate College of

Missouri State University

In Partial Fulfillment

Of the Requirements for the Degree

Master of Science, Chemistry

By

Michael Bakker

May, 2020

IMPROVING BIODIESEL THROUGH PYROLYSIS: DIRECT DYNAMICS INVESTIGATIONS INTO THERMAL DECOMPOSITION OF METHYL LINOLEATE

Chemistry

Missouri State University, May 2020

Master of Science, Chemistry

Michael Bakker

ABSTRACT

Dependence on petroleum and petrochemical products is unsustainable as it is both a finite resource and environmentally hazardous. Biodiesel is a proposed alternative, but has complications including possessing poor cold weather operability and lacking the ability to supplement other petrochemical products (e.g., ethylene, hexane, etc.) relied upon in society. Pyrolysis of biodiesel has demonstrated the formation of smaller hydrocarbons comprising many of these petrochemical products. Our aim is to computationally simulate the pyrolysis of methyl linoleate, the most prevalent component in biodiesel formed in the US (from soybean). We make use of unimolecular direct dynamics describing intramolecular processes, introducing Temperature acceleration translated in ADMP, an ensemble of trajectories was propagated with forced derived from the D3-M06-2X/6-31+G(d,p) model chemistry. The results obtained from this investigation show significant agreement between the products computed and those obtained in experimental studies. Additional validation of this method can be seen in specific products obtained and an analysis of the CO/CO2 ratio in the product distribution.

KEYWORDS: biodiesel, density functional theory, direct dynamics, thermal decomposition, pyrolysis, fatty-acid methyl esters, methyl linoleate, temperature-accelerated molecular dynamics

IMPROVING BIODIESEL THROUGH PYROLYSIS: DIRECT DYNAMICS INVESTIGATIONS INTO THERMAL DECOMPOSITION OF METHYL LINOLEATE

By

Michael Jacob Bakker

A Master's Thesis
Submitted to the Graduate College
Of Missouri State University
In Partial Fulfillment of the Requirements
For the Degree of Master of Science, Chemistry

May 2020

Matthew R. Siebert, PhD, Thesis Committee Chair

Eric Bosch, PhD, Committee Member

Ridwan Sakidja, PhD, Committee Member

Fei Wang, PhD, Committee Member

Julie Masterson, Ph.D., Dean of the Graduate College

ACKNOWLEDGEMENTS

I would like to thank the following people for their support during my graduate studies. The faculty have been vital to my success with no exceptions. Particularly I would like to thank Dr. Meints, Dr. Bhattacharya and Dr. Breyfogle who have each been fantastic advisors, professors and mentors. Additionally, I would like to thank Linda Allen, who has been a continued supporter through the entire process, an irreplaceable component of the chemistry department. I would also like acknowledge the contributions of my friends and family (Kade Bartell in particular for his last-minute support in editing/formatting), each having played a massive role in any success I have attained. Their patience, understanding, support and contributions have been integral to any achievements I have made. Furthermore, my research would not have been made possible if not for preliminary investigations made by my good friend and peer – Zach Wilson (works included in bibliography). His previous contributions and counseling, in addition to all members of the research group (Andrew Eckelmann and Will Ehrhardt in particular) made my introduction into computational chemistry possible. I would also like to acknowledge the entire chemistry department, graduate college and many of MSU's faculty and staff for all of their support.

Above all else, I would like to acknowledge the contributions of my mentor, research advisor and confidant, Dr. Matthew Siebert, without which none of this would be possible. His patience in explaining concepts and guiding students were unparalleled. Despite difficult roadblocks and complications, Dr. Siebert has been an integral part of my success and one I plan to continue to pursue intellectual pursuits collaboratively in the future.

Thankyou to all those listed above – your contributions will never be forgotten.

TABLE OF CONTENTS

LIST OF TABLES

LIST OF FIGURES

CHAPTER 1. INTRODUCTION

1.1 Petroleum and Petrochemical Dependencies

Petroleum and petrochemical products comprise a major component of many industries. As a non-renewable resource, the continued use of petroleum is unsustainable.[1-39] Coupled with environmental concerns, it is tempting to propose eliminating petroleum in favor of greener alternatives.[8, 9, 12, 19, 21-23, 25-28, 30-32, 35, 37, 39] This direction is currently unfeasible as our society is heavily reliant on petroleum for a vast number of industries.[1-39] Most contemporary liquid fuels are derived from petroleum.[1, 6, 11, 14, 17, 21] These are composed of a combination of straight-chain, branched-chain, alkenes, cyclic and aromatic hydrocarbons.[1, 3-6, 9] Each day 14.02 million barrels of gasoline, the most common liquid fuel, are produced, accounting for only 47% of all petrochemical products.[3, 20, 77] Petroleum also plays a significant role in the production of other fuels including jet and diesel (Figure 1), as well as lubricants, solvents, and other compounds commonly used in industry (Figure 2).[1, 3, 4]

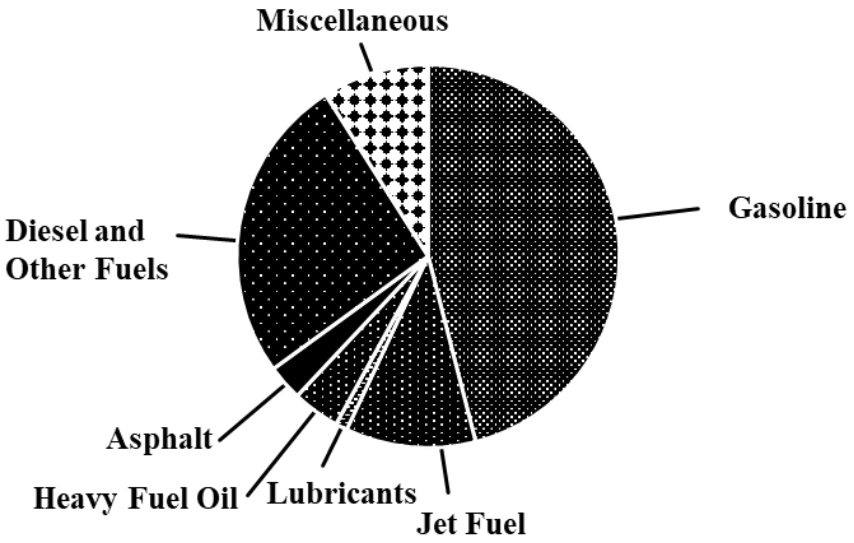

Figure 1. Distribution of commonly sold petrochemical products formed by fractional distillate after extraction. Most petroleum is sold as fuels. [1,3,4]

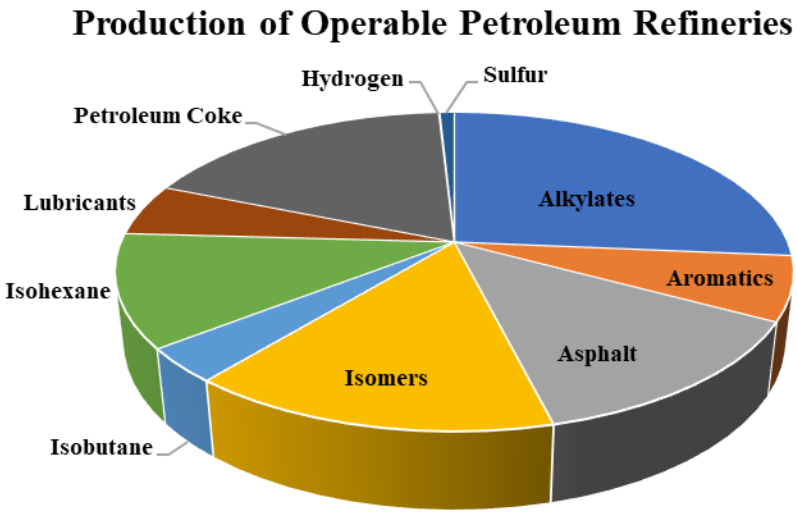

Figure 2. Description of the products produced from petroleum refineries, many of which heavily contribute to the normal progression of society.[4]

Petrochemical products are also necessary for polymer chemistry.[14] Petroleum is the largest source for olefins including ethylene, styrene and vinyl chloride (Figure 3).[86] The commercial significance for these monomers is massive. They are responsible for the creation of many plastic products including bags, bottles and PVC pipes used in plumbing. It would be next to impossible to navigate life without encountering some form of petroleum-based polymer. Even one's clothing can be made of nylon or polyester, both common petroleum-based polymers.[4]

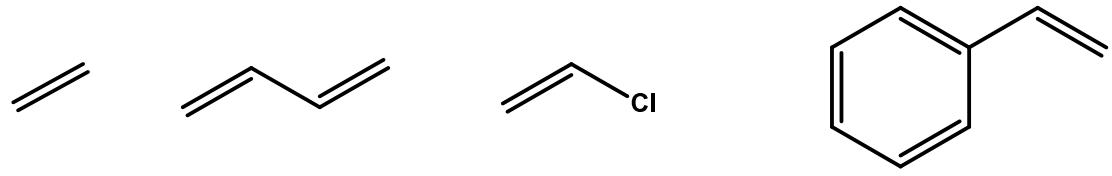

Ethene Butadiene Vinyl Chloride Styrene

Figure 3. Structures of several olefins; olefins represent a major component of the plastics industry. The primary source of these molecules is the petroleum industry.[3]

Table 1. Compilation of many of the petrochemical products that are formed from the fractional distillation of petroleum, or as a secondary byproduct. This list is illustrative and is in no way comprehensive.[1, 3, 4]

	Constituents	Uses
Hydrocarbons	Propane (C3)	
	Butane (C4)	
	Kerosene	
	Fuel Oil	Transportation, heat, power, etc.
	Gasoline (C4 – C12)	
	Jet Fuel (C8 – C16)	
	Diesel (C10 – C15)	
Olefins	Ethylene	Polyethylene; detergents, lubricants, packaging, etc.
	Vinyl Chloride	Polyvinyl Chloride (PVC); plumbing
	Styrene	Polystyrene; cheap plastic, foams, packaging, etc.
	Propylene	Polypropylene; packaging and labeling
	Butene	Polybutene; sealants, adhesives, cosmetics, etc.
	Butadiene	Polybutadiene; synthetic rubber
Aromatics	Naptha	Research, production of other aromatics, etc.
	Benzene	Production of acetone, phenol, cyclohexanes, etc.
	Toluene	Explosives, solvent, foam, paint thinner, etc.
	Xylenes	Painting, adhesives, rubber, printing, ink, etc.
	Benzoic Acid	Medicine, preservatives, artificial flavoring, etc.
	Phenol	Antiseptic, precursors to plastic, etc.
	Cylcohexanes	Nylon, recrystallization, research, etc.
Solvents	Methanol	Gasoline additive, research, formation of formaldehyde, etc.
	Formaldehyde	Crease-resistant fabrics, drug testing (Marquis reagent), etc.
	Ammonia	Fertilizer, cleaning products, agriculture, etc.
	Carbon Monoxide	Formation of ammonia, medicine, chemical industry, etc.

Another important contribution of petroleum is in the formulation of solvents, adhesives, lubricants and gels.[11] Each play roles in the pursuit of scientific research and the sustainable production of each of these solvents is vital to the furthering of chemistry, biology, engineering,

medicine, and physics. The medical field, for example, is highly dependent on petroleum products to produce antibiotics, aspirin, and antineoplastics.[2] A more complete list of the current uses of petroleum can be found in Table 1. Many of these chemicals can be produced from alternative synthetic pathways, however, approval from the FDA and increases in costs is a major consideration of any field reliant on petroleum.[3]

What should be evident is that eliminating petroleum in our society would be devastating for a variety of industries. It is therefore imperative to seek an alternative that would suitably meet the capacities supplied by petroleum in addition to energy production. Many researchers are currently investigating various renewable energy sources.[5,6,10] Each possesses advantages and disadvantages that should be considered before implementation on a large scale.

1.2 Complications with Petroleum

Though formed by biological sources, petroleum's circumstances of derivation make it effectively non-renewable.[13-15, 17, 22, 24, 27, 34, 35] This is because petroleum is formed through a combination of millions of years, temperature and pressure. Consumption statistics estimate world petroleum reserves will last no longer than 50 to 100 years.[9, 20, 22, 26] This is particularly alarming as petroleum-based fuels account for approximately 88% of the world's energy.[2, 6] In selecting a replacement, other concerns aside from sustainability should also be considered.

One major drawback of petroleum is its environmental impact. Combustion of hydrocarbons (e.g. gasoline, propane, butane, etc.) results in carbon dioxide and water (Equation 1). If the production of carbon dioxide exceeds the planet's ability to revert it back into oxygen molecules, then carbon dioxide builds up within the atmosphere, leading to both climate change and hydrosphere acidification.[41, 53, 55]

$$C_xH_y + O_2 \rightarrow CO_2 + H_2O$$

Equation 1. Depiction of a combustion reaction which results in the formation of CO_2 – a well-known greenhouse gas.

Climate change is fueled through accumulation of greenhouse gases (e.g. carbon dioxide or methane) which absorb solar radiation more efficiently than other atmospheric gases (O_2, N_2, etc.) Since humans began burning hydrocarbons as fuel, a noticeable trend has emerged, colloquially known as *global warming* (Figure 4). Ramifications of global warming include changes in precipitation patterns (droughts and floods), heat waves, and increasing tropical storm severity.[10, 42, 46-48]

Increasing CO_2 emissions also results in acidification of the hydrosphere (Equation 2). The hydrosphere includes all of Earth's readily available water sources, so even a slight change in pH has far reaching implications. One incipient consequence of this acidification is the mass extinction of marine shell-forming species.[41, 53] Another is propagation of acid rain, threatening the existence of many amphibian species.[55] The loss of biodiversity would be detrimental to the planet's ecosystem as well as potential genetic research. Areas shown in red have incurred the greatest shift in pH (Figure 5).

$$CO_2 + 2\,H_2O \quad \leftrightarrow \quad HCO_3^- + H_3O^+ \quad \leftrightarrow \quad H_2CO_3 + H_2O$$

Equation 2. Conversion of CO_2 with interaction between water.

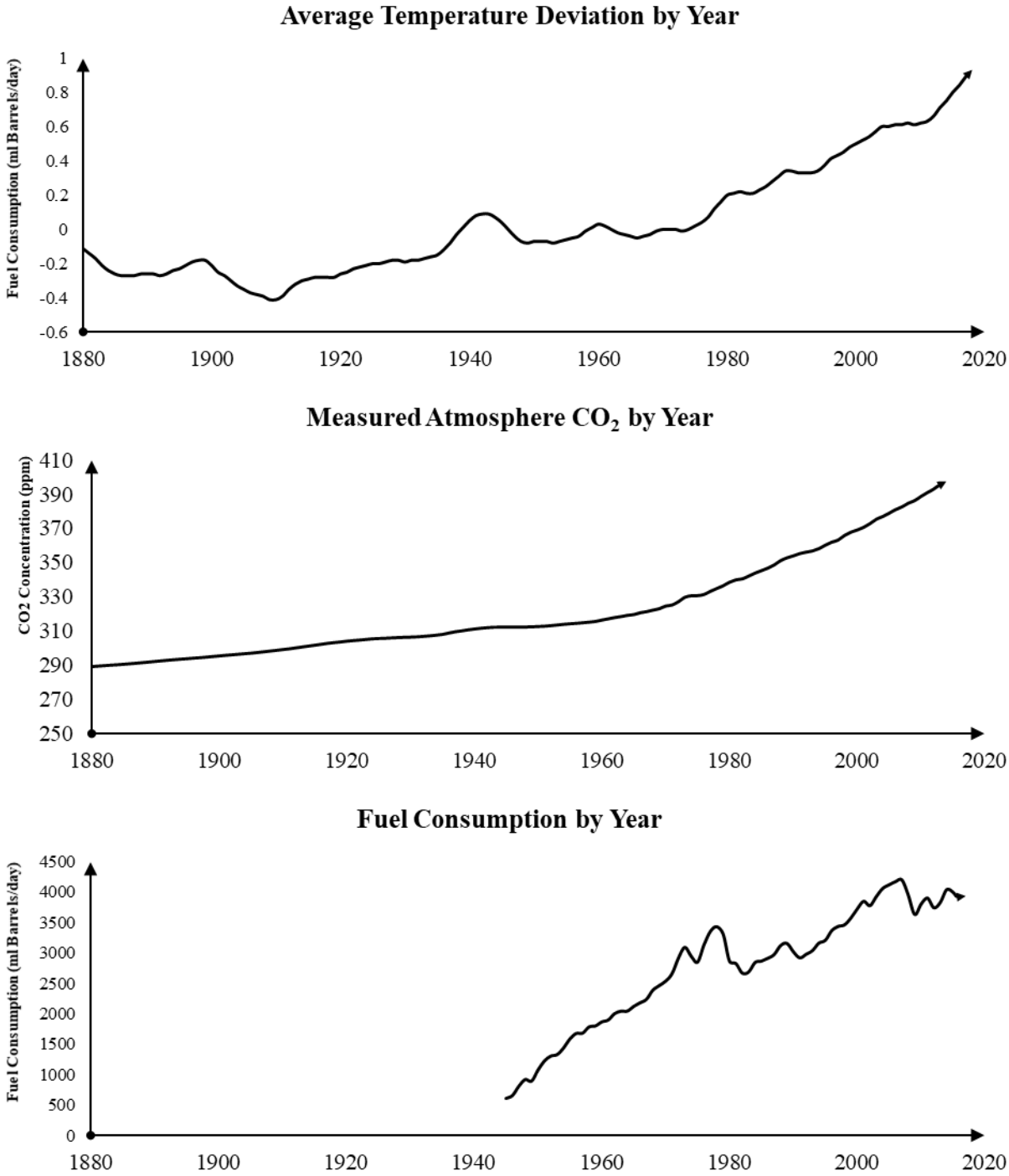

Figure 4. Trends of fuel consumption and average temperature deviation as well as the CO_2 atmosphere as a function of time collected from publicly funded available sources. Observed CO_2 increased exponentially as humans began utilizing petroleum sources.[1, 43, 45, 46]

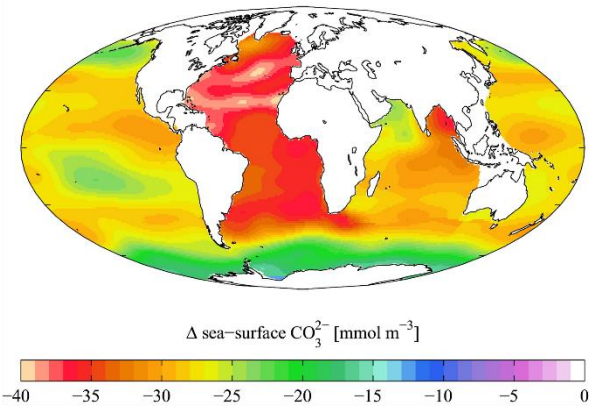

Figure 5. Concentration change of surface CO_3^{2-} over the past 10 years. Even minor changes have detrimental effects on the environment, evident by destruction in the Great Coral Reef.[55]

There are also environmental concerns associated with petroleum processing, the method through which crude oil is located, extracted, refined and distributed. Refinement of crude oil results in NO_x and SO_x emissions, which have been identified as human health and ecological hazards.[6, 15, 16, 21, 22, 27, 56, 63, 64, 65, 66, 67, 70, 71, 84, 90, 98, 105] Additionally, the risk of oil spills along each processing and transportation step impose a clear danger to the ecosystem.[57] Considering these risks, great pressure has been applied to the petroleum industry by government agencies to meet environmental standards.[58] This pressure can make it costly to meet regulatory specifications and replacing the status quo with less harmful alternatives would allow industries to comply more easily with these standards. This would be both environmentally and economically beneficial.

Petroleum has an additionally unstable quality regarding economic and geopolitical concerns. Since the first commercial well was drilled in 1857, petroleum reserves have played a crucial role in the world economy. This fact was brought to the world's attention in 1973 during the Arab Oil Embargo. Although it is now largely seen as a political failure, economists agree this event initiated a pivotal shift in the world economy. Knowledge that the world economy is vulnerable from manipulation by countries with oil reserves is unsettling. [19, 33, 34, 59] Domestically

produced fuel sources would alleviate much of the negative externalities produced by oil price instability. Although it is daunting to find an alternative that addresses all concerns, it is ethically imperative to choose a direction for society that does not leave major problems to be addressed in the future. The following is a set of criteria that describe the qualities of an ideal substitute:

- **Reliability –** Source should be domestically produced and in quantities capable of meeting demands
- **Renewability –** Source should be formed by renewable means
- **Adaptability –** Source should be capable of supplementing the various petrochemical products or propose an alternative in tandem
- **Eco-Friendly –** Source should not contribute to further accumulation of CO_2 emissions

1.3 Alternatives to Petroleum

Once humanity became cognizant of the unsustainability of petroleum, the field of renewable energies exploded. To be considered renewable, a resource's reserve must be replenishable within a realistic human timescale. Normally this would eliminate nuclear power, but its viability has kept it viewed an acceptable replacement by many.[17, 18, 23, 25, 33] Figure 6 details a variety of current renewable energy sources being investigated.

An ideal renewable energy source should meet the four criteria discussed previously: reliability, renewability, adaptability and eco-friendliness. The energy should be reliable and capable of being produced domestically to properly meet demand. Due to variety in climate and location, this can eliminate several options (e.g. wind, geothermal, tidal, solar, etc.). [8, 10, 11, 12] Excepting nuclear, all resources in Figure 6 fulfill the renewability requirement.[17, 18, 23, 25, 33] To

meet the eco-friendly quality, the source should seek to eliminate or reduce emissions of CO_2, which is applicable to most options being investigated. In the case of biodiesel or biomass, their use involves combustion of hydrocarbons, which releases CO_2. However, since the original source of the materials is through photosynthesis, which obtains the carbon from CO_2 in the atmosphere, the fuel can be considered 'carbon neutral'.[15, 18, 26, 27, 38] A cursory analysis of various alternative energies (Figure 7) demonstrates the difficulty of seeking alternatives without extreme disadvantages.

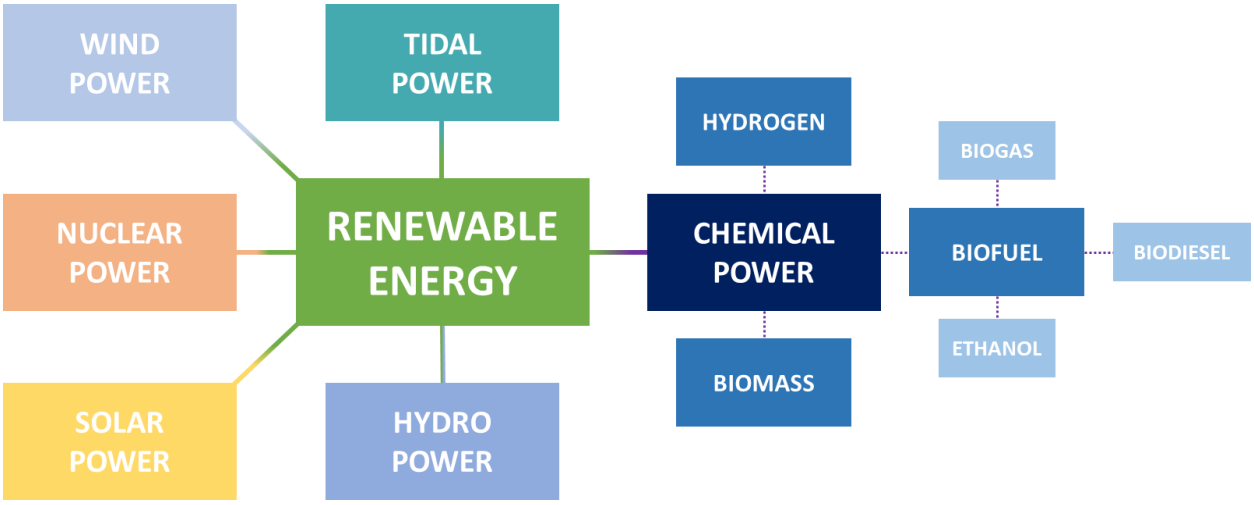

Figure 6. Categorization of various possible renewable energy directions for society. Each method of obtaining energy has specific advantages and disadvantages associated. Nuclear power is included though it requires non-renewable resources.[5, 6, 7, 8, 10, 11, 12, 13, 15, 17, 20, 22]

The final criterium is adaptability. Petroleum is essential for many petrochemical products in addition to energy production.[1,3,4] Attempting to reduce consumption by replacing it with an energy source that cannot meet these needs would be ineffective. Renewable sources such as wind, solar, or geothermal are viable energy sources, but unfortunately, they cannot be used to eliminate our dependence on fossil fuels completely. [11, 12, 13, 15, 17] However, thanks to a concept known as thermal cracking, biomass and biodiesel still hold potential in this capacity.

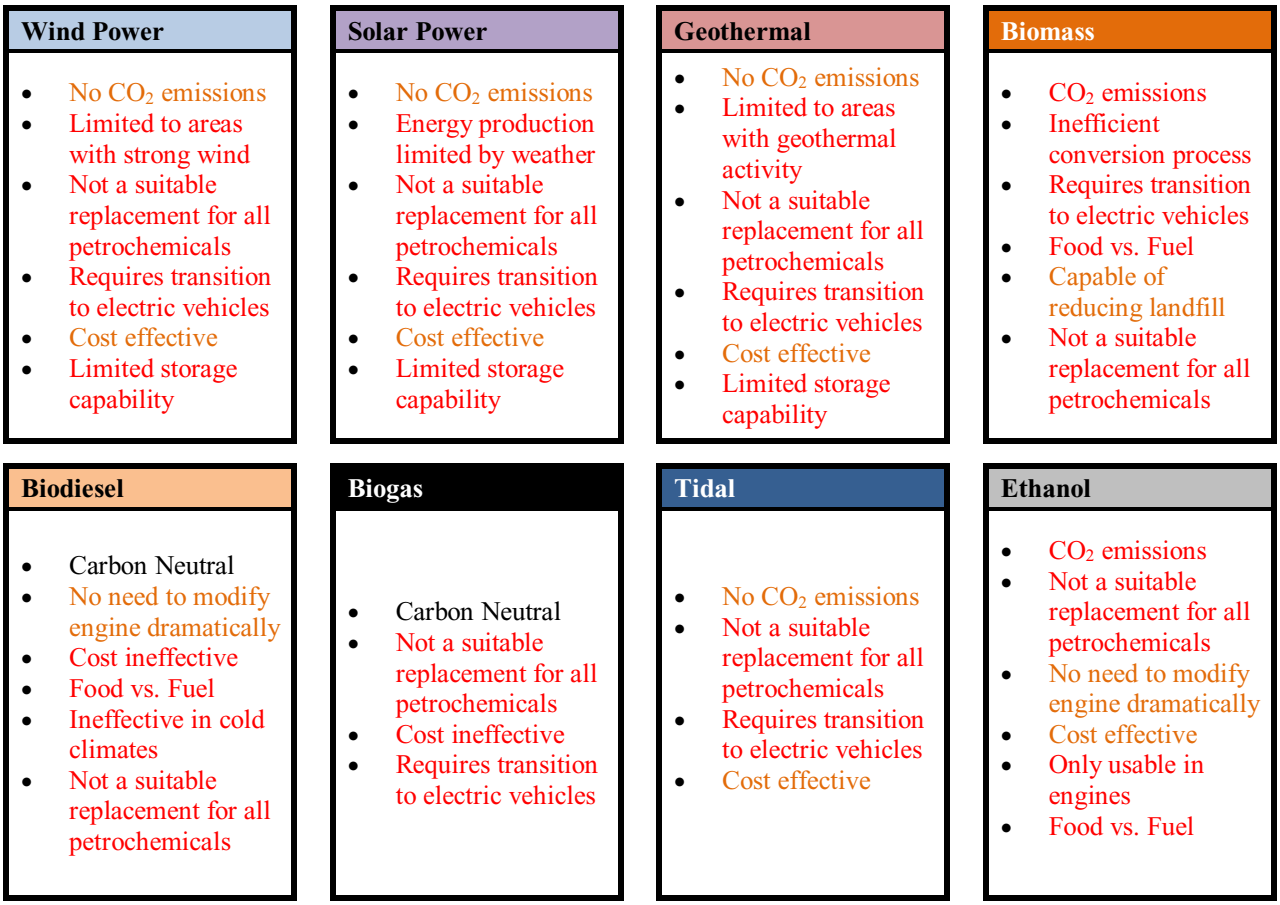

Figure 7. Cursory analysis of the various alternative energy sources available with some of the possible advantages or disadvantages (not comprehensive).[5, 6, 7, 8, 10, 11, 12, 13, 15, 17, 20, 22]

1.4 Biodiesel as an Alternative

Biodiesel is a subclass of biofuels obtainable from natural sources.[6, 18, 20, 22, 23, 25, 27, 75, 84, 94, 106] Several properties, such as its domestic production and its compatibility with existing diesel engines, make it appealing as an alternative energy source. These properties combined with its natural origin explains why many scientists are interested in its development.[6, 7, 8, 9, 10, 12, 15, 17, 20] The method of obtaining biodiesel has been existent in one form or another since World War I. The process of forming biodiesel is relevant in discussions of its potential.[26, 63 – 65, 101, 129, 133] Biodiesel feedstocks are obtainable from natural sources such as vegetable oil or animal fat.[6, 18, 20, 22, 23, 25, 27, 75, 84, 94, 106] Within the United States, soybean oil is the most commonly used

feedstock.[6, 8, 15, 20, 26, 27] Other feedstocks are used in different locations, such as in Europe which favors canola-based feedstock.[6, 8, 15, 24, 26, 27, 71] The major component in feedstock is triglycerides (Figure 8), which can be converted into biodiesel through a transesterification reaction.[6, 7, 15, 19 - 21, 25 – 27, 32, 35, 39, 63, 65, 70, 75, 76, 79, 86, 90, 98, 105, 106, 108]

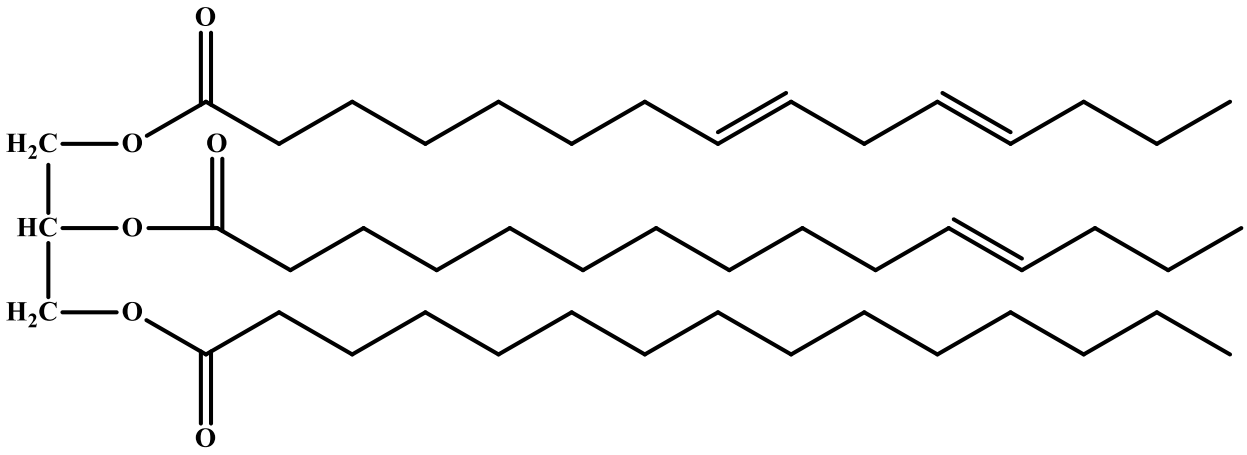

Figure 8. Example triglyceride molecule, common natural source for cooking oils. The components of the triglyceride involve a polar end and a non-polar hydrocarbon chain.[6, 7, 15, 19 - 21, 25 – 27, 32, 76, 79, 86, 90, 98, 105]

In this case, the conversion process involves methanol and a base catalyst, the products of which (Figure 9) are glycerol and FAMEs (fatty-acid methyl esters). FAMEs are organic molecules varying in homology (length) and degree of saturation (alkene characteristics).[6, 7, 15, 20, 25, 27, 63, 65, 75, 84, 93, 98, 105, 108] Numerous FAMEs comprise the resulting biodiesel. Table 2 shows a comparison between common FAMEs in relation to originating feedstock.

As well as being naturally derived, biodiesel has other qualities making it appealing. Its utilization is similar enough to petroleum that implementation would require little modification to existing infrastructure. Another positive is that in pure 100% biodiesel, there is no SO_x emission.[6, 12, 15, 27] Because of this, biodiesel has been shown to extend the life of a catalytic converters due to reduced sulfur concentration.[20, 65] Biodiesel also has a significantly lower

flashpoint than gasoline, making its storage significantly safer than traditional petroleum fuel.[6, 12, 20, 26, 63, 64, 70, 84]

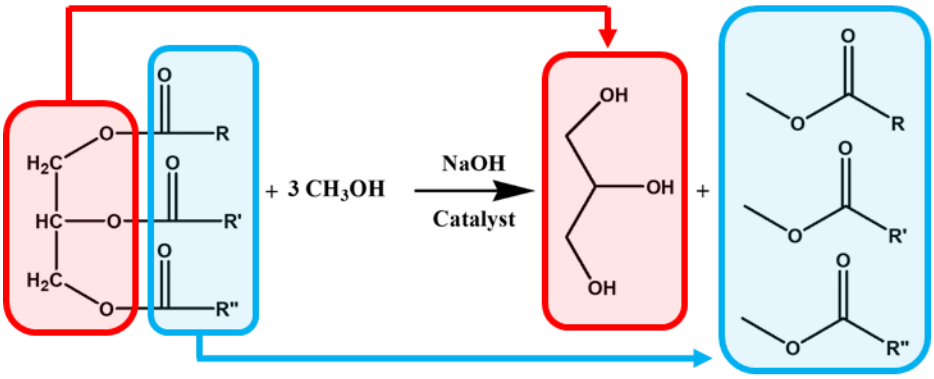

Figure 9. Chemical reaction of transesterification. The process can be done using NaOH as shown or alternatively with an acid-catalyst (i.e. HCl).[6, 7, 15, 20, 25, 27]

Table 2. Profiles of various FAMEs and concentrations of each in common biodiesel feedstock. Prolific FAMEs are methyl oleate from canola oil and methyl linoleate from soybean oil.[15, 21, 25, 27, 35, 65, 75, 76, 89, 98]

FAME		Canola	Soybean	Palm	Sunflower
Methyl Myristate	C14:0	0.0	0.0	0.8	0.0
Methyl Palmitate	**C16:0**	**4.8**	**10.9**	**43.4**	**6.8**
Methyl Stearate	C18:0	1.4	2.9	3.6	2.9
Methyl Oleate	**C18:1**	**62.4**	**24.1**	**41.1**	**31.8**
Methyl Linoleate	**C18:2**	**21.2**	**54.5**	**10.7**	**57.5**
Methyl Gadoleate	C20:1	1.1	0.2	0.2	0.2

Biodiesel has great potential as an alternative to petroleum, though downsides do exist. While SO_x emissions are lowered, NO_x emissions rise in comparison to its fossil fuel counterpart. Modified exhaust filter technology can be implemented, although any additional costs will detract from its economic appeal. In addition, biodiesel is at present costlier to produce than petroleum. Scientists predict that this inequality will be neutralized as petroleum reserves are depleted, but in its current form, biodiesel has 1.5x the production costs compared to its

petroleum-based counterpart.[6, 15, 16, 21, 22, 27, 56, 63, 64, 65, 66, 67, 70, 71, 84, 90, 98, 105] Alterations to biodiesel or the mechanism of production would certainly give it more economic appeal. The biggest complication to using biodiesel is its poor cold temperature operability. Operability is a property of fuel quantifying the minimum set of conditions that it can be used. There are methods of altering a fuel's operability, known as 'winterization,' although any additional steps for biodiesel preparation would detract from its cost effectiveness, heavily reducing its utility in colder climates.[6, 8, 15, 21, 27, 69, 70, 76, 104] Bridging the gap in operability would greatly improve biodiesel's utility.

1.5 Pyrolysis as a Possible Solution

Since operability of a fuel source is reliant on the homology of the molecules, one related solution has been suggested. Cracking long chain hydrocarbons into smaller chains would improve its operability, reduce NO_x emissions, and produce additional products which could improve its cost effectiveness. This process exposes biodiesel to high temperatures and pressure in an anaerobic environment. The lack of oxygen prevents spontaneous combustion and high temperatures allow bond dissociation.[15, 22, 23, 35, 75, 76, 80, 83, 85, 94, 95, 124, 152] The goal for thermal decomposition is the generation of smaller chain hydrocarbons, comparable to the natural formation of petroleum, only at an extremely accelerated rate.[15, 22, 23, 35, 75, 76, 80, 83, 85, 94, 95, 124, 152] The result of this method is a homogenous mix of varying length hydrocarbons similar to the fractional distillate from crude oil.

This mixture can be separated to extract useful components through a commonly used separation method based on boiling points known fractional distillation (Figure 10).[21, 161] The technique uses the intrinsic properties of substances to separate and extract them. Once complete, the components can be distributed and sold for industrial purposes. The implementation of

fractional distillation for this purpose is extremely feasible as existing petroleum infrastructure is already in place which can easily be retrofitted to process biodiesel (Figure 11).[3, 5, 15, 57, 85]

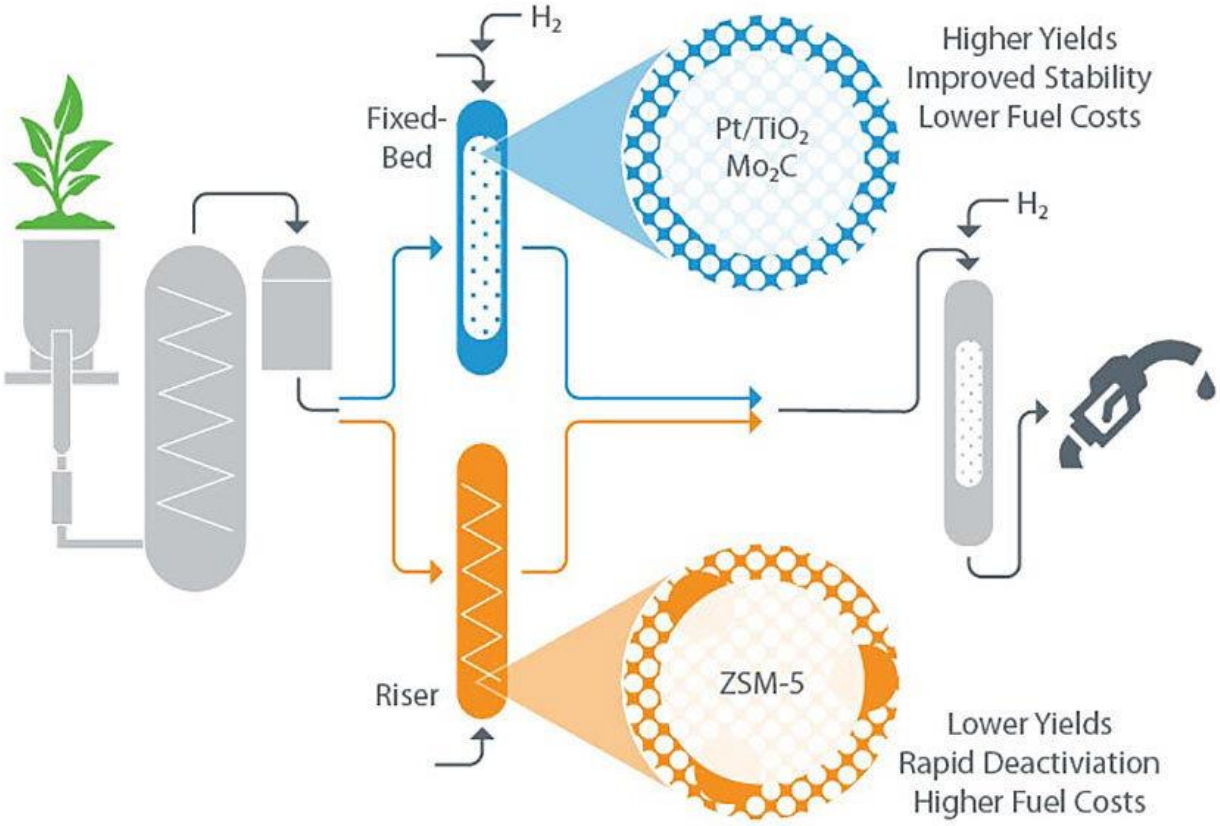

Figure 10. An example setup for pyrolysis. Alterations can be made to the schematic to improve results or decrease loss.[161]

The introduction of thermal decomposition improves biodiesel's appeal as the products are identical to those of petroleum requiring no vehicle modifications. As a bonus, fuels obtained from biodiesel contain significantly less sulfur, and the process of producing them is entirely carbon neutral.[6, 12, 15, 27] Additionally, other vital hydrocarbon products can be sold as well allowing the polymer industry to proliferate without reliance on petroleum as a source of olefins. The application of this technique to biofuels has been shown capable of producing similar

hydrocarbons to that of petroleum, as well as many of the by-products essential for the replacement of petroleum in society. Efforts to improve this process has been conducted for both industrial and academic pursuits to give the technique more wide-spread appeal. Published works on FAMEs (mixtures and pure) have investigated ideal conditions (e.g. temperature/pressure) of producing shorter chain hydrocarbons from oleic[13, 15, 64, 75, 78, 85 - 87], linoleic[15, 27, 64, 75, 85, 86] and stearic acid[28, 64, 75, 85, 86, 135]. Other investigations involve microwave-assisted[18, 38] and flash pyrolysis[143] on FAME precursors (triglycerides) in biomass and castor oil with positive results. Promising progress has also been made through introducing activated alumina to the facilitate the conversion.[24]

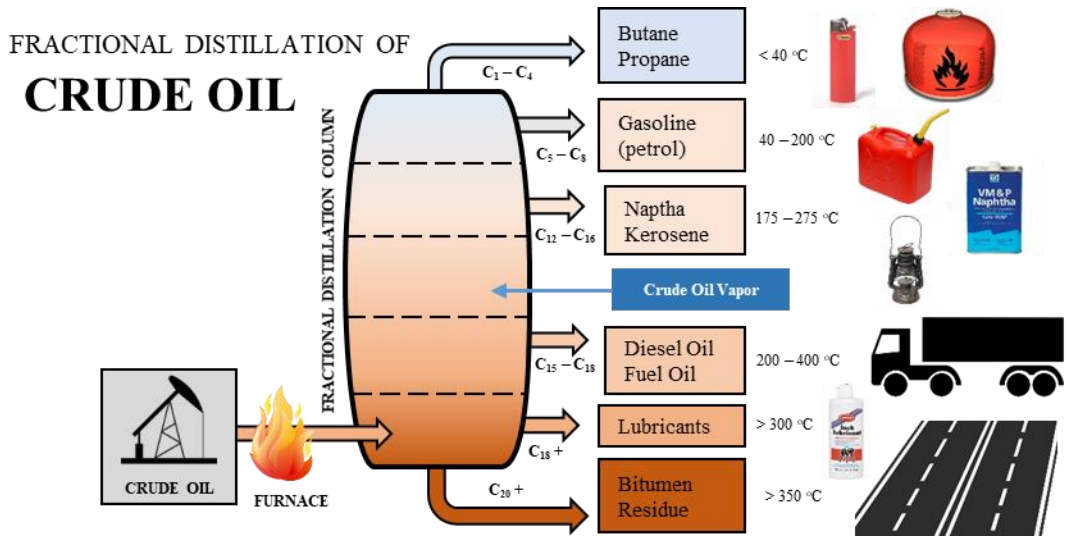

Figure 11. Flowchart describing the petrochemical process of breaking down usable components through fractional distillation of crude oil. Larger hydrocarbons settle due to low boiling points while smaller hydrocarbons ascend.[3, 5, 15, 57, 85]

While the findings of these studies show tremendous potential, a limitation to the research is that pyrolysis reactions are difficult to control or measure. Additionally, the costs of equipment and apparatus can make experimental investigations cost restrictive. Thanks to advancements in computational chemistry, a theoretical investigation would be a cost-effective

approach that would produce further elucidation into pyrolysis mechanisms – ideally to formulate ideal conditions.

CHAPTER 2. COMPUTATIONAL CHEMISTRY

2.1 Utility of Molecular Dynamics

Molecular Dynamics is a computational tool that propagates motion inter- and/or intramolecular motion over time.[32, 119, 120, 127 - 134] This technique solves equations of motion for a specified system returning trajectories from which various interpretations can be made. The purpose of computer simulations is to predict macroscopic behavior from microscopic observations and its implementation varies depending on the system.[119] It is no surprise that theoretical chemical research has become highly regarded in chemistry. Three basic properties are determined using computational chemistry (in order of increasing difficulty):

1) Structure and stability of a molecular system.

2) Free energy of the different states possible for the molecular system.

3) Reaction processes and mechanisms within molecular systems.

Computational models rely on approximations trading between accuracy and viability and predictions of properties by theoretical means must account for empirical observations in order to evaluate the method's viability. These predictions can be compared to experimental data and experimental results can be compared to computational results to interpret properties normally inaccessible.[32, 119, 126] The collaborative nature for computational and experimental investigations (Figure 12) shows the viability for its implementation.

Another advantage to theoretical investigations is its costs. An empirical investigation requires purchase of molecules of interest, chemical solvents, time, instruments, and apparatuses. Computational chemistry, on the other hand, is only limited by computing power. The modest investment required for computational chemistry is increasing in appeal due to 'Moore's Law'

which predicts the advancement of computer power to be exponential over time (Figure 13).[141, 142] Pioneer simulations had difficulties describing quantum properties within even a single atom. Advancement of technology and the development of accepted approximations/methods have allowed investigations to overcome many of these barriers (Table 3).

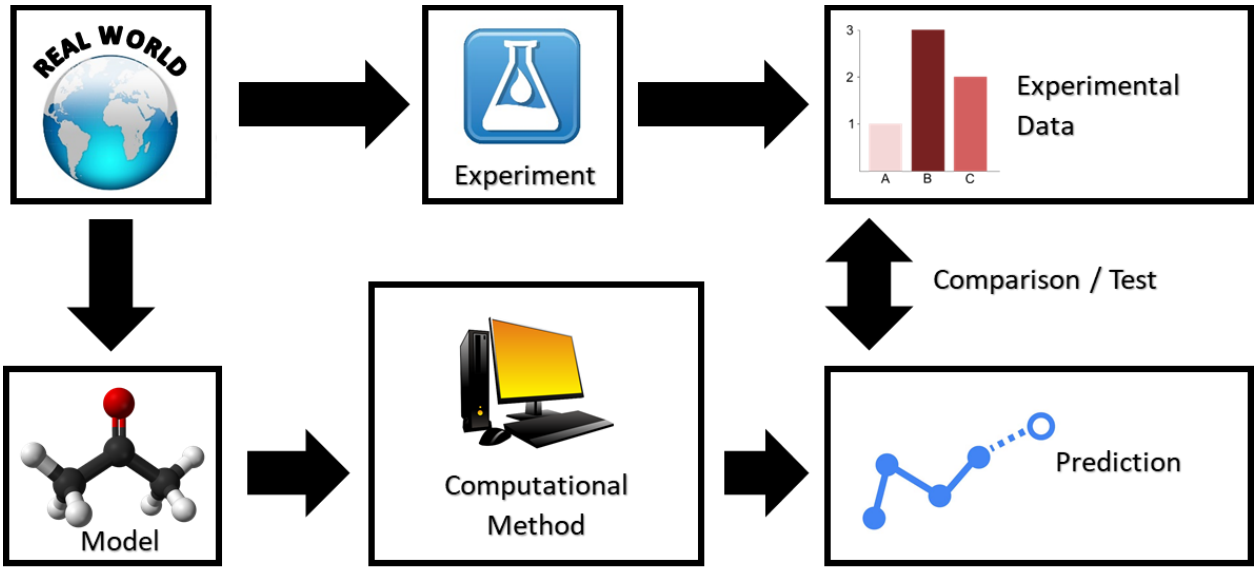

Figure 12. Flowchart describing how experimentation and computational modeling complement each other for accurate description of real-world phenomena.[119]

Table 3. Various models have developed incorporating different degrees of freedom, dependent on the complexity of the system being expressed.[119]

Model	Degrees of Freedom	Predictable Properties	
Quantum Mechanical	Nuclei, Electrons	Reactions	Complex
All Atoms (Polarizable)	Atoms Dipoles	Binding Charged Ligands	
All Atoms	Solute and Solvent Atoms	Hydration	
All Solute Atoms	Solute Atoms	Gas Phase Conformation	
Groups of Atoms (as Balls)	Atom Groups	Folding Topology of Macromolecules	Simple

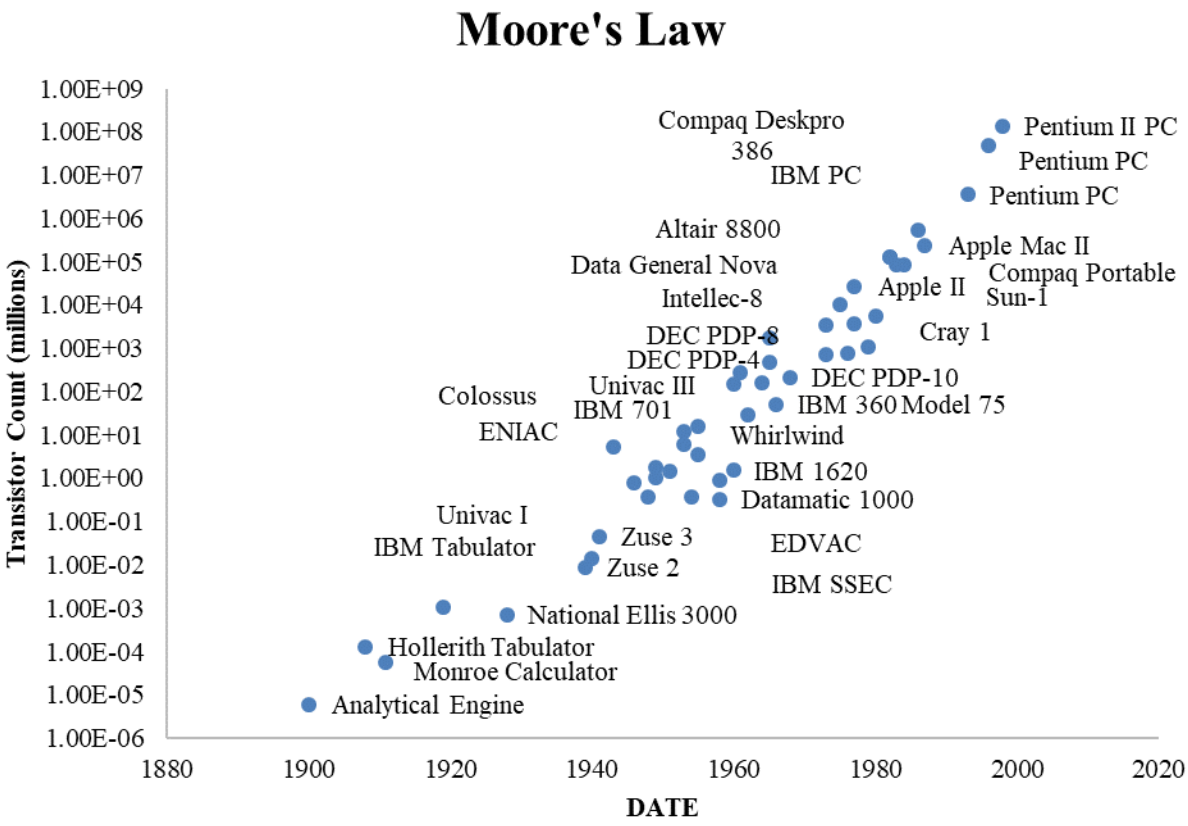

Figure 13. Exponential trend of processer transistor counts over the past century. This trend, colloquially known as 'Moore's Law' shows no sign of depreciating into the next century.[141, 142]

2.2 Equations of Motion

System behavior is determined with terms of motion as a function of time using equations of motion. Equations of motions are sets of mathematical functions used to determine matter propagation, spatial coordinates and time implemented for molecular dynamics, the simplest of which is based on classical mechanics utilizing Newton's second law of motion, F = ma.[120] Molecular dynamics at this level describe ball and stick models – simulating the individual atoms as balls with bonds based using spring mechanics. This level of theory is useful for many investigations such as molecular mechanics – remitting the quantum element for the purpose of describing larger systems.[143, 146, 147] However, electron behavior is integral to accurately describe incurred phenomena, thus a higher level of theory is required.

A quantum mechanical/molecular mechanical (QM/MM) approach computes systems using traditional equations of motions with parameterized quantum-mechanical terms. ReaxFF is a QM/MM method used in various investigations into protein folding or inter- and/or intramolecular forces.[150 - 154] Methods such as ReaxFF incorporates parameterized quantum elements making it an excellent tool for interpolation. Extrapolation relies on accurate simulations of unusual or unique cases requiring a more rigorous quantum derivation. 'Direct' dynamics regularly solves for quantum energy operators and therefore has the capability to supply a sufficient level accuracy required for this study.

2.3 Total Energy Operators

Quantum mechanics addresses electronic structure as particles and waves to properly account for the wave-particle duality of electrons. The state of the molecular system is derivable from the use of the wavefunction (Ψ). Extracting information from the state utilizes the Schrödinger equation, which can be expressed as the time-dependent (Equation 3) and time-independent (Equation 4) form.

(3) $$\hat{\mathrm{H}}\Psi = \mathrm{E}\Psi$$

(4) $$\hat{\mathrm{H}}\Psi(\mathrm{x},\mathrm{t}) = \mathrm{i}\hbar\frac{\boldsymbol{\delta}\Psi}{\boldsymbol{\delta t}} = \hat{E}\Psi(\mathrm{x},\mathrm{t})$$

Equation 3 and 4. Proper description of quantum mechanical properties is done using the Schrödinger equation, expressed in its time-independent (3) and time-dependent (4) form.

$$\widehat{H} = -\sum_i \frac{\hbar^2}{2m_e}\nabla_i^2 - \sum_k \frac{\hbar^2}{2m_k}\nabla_i^2 - \sum_i \sum_k \frac{e^2 Z_k}{r_{ik}} + \sum_{i<j} \frac{e^2}{r_{ij}} + \sum_{k<l} \frac{e^2 Z_k Z_l}{r_{kl}}$$

Equations 5. The Schrödinger equation utilizes the Hamiltonian operator ($\widehat{H}$) to obtain electron distribution with each term a contributing factor to the system (e.g. potential and kinetic energy).

The Schrödinger equation employs the Hamiltonian operator ($\widehat{H}$) on the wavefunction (Ψ) to derive the total energy of the system. When the Hamiltonian operator (Equation 5) is applied to the wave function, the result is proportional to the original wavefunction (i.e. an eigenvalue) and the proportionality describes energy of the system. The Schrödinger equation has been a staple of computational chemistry since it was originally formulated by Erwin Schrödinger in 1925.[155]

2.4 Approximations to the Quantum Model

The Lewis dot structure model is an incomplete description of chemical bonding and structure. The hybridization model illustrates geometries and electron distribution elegantly but collapse under specific circumstances. Models are still viable tools for scientists despite not entirely accurately describing phenomena. If researchers are cognizant of when significant deviations from rigorously obtained solutions occur, approximations can be employed discriminately to describe real-world phenomena. Models in computational chemistry employ approximations to support feasible computation and their influences must be considered. [143 - 149] Some computations are rigorously solved but many introduce acceptable approximations to make investigations more cost effective. Approximations might exclude calculations, supplement averages, parameterize, include variations, perturbations, or introduce other simplifications to reduce calculation complexity. The Schrödinger can only rigorously solve a hydrogen atom with

one electron, however the Born – Oppenheimer (BO) approximation is one fundamental alteration applied to the Hamiltonian allowing feasible solvation (Figure 14).[156]

The BO approximation is acceptable as nuclei are essentially stationary compared to electrons since nuclei are slower and more massive than electrons.[143 - 147] Computational chemists have a wide range of employable approximations to achieve different goals such as the Hartree-Fock (HF) approximation which accounts for the coulombic electron-electron repulsion by integrating repulsion terms.[157] The types of approximations employed is described in the functional, representing the approach for computing the system.

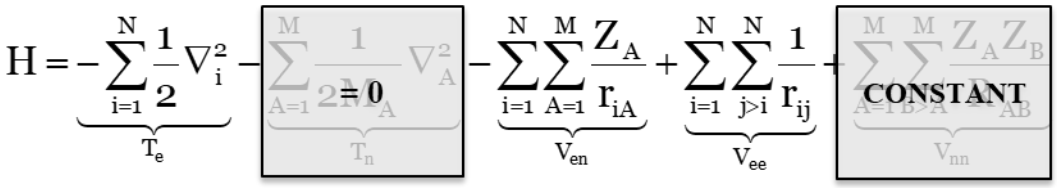

Figure 14. Mathematical description of the Hamiltonian operator. The Born-Oppenheimer approximation works using two assumptions. Nuclei move significantly slower than electrons, thus the nuclear kinetic energy is negligible. Nuclei positions remain relatively constant, thus the potential energy term for nuclei with relation to each other can be considered constant.[143 – 147]

The functional denotes half of what is called the model chemistry, the other half being the basis set which will be discussed in greater detail. Basis sets rely on linear combinations of atomic orbitals (LCAO) using either Slater-type orbitals (STO) or Gaussian type orbitals (GTO).[158] It is vital to discuss the methods of computation to describe the system effectively as the approximations involved ignore or simplify elements. Depending on the complexity and accuracy of the system required, researchers must select an appropriate method both in terms of the approximations made and the approach taken.

2.5 Density Functional Theory

One major development in computational chemistry is the emergence of Density Functional Theory (DFT). Originally disputed in its application, DFT has gained acceptance for application in chemistry and physics (Figure 15).[31, 99, 101, 103, 117, 118, 121, 126, 127, 137, 138,] Ab-initio methods solve the Schrödinger equation using the BO approximation, the most prolific of which are based on the Hartree-Fock (HF) approximation.[103, 117, 121] HF remits the electron correlation as it rigorously solves the wavefunction on a single electron basis.[157] Post-HF methods were developed using linear combinations of determinants that account for electron correlation, such as the Moller-Plesset perturbation theory (e.g. MP2).[159] While post-HF methods amount to improved accuracy, they scale at a fifth or higher power.[160]

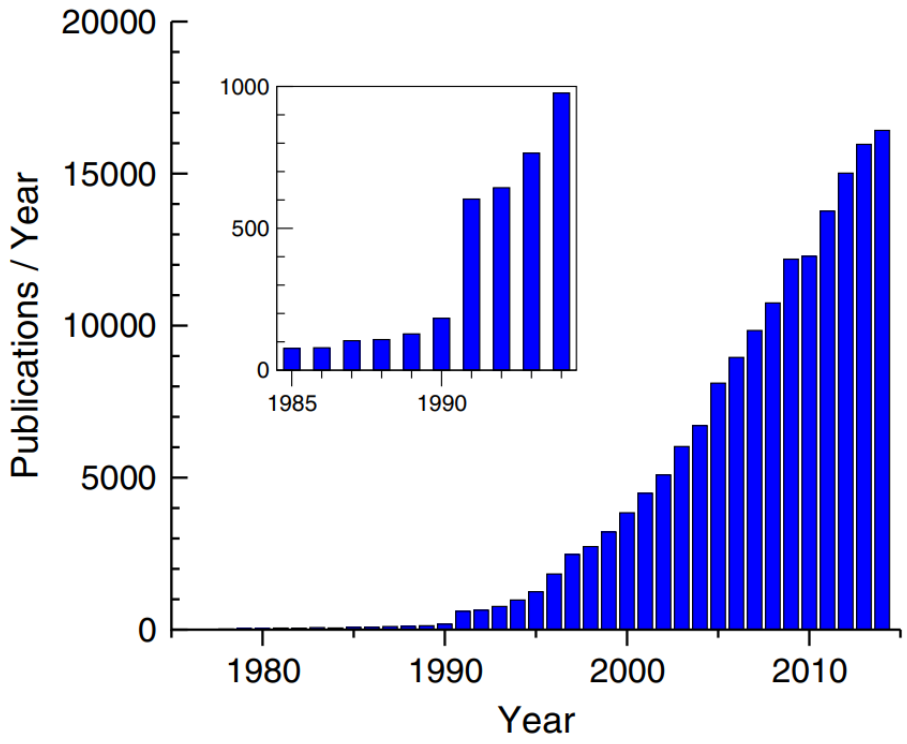

Figure 15. Graphical representation of the exponential gain in acceptance for DFT as expressed by the number of paper's including DFT in their method, logarithmic over time.[162]

The core concept for DFT replaces the complex N-electron wavefunction with electron density, ρ as a basic local variable described through Kohn – Sham orbitals (originally proposed by Pierre Hohenberg and Walter Kohn). The effective potential allows the inclusion of the external potential and accounts for coulombic interactions between the electrons such as the exchange and correlation interactions (Figure 16). The other advantage to this method is its computational scaling, as most DFT methods scale at similar levels to HF without remitting vital aspects of the system. The intractable solvation capacity for simulating larger systems was opposed originally, although the method was eventually formally recognized when Walter Kohn and John Pople were awarded the Noble prize in 1998.[162]

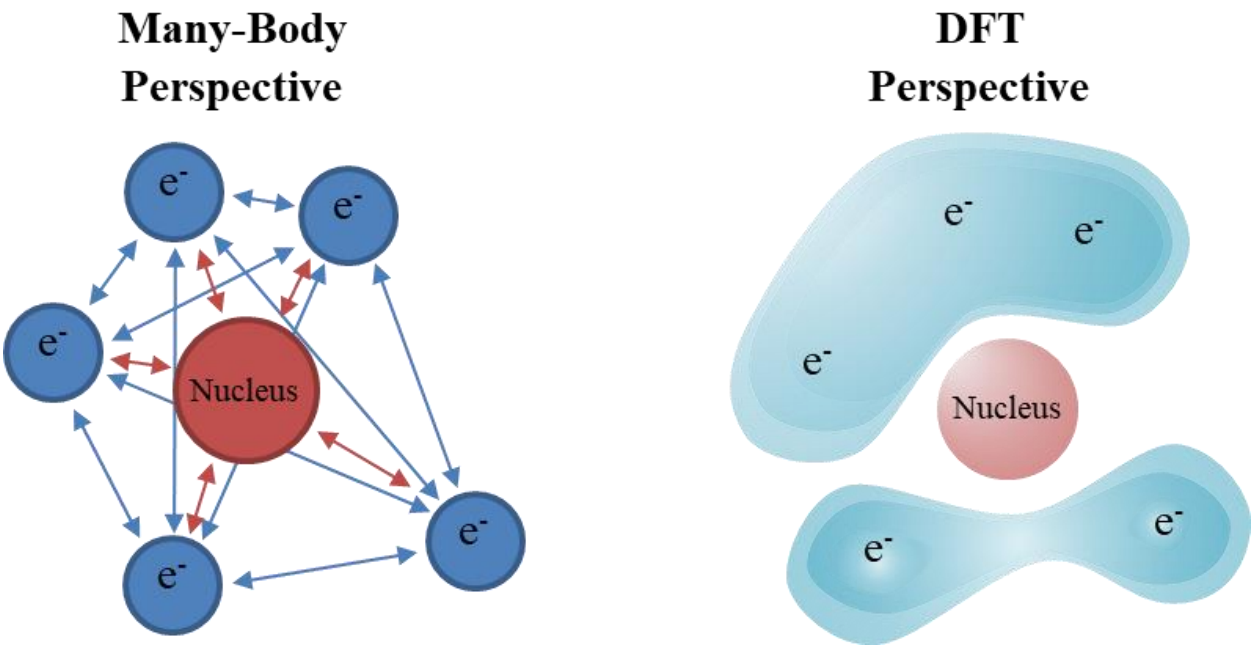

Figure 16. Graphical description of DFT vs. Many-Body perspective. Treating electrons as probability density functions allow more rigorous calculations with greater ease.

2.6 Potential Energy Surfaces (PES)

Potential energy surfaces (PES) are useful models used in methods, techniques, and concepts of computational chemistry expressing multiple states of a system as a function of energy. Mathematically challenging processes involving reaction paths, configurations or isomers are describable with notable features on a PES relevant for discussion of chemical reaction dynamics (Figure 17).

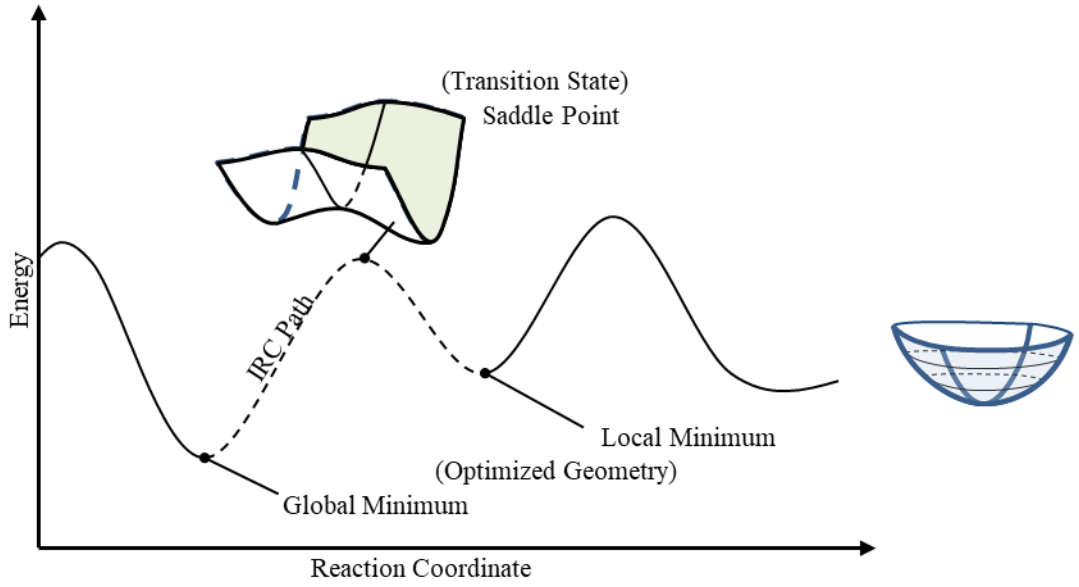

Figure 17. One-dimensional PES following the reaction of a system. Important features shown are the minima and saddle point. Typical reaction coordinates are represented by an amalgam of variables (bond angles, lengths, etc.)

The simplest PES is one-dimensional and can describe reaction pathways. The major features of a one-dimensional PES are minima, maxima, and IRC pathways (Figure 17). A minimum is a low energy configuration of a system, either local (lowest in area) or global (absolute lowest). All minima represent optimized geometry or stable states along the PES. Systems move from higher to lower energy state and a local minimum point is considered 'meta-

stable'. Maxima in one-dimensional PESs represent transition states (TS) or high energy position states between two optimized geometries and are usually unstable existing only for brief fractions of time. Transition states are useful for describing reaction pathways, activation energy (E_A) or reaction spontaneity. Many reactions involve multiple TSs and the complete mechanism can be described by an intrinsic reaction coordinates (IRC) pathway, represented by the dotted line in Figure 17. An IRC pathway is the lowest energy trajectory between two optimized geometries.[110]

PES concepts exist in higher dimensional PESs (Figure 18), in addition to more complex ones. A Valley-Ridge Inflection (VRI) point is a position on the N-dimensional PES in which the second derivative in one dimension is zero and all other derivatives negative. Second-order saddle (SOS) points represent high energy unfavorable configurations of the system which are essentially forbidden. An intuitive way of describing this is through the image of a ball balanced on a hill. Since the ball is high in potential energy, it is likely to roll down the hill, converting its potential to kinetic energy. Unless energy is applied to the system, the ball never naturally returns to the higher energy state. The Born-Oppenheimer (BO) approximation is required for establishment of a PES since the nuclei are considered stationary in relation to electrons within the system. This allows definition of system's configurations in terms of nuclei positions. To calculate a PES, minor alterations to certain features of a molecule are scanned for energy. After each alteration, a single point calculation is taken, which combined creates the surface of the PES (Figure 19).[140]

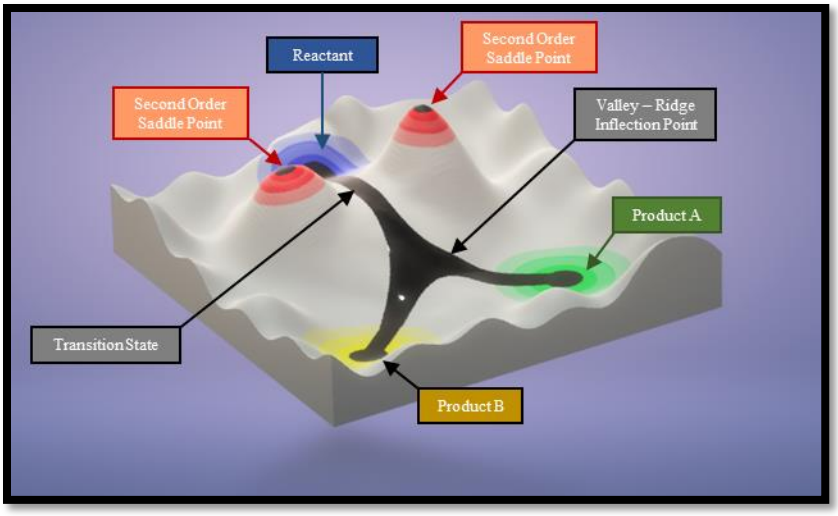

Figure 18. Potential energy surface of a two-dimensional system. Many concepts not expressible through a one-dimensional PES can be expressed with additional dimensions such as valley-ridge inflection points, second order saddle points, and bifurcation points.[172]

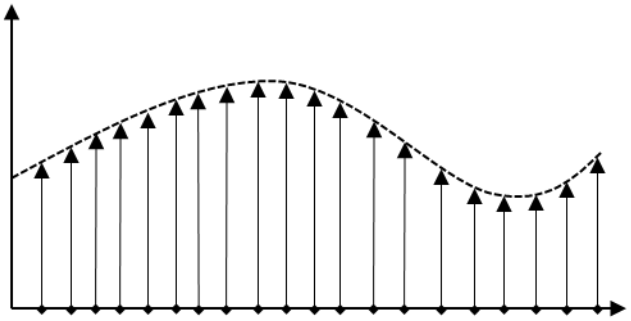

Figure 19. Graphical representation of the scanning technique used to generate a potential energy surface. An increase in dimensionality results in a grid-format scan.[110]

PESs can express many complex computational techniques such as an optimization, used to derive local minima along an N-dimensional PES. This task involves adjusting the molecule and testing for the influence on energy. If energy increases, the system reverts and if energy decreases, the system propagates. This process is repeated until further iterations no longer influence energy significantly (Figure 20).[140]

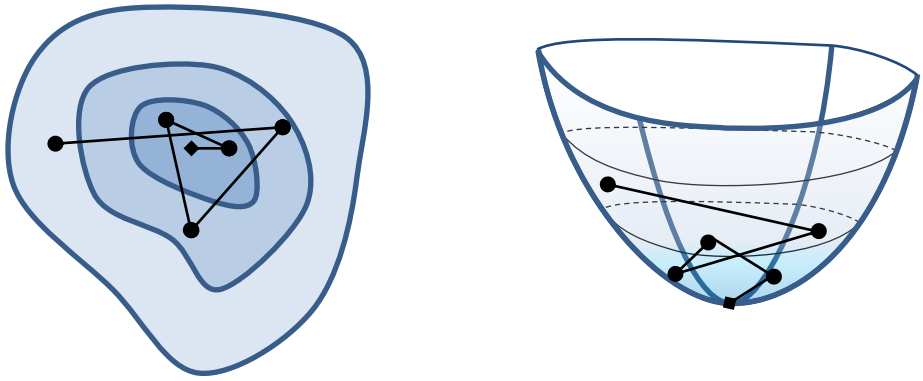

Figure 20. A two-dimensional and three-dimensional visual representation of an optimization. The process is repeated until the program determines to a degree of certainty that no further alterations can be made to significantly reduce energy in a system.[140]

2.7 Temperature – Accelerated Molecular Dynamics (TAMD)

As a method to explore and reconstruct the free-energy landscape, temperature-accelerated molecular dynamics (TAMD) has been well established to describe chemical systems. Conventional constant temperature molecular dynamics are utilized to study conformational and dynamic distributions of systems – however infrequent events such as the dissociation through pyrolysis would require a completely different timescale to simulate. Slow transitions in the configurational space can be caused by low energy regions separated by high energy barriers. These barriers provide complications when attempting to produce canonical ensembles – essential to a condensed-phase MD investigation. TAMD allows expedient propagation through these barriers by 'flooding' the PES landscape (Figure 21). Adding temperature to the system can cause potential alterations to the nuclear kinetic energy (NKE) and may permit the system to achieve states within the molecule unavailable at lower temperatures, another consideration which much be accounted for.[129 - 133]

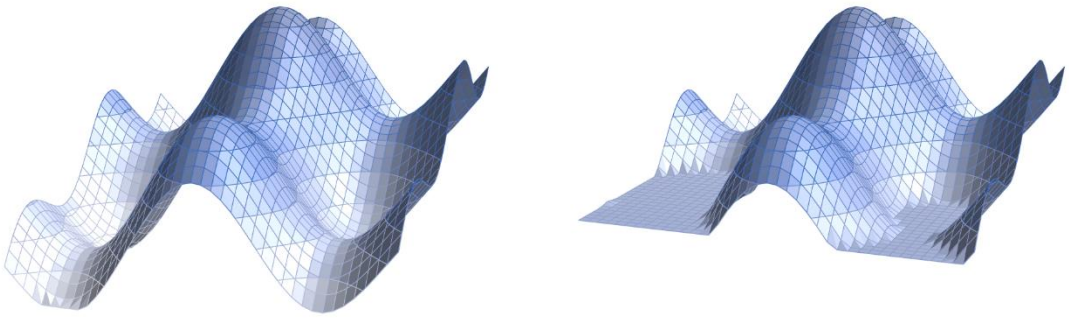

Figure 21. Conceptual representation of the TAMD approach for encouraging transfers between meta-stable states of the system. To avoid introducing forbidden states or transitions, the wells must be filled only to the extent that the barriers are reduced but not removed.[129 – 133]

2.8 Creating an Ensemble

In molecular dynamics, an ensemble of trajectories must be formed to ensure all possible pathways are considered. Each trajectory has potential to derive a set of possible products from dissociation. Just like experimental analysis, this results in a distribution of possible (or obtained) products. Deductions can be made from the product distributions of energy barriers along an n-dimensional PES. Incorporating multiple trajectories is a requirement of the ergodic hypothesis which states that for a long period of time, if the time incurred by the system within a phase space is proportional to its volume, all accessible microstates are equiprobable. MD rely on this hypothesis for validity, although it has only been rigorously proven for hard-sphere gases.[163] The achievable conclusion from this is that the average obtained by following a small number of particles over a long period of time is equivalent to averaging a large quantity of particles in a short period of time (Figure 22).[132]

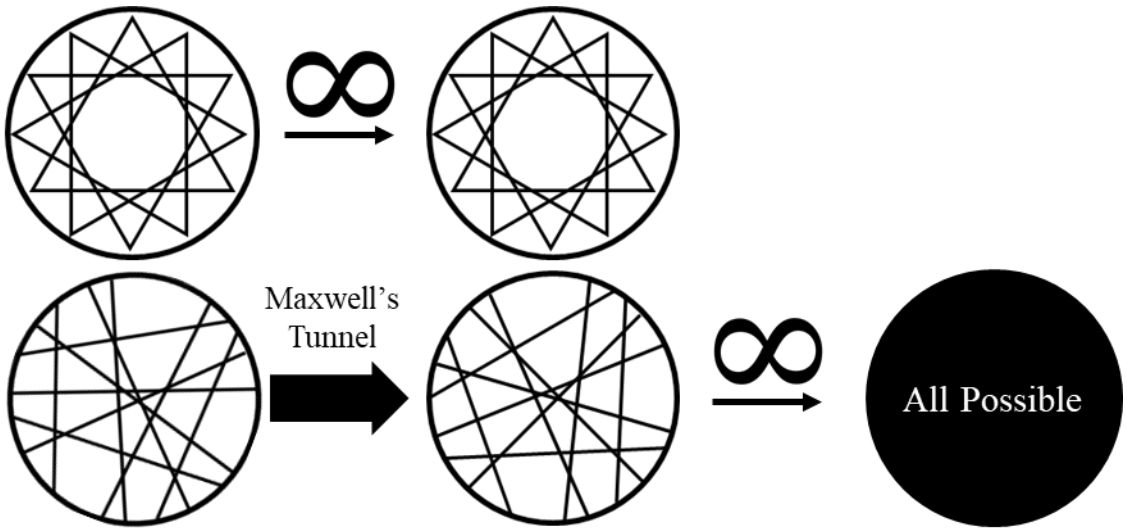

Figure 22. Representation of the Ergodic principle. The top model represents a repeating system thus not all configurations in the phase space are achievable, even when run to infinity. The bottom is ergodic because as the system approaches infinity, all states become equiprobable.[164]

CHAPTER 3. METHODOLOGY

3.1 Model Chemistry – Functional and Basis Set

Herein we make use of direct dynamics simulations by integrating Newton's classical equations of motion with forces derived from an electronic structure method. The Gaussian09[165] suite of programs was used to compute all trajectories. As discussed earlier, the model chemistry determines the accuracy and cost effectiveness of the project through multiple considerations. There are two major components that help define the model chemistry: the functional and the basis set in the format FUNCTIONAL / BASIS SET. [99, 120 - 123, 139]

The functional defines the calculation approach, as described in the discussion of DFT methods. The most common DFT functional is B3LYP, representing the Becke, 3-parameter, Lee-Yang-Parr method (Figure 23).[101] B3LYP is a parameterized hybrid DFT functional created by Axel Becke in 1993. Hybridization with HF exchange improves the accuracy of many molecular properties in the system. Since its creation, B3LYP has been widely used, incurring criticism from many experts.[121, 126] It has been argued that the popularity of B3LYP's application is not simply its accuracy but its versatility for application in a wide variety of investigations. Since B3LYP, many new parameterized DFT functionals have emerged for application in specific pursuits of computational chemistry, although none yet exhibit more general appeal.[99, 102, 121]

Other functionals perform better in more specific cases. An analysis of the individual components of the system must be made to determine an appropriate functional. A benchmark study on 44 chemical moiety representative (CMR) reactions was undergone in relation to experimentally determined bond dissociation energies (BDEs) to derive the efficacy of various

model chemistries describing the thermodynamic properties of methyl linoleate.[28] The result found the deviation of B3LYP/6-31+G(d,p) to be 5.7 ± 11.4 kcal/mol, significantly higher than M06-2X/6-31+G(d,p), which was found to be 0.5 ± 9.4 kcal/mol.[15]

Figure 23. Word cloud containing commonly employed DFT functional methods (credit to Peter Eliot for compiling 500 computational research articles). More commonly used functionals are shown larger; the most commonly employed is B3LYP.[121]

M06-2X is a group of highly parameterized exchange-correlation energy functionals developed by Dr. Donald Truhlar's research group at the University of Minnesota (namesake). This functional is particularly accurate for descriptions of thermochemistry in main-group elements – very pertinent to this investigation.[102] The functional is only half of the complete model chemistry, and a suitable basis set was chosen to complement the functional. It has been noted that applying an accurate functional to a simple basis set increases the cost while not contributing well to the improvement of accuracy.[121, 125] The same was found with the inclusion of a simple functional and a complex basis set. The correlation between the two methods must be complementary to best obtain the benefits of both basis set and functionals, without loss of either accuracy or cost effectiveness.

A good analogy for using unsuitable pairs of functionals and basis sets is when one attempts to determine the density of a liquid using an accurate scale but an imprecise volumetric

flask. Since the bottleneck for accuracy in density is a combination of the volume and mass, improving the accuracy of the mass measurements without improving the volume determination would be inefficient to improve an investigations accuracy. An amalgam of similar such considerations in molecular dynamics can be seen in Figure 24, including a Pople diagram describing the correlation between functionals and basis sets.[170]

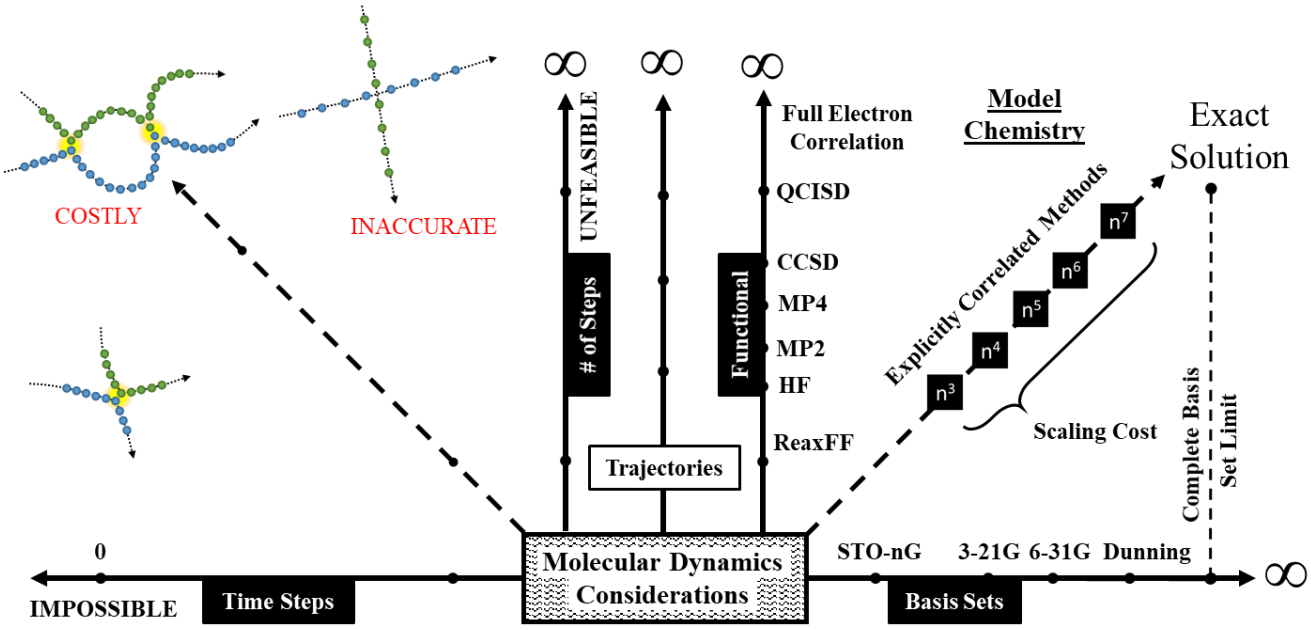

Figure 24. Graphical description of the considerations for choosing a proper functional and basis set in properly simulating a system.[170]

Theoretically, as the number of basis functions are expanded ad infinitum, they approach the complete basis set (CBS) limit. The CBS limit represents the point where the inclusion of additional basis functions no longer improves the accuracy (presumably infinite).[125] These basis functions are derived from calculations of the wavefunction for either atomic orbitals (AO) or molecular orbitals (MO). Unfortunately, the function that this is calculated through is dependent

on slater functions (Figure 25). These functions, while accurate, pose problems when attempting to integrate under the curve (required for calculations of electron density).[126]

$$\Psi_{1s} = \left(\frac{x^3}{\pi}\right)^{\frac{1}{2}} e^{-x|r-R|}$$

Slater Type Wavefunction

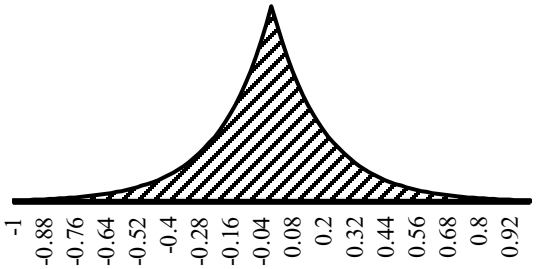

Figure 25. Slater functions (see above) are the most accurate method for simulating the motion and position of electrons in a system.

Many computational methods rely on similar functions known as gaussians, which exhibits similar mathematical properties deviating with the inclusion of an exponential square factor on the radius. Integrating Gaussian Type Orbitals (GTOs) do not produce undefined regions thus are commonly utilized as a replacement for Slater Type Orbitals (STOs). There are consequences to this alteration as the accuracy of GTOs breaks down in areas far away from and close to the nucleus (Figure 26). To compensate for this, basis sets are derived through linear-combination of gaussian-type orbitals (excluding plane-wave basis sets).[126]

$$\Psi_{1s} = \left(\frac{x^3}{\pi}\right)^{\frac{1}{2}} e^{-x(r-R)^2}$$

Gaussian Type Wavefunction

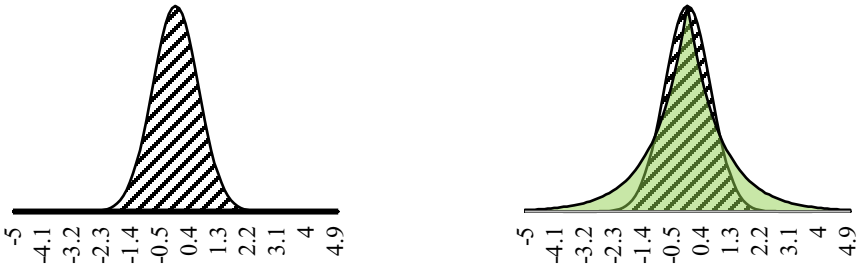

Figure 26. Gaussian type wavefunction (left) graphically shown (middle) and compared to slater type orbitals for comparison (right). The right graph shows a problem with implementing a gaussian when a slater type is more accurate (close to center and farther out).

Figure 27 gives a good representation of combined GTOs attempting to simulate an accurate STO. The more GTOs included, the closer an approximation is to the actual STO. STO-XG is an extremely simple basis set, where X relates to the number of GTOs included. Another commonly used basis set are the Pople basis sets, named after the individual who derived them.[171] Integral to the very concept of these is the idea of split-valence basis sets, which includes sets of GTOs describing the valence electrons separate from the local AOs or MOs. The format typically used for a Pople basis set is generally X-YZG or X-YZW depending on the number of split valences involved.[171]

To align the functional with a correlative complex basis set, 6-31+G(d,p) was selected for computation. The additional parameterizations (i.e. '+' 'd' and 'p') represent diffuse functions and polarization functions respectively. Since the dissociation of fatty acid methyl esters requires diffusion, and the specific moieties within the molecule include polarized heteroatoms, these are necessary to successfully describe the molecular system. Based on a previously mentioned investigation, M06-2X/6-31+G(d,p) was determined to be an accurate model chemistry for this investigation.[15, 27]

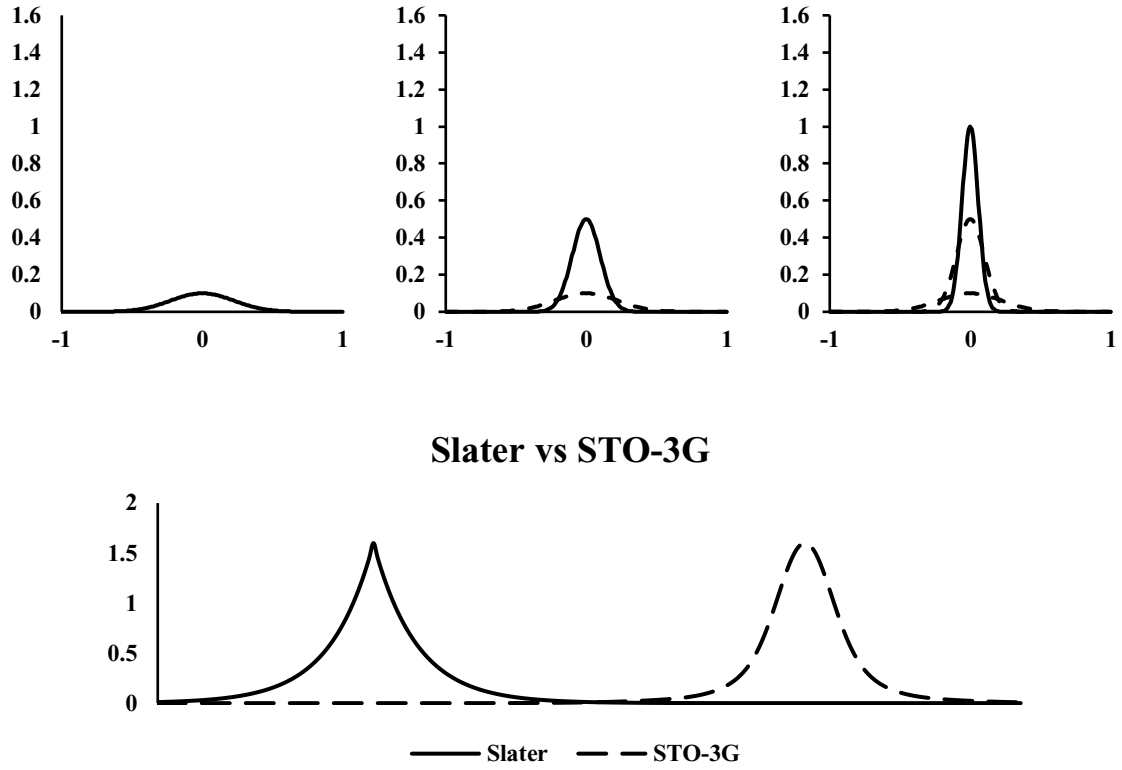

Figure 27. Linear combination of GTOs (top) form a STO-3G (bottom-right) that is comparable to the STO (bottom-left). The linear combination of GTOs in parameterized basis functions allow closer approximations to STOs without complications in areas where singular GTOs fail.

3.2 Molecular Dynamics Parameters

Molecular dynamics requires additional considerations to accurately depict properties specifically related to time. There are two components, highly vital to this investigation: the ability to simulate the desired process accurately, and to be able to do so in a reasonable amount of time. The time step describes the interval of time that elapses between each 'frame' of the simulation calculating the current state of the reaction. Think of it like trying to take a video of an event in motion, for example a basketball game, by taking a series of still images. If the time between taking the images is too long, then one would miss important movements of the players or even the moment that a team scores. If one decreases the time between the images, they are more likely to capture all the critical details of the game. Of course, this is how video works; a

rapid series of still images that we perceive as continuous, fluid motion. However, there is also a point where taking the images too fast will cease to yield further meaningful information and will only serve to take up extra space on the storage device. The rule of thumb for determining an appropriate interval is the $1/10^{th}$ rule – which states that the length of the time step should be no more than one tenth of the time for the shortest phenomena.[140] Since the fastest vibration persistent in the molecule is the C = C – H stretch occurring around 3100 cm^{-1}, this value can be used to reverse engineer an ideal time step as 0.0000000107 s or approximately 1.0 femtoseconds (fs).

Additionally, the simulation must be permitted to run for a length of time sufficient to observe the phenomena. If the simulation is not permitted to persist to a suitable degree, the entire computation becomes pointless. On the other hand, if the computation continues far beyond the point of dissociation, there comes a point where additional time steps does not contribute to the purpose of the investigation. Using the previous example of a basketball game, one would not want to stop taking pictures before the game was over, nor would they want to keep taking pictures after everyone had left the court. The chosen duration used for this investigation was 2000 fs (which corresponds to 2000 time steps.) Unfortunately, 2000 fs is an extremely short quantity of time, and nowhere near the duration described by empirical studies. This is a problem common to many variations of molecular dynamics, and multiple workarounds have been established to compensate for this. One postulated method of doing so is through temperature-accelerated molecular dynamics (TAMD) as discussed previously.

The introduction of the temperature-accelerated molecular dynamics method (TAMD) has shown validity in describing processes exceeding the normal limitations of the calculation. TAMD was introduced to increase the speed of conformational and constitutional alterations in

the molecule. Yet if the temperature is set too high within the molecule, energetically forbidden states can be achieved. For this reason, the temperature of 3500 K was selected as it showed no significant problematic results in the preliminary investigation.[15, 27] In addition to forbidden states, TAMD also further deviates the system from the BO potential energy surface.[129 - 133] The value for the nuclear kinetic energy (NKE) over the extension of time was calculated using Equation 6 and incorporated in the randomized velocities of the nuclei.

$$NKE = \frac{3}{2}(N-1)k_B T$$

Equation 6. Calculations for the nuclear kinetic energy (NKE) were done to compensate for deviations in the BO potential energy surface.

3.3 Atom - Centered Density Matrix Propagation (ADMP)

For the purpose of performing direct dynamics trajectories, atom-centered density matrix propagation was employed treating electronic structure simultaneously with nuclear motion. ADMP is a form of extended-Lagrangian molecular dynamics (ELMD) which utilizes extended-Lagrangian mechanics to propagate the system over degrees of freedom in the nuclei.[172] The extended-Lagrangian function used can be seen in equation 7 below. ***Tr*** represents a trajectory-dependent term, as the seed determines the distribution of forces and is randomized for each. The $\boldsymbol{V^T MV}$ term denotes the momentum scaling term. **μ** represents the fictitious mass tensor while **W** represents the density matrix velocity. E(R, P) represents the potential energy as a function of the position (R) of the nuclei, as well as the single-electron density matrix (P). Finally, the Lagrangian multiplier matrix (Λ) ensures electrons are not counted duplicitously.

$$L_{ADMP} = \frac{1}{2}Tr(V^T MV) + \frac{1}{2}Tr\left(\left[\mu^{\frac{1}{4}} W \mu^{\frac{1}{4}}\right]^2\right) - E(R,P) - Tr[\Lambda(PP - P)] \qquad (2)$$

Equation 7. Depiction of the equation used to propagate the system over degrees of freedom in the nuclei.[172]

3.4 Formation of the Input Stream

Having discussed the various components of each of the considerations of this project, there is a small discussion of the logistics of communicating with the quantum computational program. An Input Stream File (ISF) communicates commands and system properties to Gaussian for calculation (Figure 28). The format of this file is separated into sections:

- **Link 0 Commands**: used to locate and name scratch files (optional) as well as specify computer resource information (memory, nodes, etc.)
- **Route Section**: specifies the computation's type, model chemistry, and other parameters.
- **Title Section**: arbitrary title given to easily distinguish the job file
- **Molecule Specification**: defines the molecular system.
- **Additional Section**: additional molecular specification (if desired)

%NProcShared=12 %Mem=1500MB	**Link 0 Commands**
# B3LYP/6-31G(d) Opt Freq	**Route Section**
Water Optimization	**Title Section**
0 1 H -5.07739934 0.97523218 0.00000000 O -4.72074492 -0.03357782 0.00000000 H -4.72072650 1.47963037 -0.87365150	**Molecule Specification**
	Additional Section

Figure 28. Example ISF for the optimization of a water molecule. Each component of the ISF describes a modality of the computation for the determination of energy.

The two most relevant components of the ISF are the Route Section (RS) and Molecule Specification (MS). For jobs of our purposes, the RS is a combination of the following codes:

M06-2X/6-31G(d,p)

- **Model Chemistry**: The model chemistry is a combination of the functional and the basis set. In the case of this investigation, M06-2X was chosen as the functional and 6-31G(d,p) was chosen as the basis set.

ADMP=(MaxPoints=2000,FullSCF,NKE=897791,StepSize=10000)

- **ADMP.** Atom-centered Density Matrix Propagation was selected as the form of MD. The MaxPoints represents the number of steps included in the computation, at a StepSize of 10000 *n*, or 1 fs. The code incorporated the FullSCF command to have the dynamics conducted with converged SCF results at each stage. The NKE was calculated to compensate for deviations ignored by the BO approximation.

EmpiricalDispersion=GD3

- **Empirical Dispersion.** Despite its many advantages, DFT has difficulties describing Van der Waal forces. To compensate for this, code shown above is included in the RS. The GD3 tells the code to include the D3 version of Grimme's Dispersion.[124]

guess=(mix,always)

- **Guess.** The inclusion of this line refers to the method by which the program conducts an initial guess for self-consistent field optimization. The parameters shown above tell the code to mix the HOMO and LUMO. This request is introduced to destroy α-ß and spatial symmetries.

SCF=(xqc,MaxConventionalCycles=250,NoSymm)

- **SCF.** The SCF, or self-consistent field, requires that the final field computed from charge distribution be 'sef-consistent' with the assumed initial field. The XQC line incorporates an additional QC (quadratically convergent SCF) in case the first-order SCF has not converged. The MaxConventionalCycles limits the number of SCF cycles to 250. NoSymm was included to lift all orbital symmetry constraints.

  Symmetry=None

- **Symmetry.** This line fully disables symmetry in the calculation.

  IOp(1/44=-1,1/80=1000000,1/81=10,1/82=3500,1/89=2)

- **IOp.** The IOp (Internal Options) is a vast number of commands that alter how Gaussian operates with specific calculations (Table 4).

Table 4. Description of various pertinent IOp commands for the proper simulation to be described and operated in Gaussian.

IOp	Purpose
1/44=-1	Uses system time initialize iseed (each run should produce different results)
1/80=1000000	Introduces Velocity Scaling throughout the simulation, in order to compensate for the Nuclear Kinetic Thermostat option.
1/81=10	Step Size by which the temperature is checked and scaled.
1/82=3500	NKE Thermostat temperature.
1/89=2	Minimum allowed deviation, in Kelvin, from average NKE

  Temperature=3500

- **Temperature.** Thermochemistry analysis utilizes a set temperature option. In this case, the temperature was set to 3500 K. The default is 298.15 K.

The other important feature in the ISF is the Module Specification (MS) describing the system by cartesian or internal coordinates. A Cartesian MS (Figure 28) expresses atom positions in the format "$atom\ type\ x\ y\ z$". The molecule can also be expressed with reference to another format that relies on internal coordinates using three non-degenerate dimensions of the system instead of its relationship to the origin (Figure 29). The advantage of this description is that it requires 6 less dimensions (12 including velocity) and describes the system in terms of spherical coordinates instead of Cartesian allowing a direct relationship between the system and the bonds in the molecule described by 3 terms: bond lengths, bond angles, and dihedral angles. Future endeavors would benefit greatly in how the system is defined.

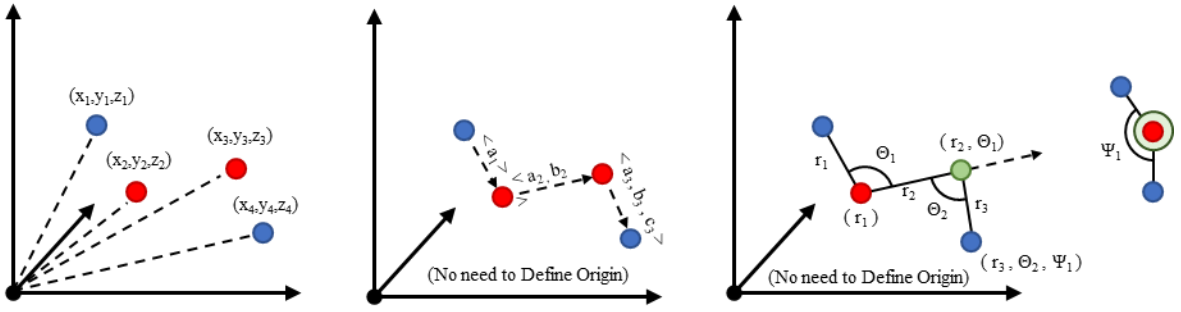

Figure 29. Description of a system using different coordinate systems. a) describes the system using Cartesian coordinates relative to the origin. b) describes the system with internal coordinates which omits the existence of the origin. c) describes the system ideally for our purposes to permit direct alterations of the ISF. Instead of the traditional Cartesian format (x,y,z) the polar coordinate system is implemented (r, Θ, Ψ).[140]

CHAPTER 4. RESULTS AND DISCUSSION

4.1 Ensemble Analysis

The results of this investigation are interpretable from different perspectives. A total of 100 trajectories dissociated (33%) comprising the theoretical ensemble. The average trajectory incurred 2.27 bond cleavages after 1189 fs. A graphical depiction of these dissociations (Figure 30) shows the first dissociation for each trajectory in terms of bond distances (Å). This shows significant support that bond dissociations are heavily co-entangled, meaning a simple calculation of the bond dissociation energy (BDE) for individual bonds would be insufficient in extrapolating the possible results obtained from pyrolysis. Understanding the times at which a trajectory dissociates in comparison to when it first dissociates is important for discussion of the mechanics involved (Figure 31). The complete product distribution can be seen in the supporting information.

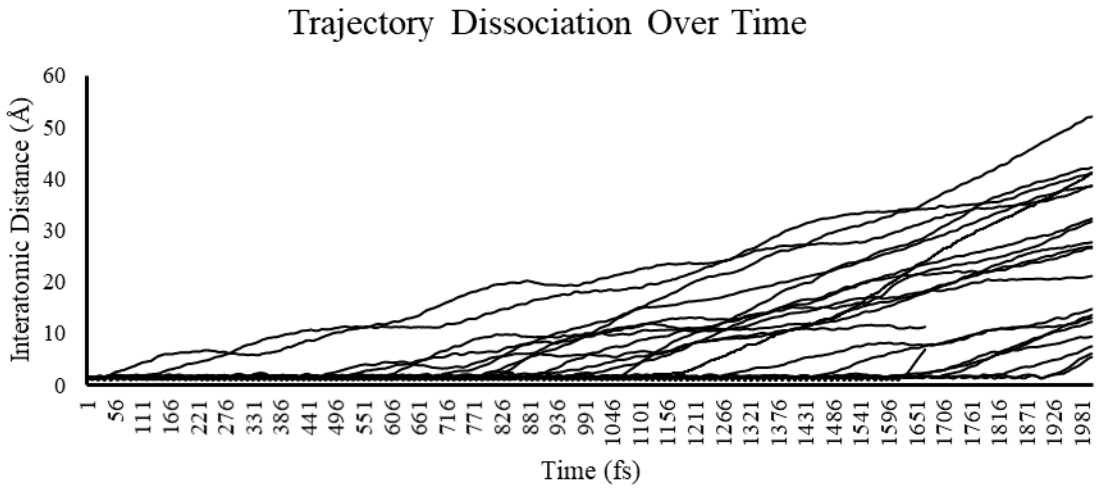

Figure 30. Description of trajectories as a function of bond distance over time. Several trajectories involve multiple separations, but only the first dissociation is described in the above.

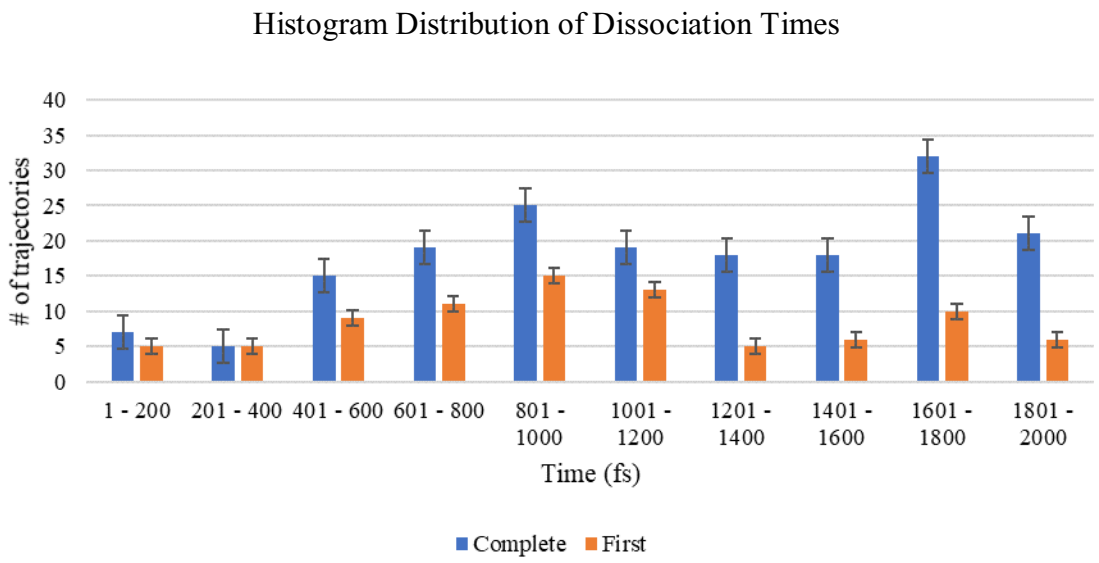

Figure 31. Distribution of the dissociations as a function of number of trajectories within specified time regions. Inferences can be made that a first dissociation acts to encourage latter dissociations.

In investigations into thermal cracking procedure, it must be determined the point at which bonds no longer are considered bonded. The energy incorporated within a bond can be represented by the Morse potential energy function (Figure 32). In this function, r_e represents the equilibrium bond distance and D_e is the well depth. Experimentally, these values can be determined by methods including X-ray diffraction, electron diffraction or other spectroscopic methods. The distance between the two species is never constant, as bonded systems acts akin to springs. As molecules vibrate, the system rocks back and forth in the potential energy dip. At some point, the energy of the vibrational supersedes the attractive force between the species and the bond can formally be considered "broken".[167]

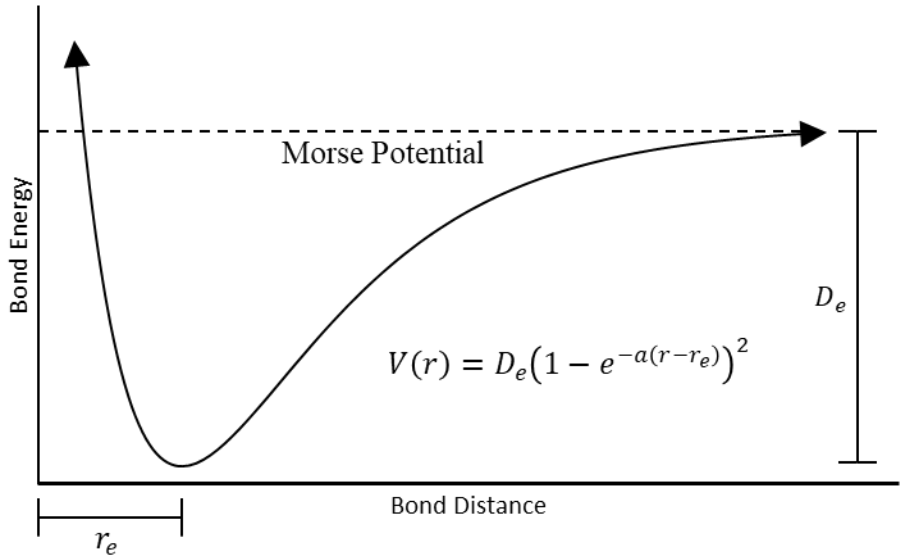

Figure 32. Bond Energy as a function of Internuclear separation. The dotted line represents the dissociation energy, which can be achieved by expanding the asymptote to the Morse potential.[166]

The chosen value for this analysis was based on Van der Waals (VdW) radius representing the distance of closest approach for another atom. This value changes depending on the size of the species' nuclei derived from literature investigations (Table 5). If the interatomic distance between atoms exceeds the sum of the individual species' VdW radius, then for the purposes of this analysis the bond is considered severed.[167]

Table 5. Various Van der Waal radii used to determine the point at which a bond can no longer be considered based on literature values.[168]

Element	VdW Radius
H	120 pm
C	170 pm
O	152 pm

A comparison between experimental and theoretical results can be insightful to the validity of the method employed. One investigation by Ming Chai analyzed the thermal

decomposition of 3 relevant FAs (stearic acid, oleic acid, and linoleic acid) which share many of the features to methyl linoleate (Figure 33).[169] The results of this investigation described the quantity of FAs converted (or converged) and the distribution of the products obtained. Of the three FAs investigated, the amount at which each of these were conserved were 3% (stearic acid), 22% (oleic acid) and 68% (linoleic acid). This trend indicates that the presence of unsaturation plays a major role in how the molecule dissociates and agrees with simulations as even at elevated temperatures a lack of dissociation was observed in 66% of trajectories in the ensemble.

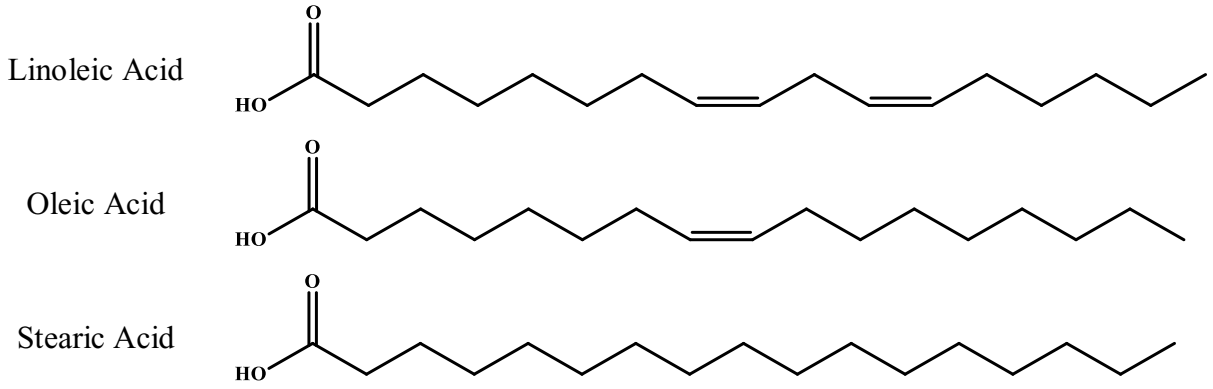

Figure 33. Three individual FA interpreted in a study by Ming Chai. It should be noted the only deviation between the three is the level of unsaturation incorporated.[169]

The experimental results by Ming were also interpreted for the products formed. Without an atomic level perspective, interpretations were limited to phase analysis, IR and GC/MS. It was determined that two major phases formed – gas and liquid – indicating that little products of the reaction appeared in solid form.[169] This is important for validifying this investigation, as an important assumption is that at high temperatures, the probability of bond dissociation is far higher than bond formation. This is supported by both the experimental and theoretical results, as both show little or no presence of higher weight products than the original molecule. The gas-phase was determined with GC/MS to be consistent of low weight hydrocarbons (C1 – C4) and

light deoxygenated products (CO_2, CO, etc.). As discussed in Ming's analysis, there is some difficulty in interpreting the quantifiability of these results, as these products were difficult to contain (loss in apparatus) and measure (interaction with DCM).[169] The distribution of gas-phase products is comparable to the obtained theoretical ensemble (Figure 34) with two important molecules for discussion being CO_2 and CO, the result of decarboxylation and deoxygenation. Without atomic-level analysis, the ratios of these components are used in similar experimental studies to determine likely mechanisms of dissociation.

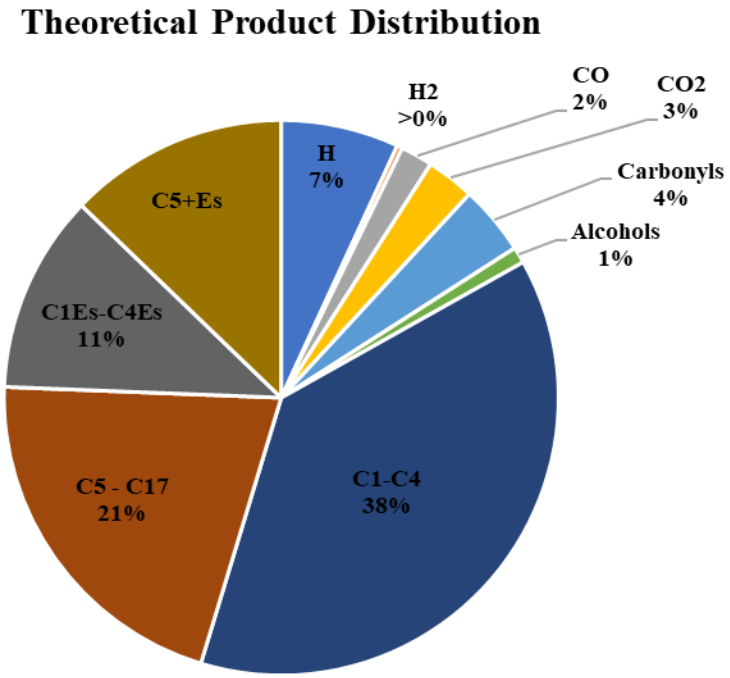

Figure 34. Product distribution obtained from trajectories categorized based on properties observable in experimental investigations.

Another study analyzed the thermal decomposition of methyl oleate with a heavier focus on containing and categorizing gaseous product distributions.[28] In theory, the ratio between CO_2 and CO can be used to elucidate preferred routes of dissociation. Figure 35 gives the product

distribution of CO and CO_2 obtained in Asomaning's data as a function of temperature. The ratio of these two obtained from the theoretical ensemble was (2.8 ± 0.2% CO_2, 1.87 ± 0.6% CO, 1:1.497), agreeing with experimental observations of lower temperature pyrolysis. A complete description of deoxygenation reactions observed in the theoretical ensemble is described in greater detail in the atomic-level analysis (Figure 43).

As is noted by Asomaning, the production of CO and CO_2 is affected additionally by post-pyrolysis reactions, where water or methanol react during the cool-down portion of experimentation. CO_x methanates in the presence of H_2, producing methane and water while CO can undergo a water-gas shift through reactions with water to produce H_2 and CO_2. It is important to note that the simulations discussed herein air to determine the unimolecular reaction dynamics and do not account for post-pyrolysis cool-down mechanisms.[13]

Asomaning's exploration into experimentally obtained results also interpreted the results based on the homology of hydrocarbon products (using GC/MS). The distribution of products obtained from pyrolysis of methyl oleate (a similar FAME to methyl linoleate) was run at multiple temperatures (Figure 36b) and the data obtained theoretically (Figure 36a) most closely associates with the distribution at 350°C. This in tandem with CO/CO_2 interpretation suggests that the temperature selected to accelerate the system with TAMD (3500 K) was in line with a lower temperature pyrolysis. More descriptive homology descriptions can be found in Figure 48 and 49 in Appendix C.[28]

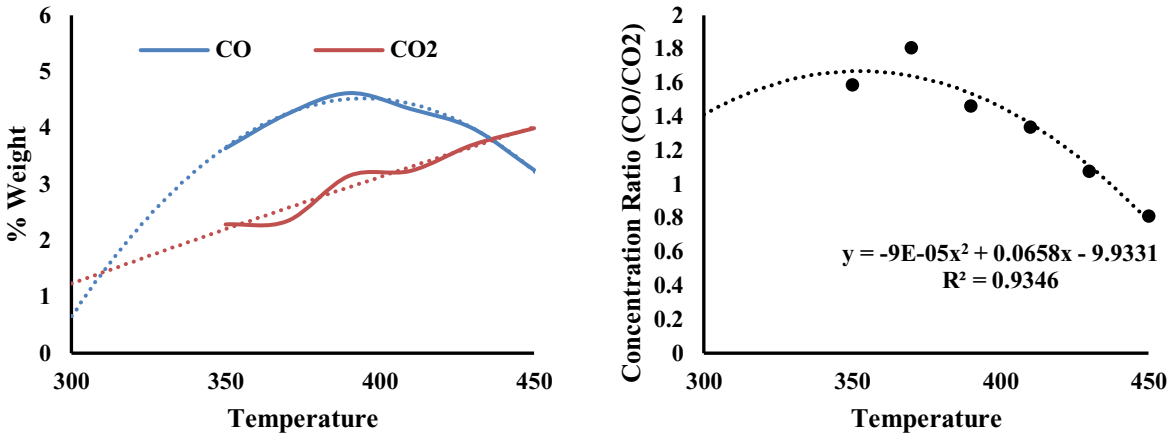

Figure 35. (a) Comparison of CO and CO_2 production from experimental data. As is represented in (b) there are specific temperatures in which both the ratio of the two and concentrations fit, at temperatures higher than the experimental results.[28]

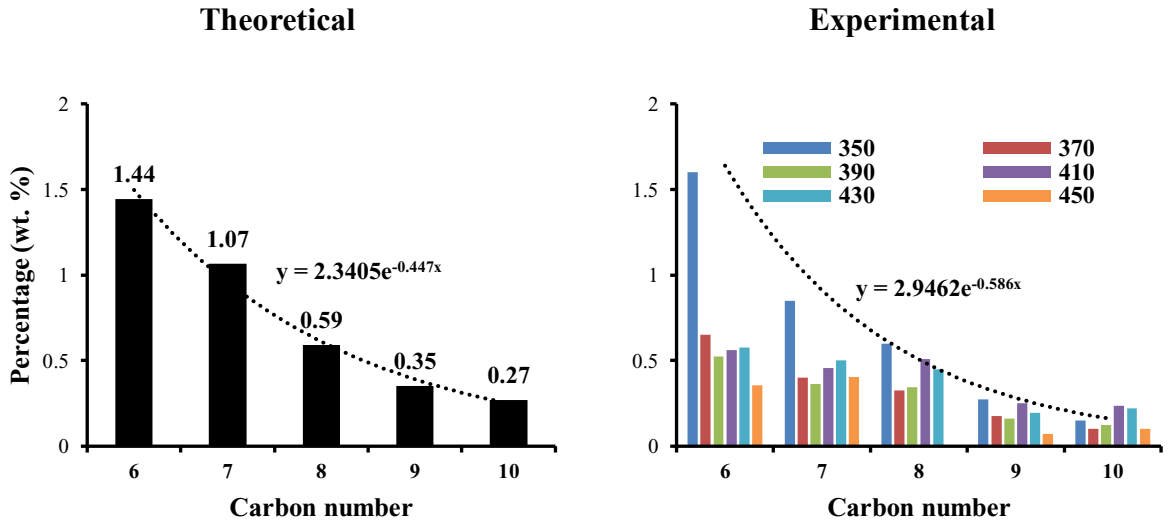

Figure 36. Comparison between experimental and theoretical results showing the correlation between pyrolysis reactions achieved at 350°C and those obtained using theoretical means.[28]

4.2 Individual Product Analysis

As discussed in the introduction, another focus for analyzing pyrolysis of biodiesel with theoretical methods is an additional focus on individual unique products obtained. Multiple experimental analyses of this process left individual products unidentified (Karne de Boer and Parisa A. Bahri, 2010) although others noted general trends emerging in the formation of cyclic

or aromatic hydrocarbons (Kubatov, 2011).[88, 95, 106, 173, 174] It has additionally been recognized that cyclic product formation in free-radical-based petrogenic processes have not been thoroughly investigated. The formation of cycloalkanes and aromatic precursor molecules, such as those observed in theoretical trajectories (Figure 37) were observed in the theoretical ensemble.

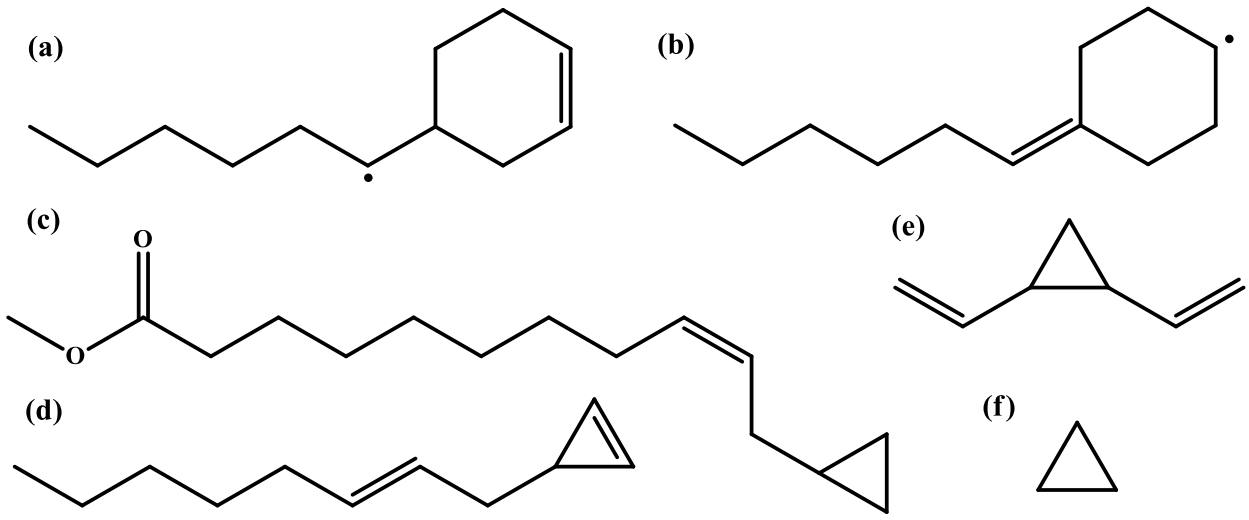

Figure 37. Collection of various hydrocarbons and esters with cycloalkane moieties, observed in both experimental and theoretically obtained results. Structures (a) and (b) corroborate with Kubatov's observance of cyclic hydrocarbons and products (c – f) agree with Ming's identification of cyclopropyl moieties. Structure (e) was found prominently in the ensemble, and its presence will be discussed further in atomic-level mechanism analysis.

4.3 Alignment of Ensemble Results and Bond-Dissociation Energy Analysis

An important aspect of this investigation is ascertaining if this method is better suited to simulate multi-step reaction mechanisms than other theoretical methods. Previous attempts at understanding the thermochemical properties of a system utilize bond-dissociation energy (BDE) analysis to understand individual energies contained in a system (Figure 38). One major caveat to this method is its inability to describe a systems progression over time from a singular starting

state (initial condition). Upon primary dissociation, to accurately assess the progression of the system, a new benchmark BDE analysis must be employed to determine the next likely dissociation. At its face value, BDE analysis is an excellent tool for determining relative strength of the bonds as they are distributed in molecular system, requiring only a frequency and optimization on 34 dissociations. Analysis of subsequent products of 34 bond cleavages would require recalculations of no less than 33 of the 34 primary dissociations. This continues for each subsequent dissociation thus an accurate assessment of the distribution of 5 bonds being cleaved would require about 66,781,440 (2x34x33x32x31x30) optimization frequency jobs at an already expensive model chemistry. This is significantly more expensive than running 2,000 optimization and frequency jobs 100 times (200,000) at approximately 300x less runs. In addition, performing multiple BDEs is incapable of describing an end point for decomposition once the trajectory achieves a stable state.

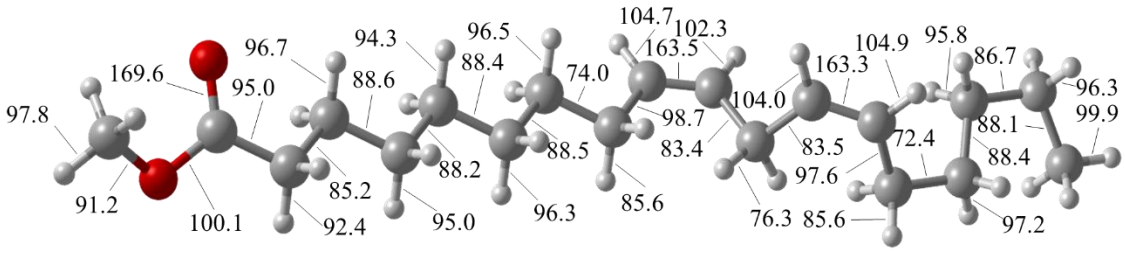

Figure 38. Bond dissociation energies for methyl linoleate (expressed as kcal mol^{-1}).[28]

A comparison of the two methods (Figure 39) show fantastic agreement between the dissociation predictions of a BDE and trajectory analysis. In instances of particularly high BDE ($C_9 - C_{10}$ and $C_{11} - C_{12}$) no trajectories observed dissociation and the inverse is true for bonds with particularly low BDEs ($C_7 - C_8$ and $C_{14} - C_{15}$). This relates to the specific nature of these bonds as π bonds have significantly higher energy and are harder to dissociate that σ bonds. Additionally, the lowest energy BDE and highest trajectory frequency are highly correlated to

the allylic bonds whose dissociation produces highly stable resonance. Homolysis of the $C_8 - C_9$, $C_{10} - C_{11}$, $C_{11} - C_{12}$, and $C_{13} - C_{14}$ are reasonably higher energy bonds (and correspondingly lower frequency of dissociation) due to the instability of the formed vinyl radical structure. The center bonds ($C_{10} - C_{11}$, $C_{11} - C_{12}$) are more likely to dissociate of the four, due to competing influences between the stability of allylic and instability of vinylic radical products.

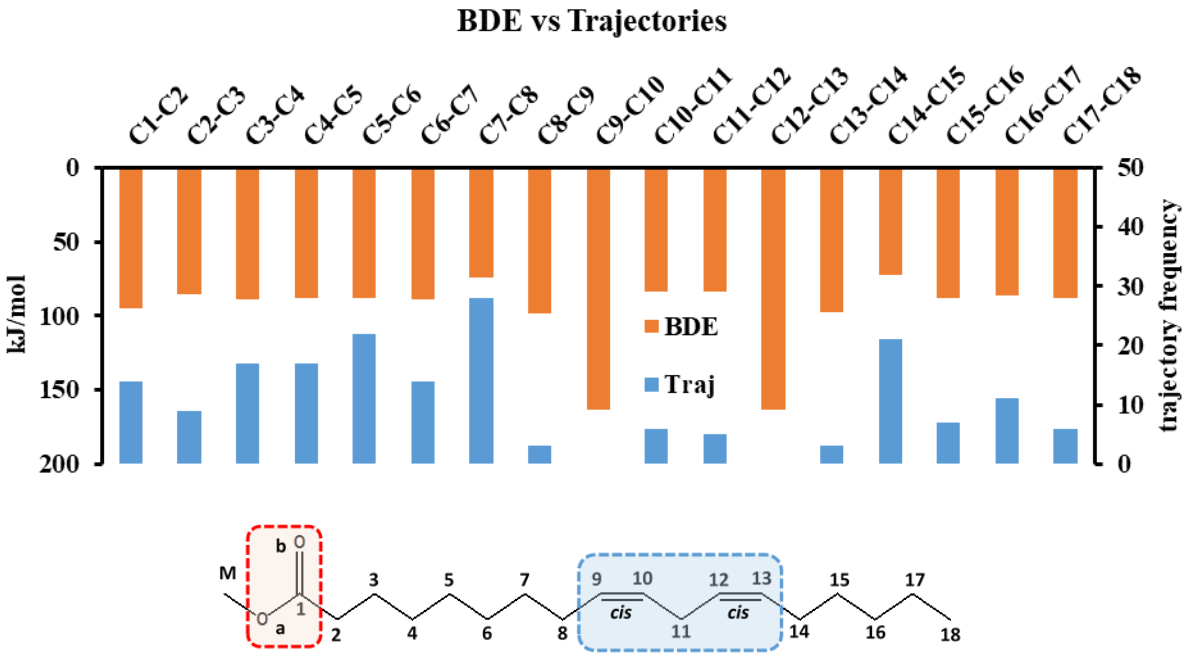

Figure 39. Comparison of 'direct' dynamics trajectories and benchmark BDE calculations for bond cleavage distribution within methyl linoleate.

While many instances of agreement were found for the two method, the BDE analysis is limited to a single dissociation analysis and neglect additional dissociations producing notable deviations between the methods. Bonds located in the $C_2 - C_7$ and $C_{15} - C_{18}$ region of the molecule have near identical computed BDEs but vary widely in frequency of dissociations. One prospective interpretation supported by the observation of trajectories' mechanisms is a chain-reaction ß-scission process that exhibits a 'zipper effect' along the chain. Similar to FA

formation *in vivo* by ß-oxidation metabolism, this process acts in reverse. Once the initial bond cleavage occurs, the bond ß now has a significantly higher chance of dissociating (lower BDE). This process propagated to produce large concentrations of ethene, CO_2, lengthier hydrocarbons and methyl radicals (Figure 40) supported by the ensemble distribution of products, experimental evidence (CO_2, ethene, and molecule f in Figure 37) and a reasonable interpretation of organic chemistry mechanisms.

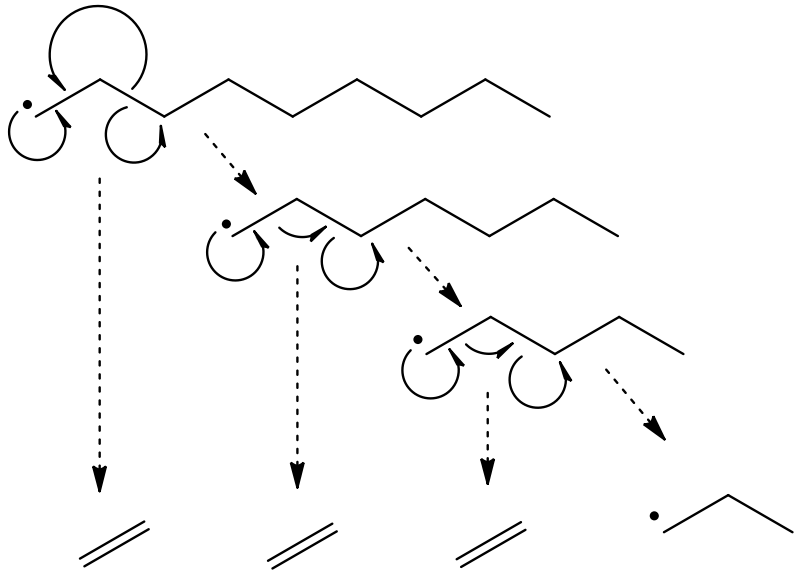

Figure 40. Description of the 'zipper' effect on hydrocarbons. Formation of a free-radical on the terminal carbon facilitates the dissociation of the ß C – C bond, presumably indefinitely producing numerous ethene molecules and smaller chain hydrocarbons.

Another deviation between the BDE and the trajectories observed both in experimental and theoretical results is the decarboxylation/deoxygenation reactions. Reaction schemes below show the original interpretation used to calculate the BDE of the $C_1 – C_2$ bond. The $C_2 – C_3$ bond was calculated more likely to cleave, however interpretation of the ensemble results shows a higher frequency of $C_1 – C_2$ cleavage. The explanation lies in latter bond cleavage, as seen in Figure 41. The energies were calculated for the products obtained for such a cleavage to reinforce the pertinence of this bond cleavage and was found to

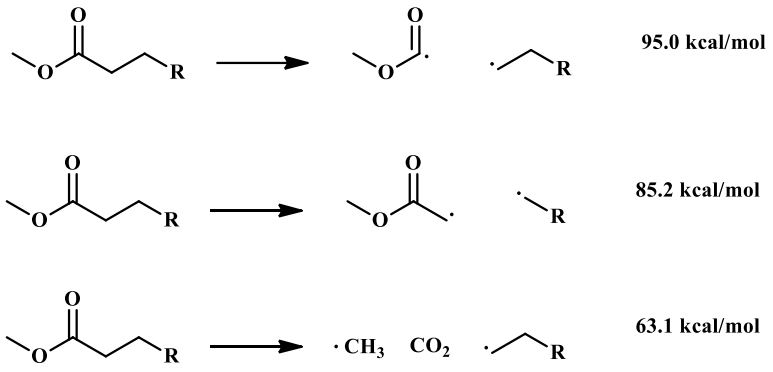

Figure 41. Description of the influence of secondary bond cleavage on proper calculation for BDE. Formation of stable CO_2 product reinforces the dissociation of the $C_1 - C_2$ bond.[15]

4.4 Atomic Level Analysis – Free Radical Mechanisms

The final interpretation of the trajectories was one that cannot be done directly through experimental means – atomic level analysis. The lifetime of a radical is short and turbulent and any attempts to derive pyrolysis mechanisms has been met with difficulty. Free-radical reactions can be described in 3 stages (Figure 42) initiated by homolytic cleavage usually through high energy (such as that in thermal decomposition). The radicals then propagate until they meet another free radical, when the process terminates.

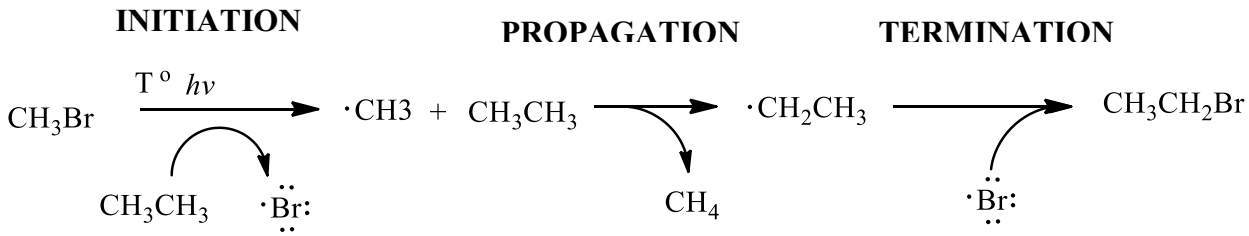

Figure 42. Example free-radical mechanisms similar to those expressed in thermal decomposition mechanisms.

The initiation and termination process' are extremely relevant to this research investigation as the chemistry of pyrolysis is heavily dominated by radical based reactions. One

of the interesting results of the investigation is that the products produced by the homolytic cleavages must terminate at some point during a cooling phase. This process is well documented and has been observed by several studies. The result of this is the elimination of the free radical products by forming longer chain hydrocarbons.

Since this investigation is a unimolecular analysis, the products of termination are not included in the trajectories produced. A statistical analysis of the result is then required to determine the most feasible stable products, since free radicals are commonly considered to be 'meta-stable'. One method of doing so is imaging a pool of products from the 100 trajectories simulated. In this solution, there is an equal chance that any of the free-radicals are incorporated in a termination step with another free-radical. Since the distribution of the radicals has already been determined, a cross-analysis of these results in a binomial expansion (since trimolecular reactions are exceedingly uncommon) would produce a viable statistical probability of forming longer-chain hydrocarbons (Figure 43) representative of the binomial distribution for a dissociation involving five radical products. 53 distinct radical products were determined by the data, with varying homology and radical placement. The homology of this analysis can be seen in the distribution below (Figure 44).

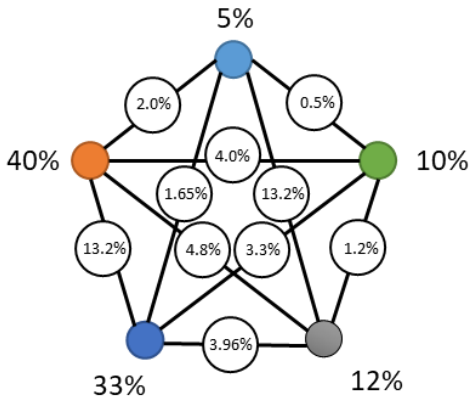

Figure 43. Example binomial recombination distribution of products assuming all possible share and equal probability for encountering each other and terminating.

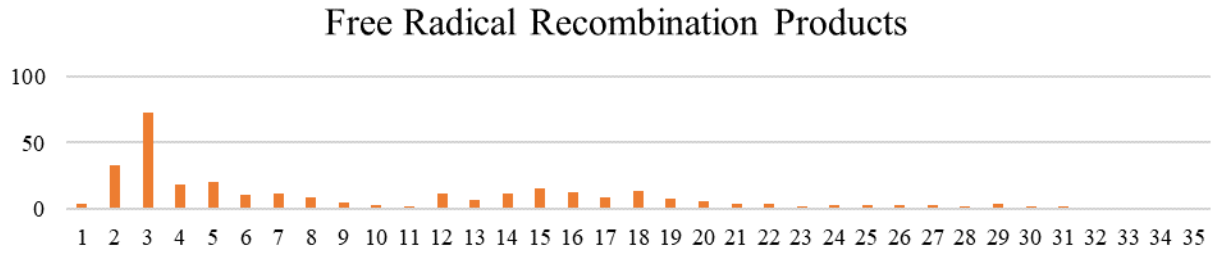

Figure 44. Homology distribution compilation of theoretically obtained free radicals combined with stable non-free-radical products.

4.5 Atomic Level Analysis – Deoxygenation Mechanisms

As described earlier in the experimental results, the presence of CO_2/CO products and deoxygenated hydrocarbons in indicative of deoxygenation/decarboxylation reactions. This has been proposed by experimental studies (Kubatov) though lacking an atomic-level interpretation no specific mechanisms were proposed.[13, 88, 95, 106] Through analysis of trajectory propagation, several theorized reaction schemes were elucidated associated with C – O bonds (Figure 45). These are the six primary pathways for dissociation: decarbonylation, decarboxylation, pericyclic deoxygenation, methyl free-radical deoxygenation, α free-radical deoxygenation and ß free-radical deoxygenation. All products of these pathways were observed in experimental analysis.[13, 88, 95, 106, 169] Formaldehyde (CH_2O) was formed through methyl free-radical deoxygenation, decarbonylation and ß free-radical deoxygenation. Carbon monoxide (CO) was formed through ß free-radical deoxygenation and decarbonylation. Carbon dioxide is formed through either decarboxylation, or through a water – gas shift with carbon monoxide (as discussed earlier). Methanol was produced either through a peri-cyclic deoxygenation pathway or a termination reaction between a hydrogen and methoxy radical.[169]

In addition to describing the formation of products obtained through analysis of the deoxygenation/decarboxylation/deoxygenation reactions, there is some discussion (specific to methyl linoleate) concerning the ß-chain scission pathways (Figure 46). In addition to the 'zipper' effect described previously, logically extending the pathway results in the formation of product (e) in Figure 37. The existence of this molecule is extremely relevant for the formation of cyclic hydrocarbons pronounceably found in experimental distributions. Ring expansion reactions such as vinylcyclopropane rearrangements (Equation 8a) and divinylcyclopropane-cycloheptadiene rearrangement (Equation 8b) show the mechanisms associated.

The relevance of these rearrangements lies in both their kinetic and thermodynamic properties associated. The actual mechanism that Equation 8 undergoes is disputed to be either a diradical-mediated two-step or a fully concerted orbital-symmetry-controlled mechanism. It has been established is that the energy released from the system is thermodynamically favored (driven by the ring strain associated with cyclopropane) suggesting the former. However, the kinetics seems to suggest the latter mechanism through stereospecific analysis, meaning that *both* rearrangements occur slow compared to pyrolysis dissociation processes.[175] This would explain a significant lack of cycloheptane and cyclopentane seen in distributions obtained experimentally, as the timestep allotted does not permit the observance of these rearrangements.

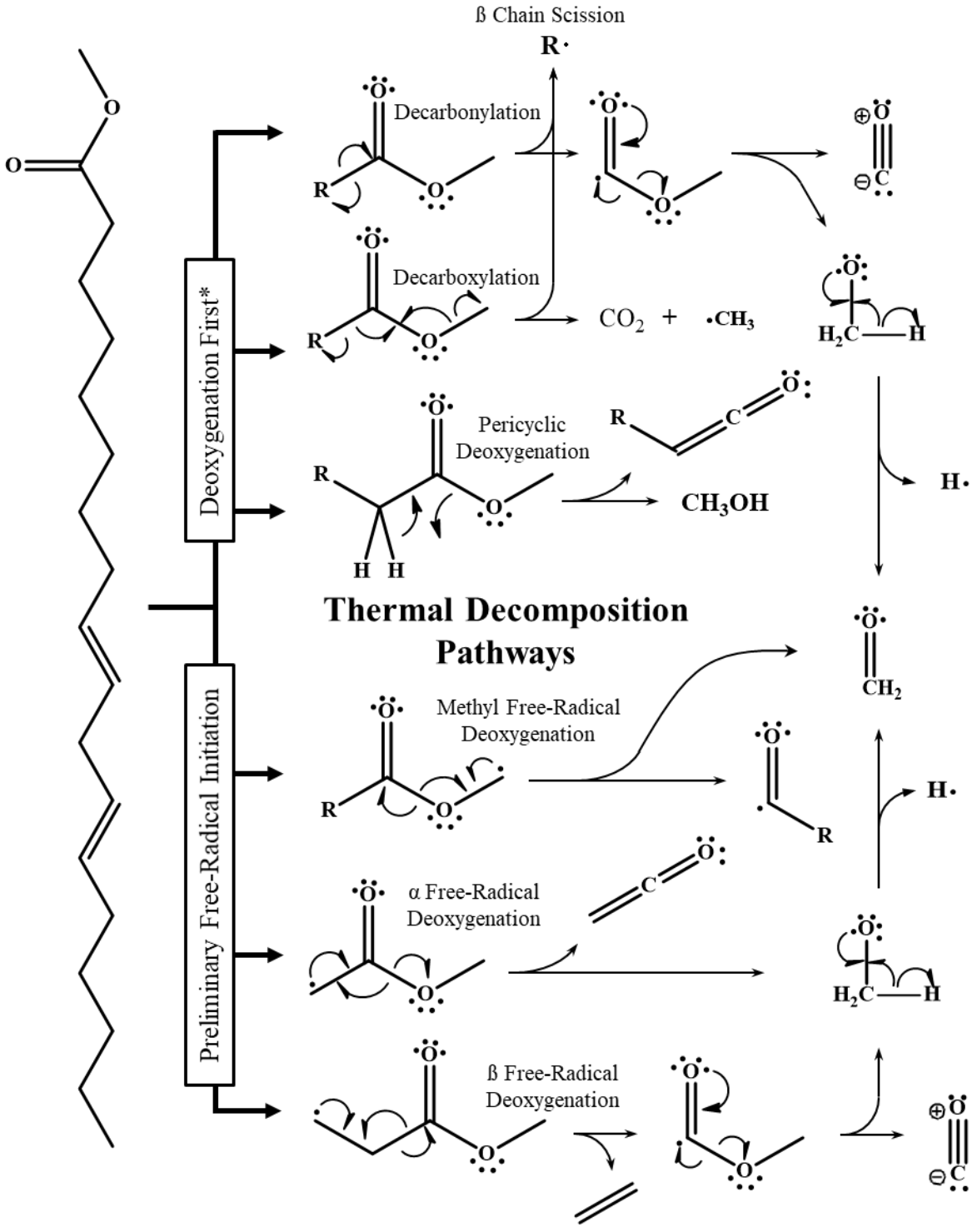

Figure 45. Thermal decomposition pathways observed for the deoxygenation/decarbonylation reactions. Remaining hydrocarbon allylic radicals are further decomposed through the ß – scission process described above (Figure 40).

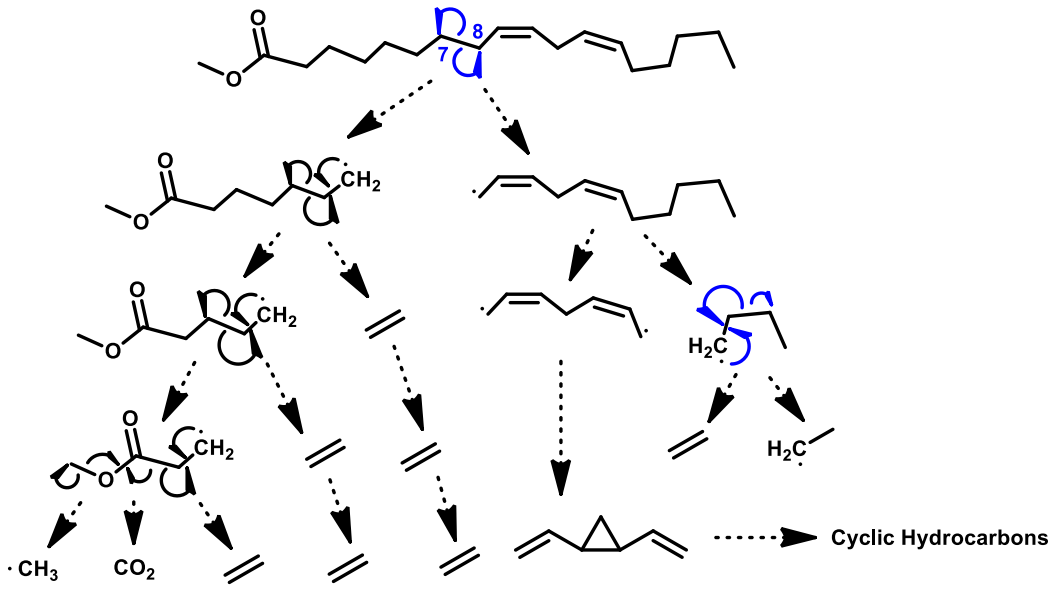

Figure 46. Reaction scheme describing a probable complete dissociation of hydrocarbons. While this is a theoretical dissociation, each step was observed in heightened frequency compared to abnormal dissociations.

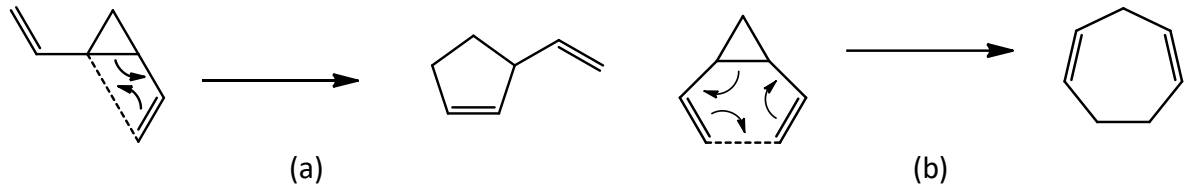

Equation 8. Pericyclic reactions pertinent to the divinylcyclopropane molecule observed heavily in the experimental distribution (Appendix A). (b) Vinylcyclopropane rearrangement is a more common ring expansion reaction relevant as a key reaction for complex natural product synthesis. (a) Divinylcyclopropane-cycloheptadiene rearrangement, related to the Cope rearrangement derives much of its thermodynamic drive by the release of ring strain.[175]

CHAPTER 5. CONCLUSION AND FUTURE WORK

M06-2X/6-31+G(d,p) was used to simulate thermal decomposition of methyl linoleate. TAMD was employed at 3500 K to simulate pyrolysis over an acceptable time period. Theoretical results were compared to experimental investigations showing agreement to lower temperature pyrolysis. Unusual and unique products identified in experimental results were observed in theoretical ensembles with the addition of atomic-level mechanistic interpretation for formation. Previous attempts at describing pyrolysis of such molecules computationally were deemed insufficient to direct dynamics due to the inability to describe multiple dissociations properly. Additionally, observations of unique products such as divinylcyclopropane found in scarce quantities in experimental distributions adds to our understanding of pyrolysis mechanism and could potentially supply and additional source of alternative energy chemically obtained.[175]

This investigation is an ongoing study interpreting the influence of energy on large organic systems. The method, while showing great promise has several points for prospective improvements. One such direction is increasing in alignment with the ergodic hypothesis. As discussed earlier, one essential facet to the establishment of valid results is in the significance of the ergodic nature of the simulation. While the propagation of the system is done through pseudo-random incorporation of ADMP, one constant component has been the initial condition the system seems to propagate from. One method to increase the stochastics involved is the incorporation of randomly selected initial condition sampling. The trajectories through inclusion of a simple macro can propose a randomized structure by altering the intrinsic reaction coordinates from a polar perspective. The resultant structure can then be optimized to obtain the energy of the system. This energy can be related to the Boltzmann Distribution to determine the

probability said molecule will be found in said state. The prospective advantage of this technique is the possibility of accessing states not forbidden but inaccessible from the starting geometry in the allotted time span. Figure 47 gives a good graphical representation of introducing this method.

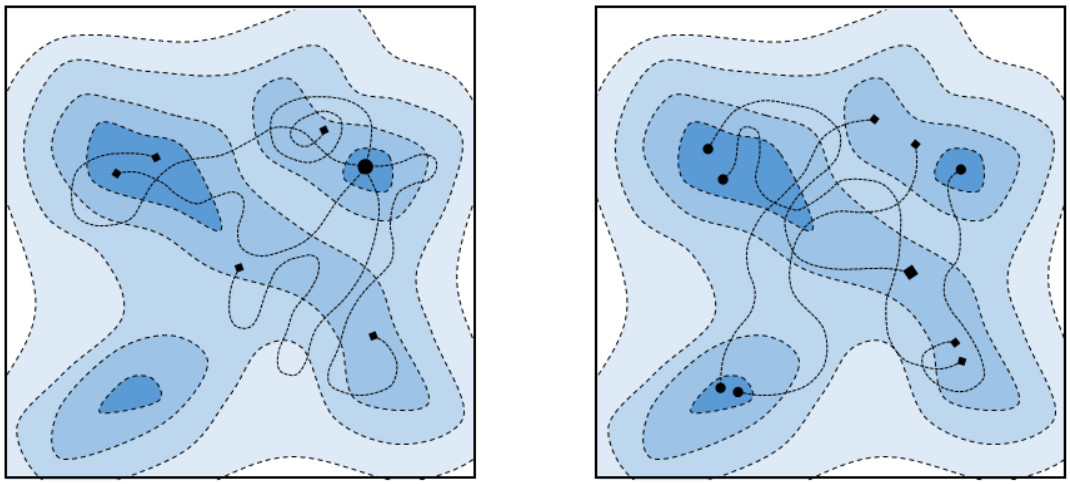

Figure 47. Graphical representation of trajectories over a PES. Starting from different initial states has a greater probability of achieving a sufficient level of ergodicity for valid molecular dynamics trajectory ensembles.

Another possibility for improving product distribution is in extending the timespan beyond 2,000 fs. One method to do so efficiently would be separating the individual products from dissociated trajectories and running them separately. Due to the way that DFT scales, in this case $O(n^3)$, running a job containing 10 atoms might take 1,000 seconds. Running two separate jobs of 5 atoms each would only take 250 seconds (2×5^3) making the calculation 4x more efficient by neglecting interatomic contributions between dissociated products. As the interatomic distance between pertinent atoms approach the Morse potential, their contributions become negligible. A python program was created and tested successfully for future investigations (Appendix D).

Since the method has shown validity for the methyl linoleate molecule investigating other similar FAMEs (methyl linolenate, methyl stearate, methyl oleate, etc.) would be fruitful in determining the influence of molecular structure on dissociation pathways. On this consideration, the investigation can be implemented for other molecules of its ilk. Following this pursuit can lead to the formulation of ideal FAMEs for dissociation into useful industrial components. This information can be insightful if applied in tandem with algae biofuel studies. Since algae has a relatively adaptable genome, deriving a cheap efficient source to create the ideal biofuel is more than a possibility.[33, 38, 67, 84, 106]

REFERENCES

(1) https://www.eia.gov/dnav/pet/hist/LeafHandler.ashx?n=PET&s=MDIUPUS2&f=A (accessed Oct 27, 2019).

(2) Hess, J.; Bednarz, D.; Bae, J.; Pierce, J. Petroleum and Health Care: Evaluating and Managing Health Cares Vulnerability to Petroleum Supply Shifts. *American Journal of Public Health* **2011**, *101* (9), 1568–1579.

(3) Al-Sharrah, G.; Elkamel, A.; Almanssoor, A. Sustainability Indicators for Decision-Making and Optimisation in the Process Industry: The Case of the Petrochemical Industry. *Chemical Engineering Science* **2010**, *65* (4), 1452–1461.

(4) Namazi, H. Polymers in Our Daily Life. *BioImpacts* **2017**, *7* (2), 73–74.

(5) Clark, J.; Farmer, T.; Hunt, A.; Sherwood, J. Opportunities for Bio-Based Solvents Created as Petrochemical and Fuel Products Transition towards Renewable Resources. *International Journal of Molecular Sciences* **2015**, *16* (8), 17101–17159.

(6) Huang, D.; Zhou, H.; Lin, L. Biodiesel: an Alternative to Conventional Fuel. *Energy Procedia* **2012**, *16*, 1874–1885.

(7) Graboski, M. S.; Mccormick, R. L. Combustion of Fat and Vegetable Oil Derived Fuels in Diesel Engines. *Progress in Energy and Combustion Science* **1998**, *24* (2), 125–164.

(8) Bouaid, A.; Boulifi, N. E.; Hahati, K.; Martinez, M.; Aracil, J. Biodiesel Production from Biobutanol. Improvement of Cold Flow Properties. *Chemical Engineering Journal* **2014**, *238*, 234–241.

(9) Aboim, J. B.; Oliveira, D.; Ferreira, J. E.; Siqueira, A. S.; Dallagnol, L. T.; Filho, G. N. R.; Gonçalves, E. C.; Nascimento, L. A. Determination of Biodiesel Properties Based on a Fatty Acid Profile of Eight Amazon Cyanobacterial Strains Grown in Two Different Culture Media. *RSC Advances* **2016**, *6* (111), 109751–109758.

(10) Owusu, P. A.; Asumadu-Sarkodie, S. A Review of Renewable Energy Sources, Sustainability Issues and Climate Change Mitigation. *Cogent Engineering* **2016**, *3* (1).

(11) Prado, C. M.; Filho, N. R. A. Production and Characterization of the Biofuels Obtained by Thermal Cracking and Thermal Catalytic Cracking of Vegetable Oils. *Journal of Analytical and Applied Pyrolysis* **2009**, *86* (2), 338–347.

(12) Candeia, R.; Silva, M.; Filho, J. C.; Brasilino, M.; Bicudo, T.; Santos, I.; Souza, A. Influence of Soybean Biodiesel Content on Basic Properties of Biodiesel–Diesel Blends. *Fuel* **2009**, *88* (4), 738–743.

(13) Zandonai, C.; Bravo, C. O.; Machado, N. F. Biofuel Production from Thermocatalytic Processing of Vegetable Oils: a Review. *Revista Fuentes el Reventón Energético* **2015**, *13* (2), 83–101.

(14) Frumkin, H.; Hess, J.; Vindigni, S. Peak Petroleum and Public Health. *Jama* **2007**, *298* (14), 1688.

(15) Wilson, Z. R.; Siebert, M. R. Methyl Linoleate and Methyl Oleate Bond Dissociation Energies: Electronic Structure Fishing for Wise Crack Products. *Energy & Fuels* **2018**, *32* (2), 1779–1787.

(16) Eneh, O. C. A Review on Petroleum: Source, Uses, Processing, Products and the Environment. *Journal of Applied Sciences* **2011**, *11* (12), 2084–2091.

(17) Hannon, M.; Gimpel, J.; Tran, M.; Rasala, B.; Mayfield, S. Biofuels from Algae: Challenges and Potential. *Biofuels* **2010**, *1* (5), 763–784.

(18) Microwave-Assisted Pyrolysis of Biomass for Liquid Biofuels Production. *Biofuels* **2016**, 163–182.

(19) Asomaning, J.; Mussone, P.; Bressler, D. C. Pyrolysis of Polyunsaturated Fatty Acids. *Fuel Processing Technology* **2014**, *120*, 89–95.

(20) Vasudevan, P. T.; Briggs, M. Biodiesel Production—Current State of the Art and Challenges. *Journal of Industrial Microbiology & Biotechnology* **2008**, *35* (5).

(21) Parvizsedghy, R.; Sadrameli, S. M.; Darian, J. T. Upgraded Biofuel Diesel Production by Thermal Cracking of Castor Biodiesel. *Energy & Fuels* **2015**, *30* (1), 326–333.

(22) Jahirul, M.; Rasul, M.; Chowdhury, A.; Ashwath, N. Biofuels Production through Biomass Pyrolysis —A Technological Review. *Energies* **2012**, *5* (12), 4952–5001.

(23) Vamvuka, D. Bio-Oil, Solid and Gaseous Biofuels from Biomass Pyrolysis Processes-An Overview. *International Journal of Energy Research* **2011**, *35* (10), 835–862.

(24) Boocock, D.; Konar, S.; Glaser, G. The Formation of Petrodiesel by the Pyrolysis of Fatty Acid Methyl Esters Over Activated Alumina. *Progress in Thermochemical Biomass Conversion* 1517–1524.

(25) Lin, L.; Cunshan, Z.; Vittayapadung, S.; Xiangqian, S.; Mingdong, D. Opportunities and Challenges for Biodiesel Fuel. *Applied Energy* **2011**, *88* (4), 1020–1031.

(26) Demirbas, A. Importance of Biodiesel as Transportation Fuel. *Energy Policy* **2007**, *35* (9), 4661–4670.

(27) Wilson, Z. R.; Siebert, M. R. Methyl Linoleate and Methyl Oleate Bond Dissociation Energies: Electronic Structure Fishing for Wise Crack Products. *Energy & Fuels* **2018**, *32* (2), 1779–1787.

(28) Amber, S.; Kamal, M. A. Production of Hydrocarbons by Catalytic Cracking of Stearic Acid under Atmospheric Pressure for Petrochemical Replacement. *Petroleum Science and Technology* **2018**, *37* (2), 146–154.

(29) Gallagher, B. J. The Economics of Producing Biodiesel from Algae. *Renewable Energy* **2011**, *36* (1), 158–162.

(30) Demiral, I.; Atilgan, N. G.; Şensöz, S. Production Of Biofuel From Soft Shell Of Pistachio (Pistacia Veral.). *Chemical Engineering Communications* **2008**, *196* (1-2), 104–115.

(31) Abdel-Rahman, M. A.; Al-Hashimi, N.; Shibl, M. F.; Yoshizawa, K.; El-Nahas, A. M. Thermochemistry and Kinetics of the Thermal Degradation of 2-Methoxyethanol as Possible Biofuel Additives. *Scientific Reports* **2019**, *9* (1).

(32) Oliveira, I. P. D.; Caires, A. R. L. Molecular Arrangement in Diesel/Biodiesel Blends: A Molecular Dynamics Simulation Analysis. *Renewable Energy* **2019**, *140*, 203–211.

(33) Biodiesel from Microalgae. *SpringerReference*.

(34) Owen, N. A.; Inderwildi, O. R.; King, D. A. The Status of Conventional World Oil Reserves—Hype or Cause for Concern? *Energy Policy* **2010**, *38* (8), 4743–4749.

(35) Wang, X.; Läu, J.-L.; Zhang, Y.-P. Pyrolysis Characteristics and Thermal Kinetics of Degradable Films. *Pedosphere* **2007**, *17* (5), 654–659.

(36) Difiglio, C. Oil, Economic Growth and Strategic Petroleum Stocks. *Energy Strategy Reviews* **2014**, *5*, 48–58.

(37) Hill, J.; Nelson, E.; Tilman, D.; Polasky, S.; Tiffany, D. Environmental, Economic, and Energetic Costs and Benefits of Biodiesel and Ethanol Biofuels. *Proceedings of the National Academy of Sciences* **2006**, *103* (30), 11206–11210.

(38) Du, Z.; Li, Y.; Wang, X.; Wan, Y.; Chen, Q.; Wang, C.; Lin, X.; Liu, Y.; Chen, P.; Ruan, R. Microwave-Assisted Pyrolysis of Microalgae for Biofuel Production. *Bioresource Technology* **2011**, *102* (7), 4890–4896.

(39) Ma, Y.; Liu, Y. Biodiesel Production: Status and Perspectives. *Biofuels: Alternative Feedstocks and Conversion Processes for the Production of Liquid and Gaseous Biofuels* **2019**, 503–522.

(40) Swenberg, J. A.; Moeller, B. C.; Lu, K.; Rager, J. E.; Fry, R. C.; Starr, T. B. Formaldehyde Carcinogenicity Research. *Toxicologic Pathology* **2012**, *41* (2), 181–189.

(41) Feely, R. A.; Orr, J.; Fabry, V. J.; Kleypas, J. A.; Sabine, C. L.; Langdon, C. Present and Future Changes in Seawater Chemistry Due to Ocean Acidification. *Carbon Sequestration and Its Role in the Global Carbon Cycle Geophysical Monograph Series* **2009**, 175–188.

(42) Solomon, S.; Plattner, G.-K.; Knutti, R.; Friedlingstein, P. Irreversible Climate Change Due to Carbon Dioxide Emissions. *Proceedings of the National Academy of Sciences* **2009**, *106* (6), 1704–1709.

(43) User, S. Historical CO2 Datasets. https://www.co2.earth/historical-co2-datasets (accessed Oct 27, 2019).

(44) Florides, G. A.; Christodoulides, P. Global Warming and Carbon Dioxide through Sciences. *Environment International* **2009**, *35* (2), 390–401.

(45) Global Surface Temperature | NASA Global Climate Change. https://climate.nasa.gov/vital-signs/global-temperature/ (accessed Oct 27, 2019).

(46) Mann, M. E.; Jones, P. D. Global Surface Temperatures over the Past Two Millennia. *Geophysical Research Letters* **2003**, *30* (15).

(47) The Effects of Climate Change. https://climate.nasa.gov/effects/ (accessed Oct 27, 2019).

(48) Trenberth, K. E.; Dai, A.; Schrier, G. V. D.; Jones, P. D.; Barichivich, J.; Briffa, K. R.; Sheffield, J. Global Warming and Changes in Drought. *Nature Climate Change* **2013**, *4* (1), 17–22.

(49) Emanuel, K. Global Warming Effects on U.S. Hurricane Damage. *Weather, Climate, and Society* **2011**, *3* (4), 261–268.

(50) Botkin, D. B.; Saxe, H.; Araújo, M. B.; Betts, R.; Bradshaw, R. H. W.; Cedhagen, T.; Chesson, P.; Dawson, T. P.; Etterson, J. R.; Faith, D. P.; Ferrier, S.; Guisan, A.; Hansen, A. S.; Hilbert, D. W.; Loehle, C.; Margules, C.; New, M.; Sobel, M. J.; Stockwell, D. R. B. Forecasting the Effects of Global Warming on Biodiversity. *BioScience* **2007**, *57* (3), 227–236.

(51) Elliott, M.; Hutzinger, O.; Hrubec, J.; Einax, J.; Kouimtzis, T.; Samara, C.; Kruk, I.; Boule, P.; Fabian, P.; Singh, O. N.; Wangersky, P. J.; Beck, B.; Paasivirta, J.; Beek, B.; Aboul-Kassim, T. A. T.; Simoneit, B. R. T.; Metzler, M.; Neilson, A. H.; Nikolaou, A.; Rimkus, G. G.; Pluschke, P.; Kassim, T. A.; Williamson, K. J.; Hargrave, B. T.; Saliot, A.; Hocking, M. B.; Kostianoy, A. G.; Kosarev, A. N.; Volkman, J. K.; Bilitewski, B.; Hites, R. A.; Konstantinou, I.; Knepper, T. P.; Barceló Damià; Petrovic, M.; Eyerer, P.; Weller, M.; Hübner Christof; Brack, W.; Eljarrat, E.; Darbra, R. M.; Guasch, H.; Ginebreda, A.; Geiszinger, A.; Barcelò Damià; Lange, F. T.; Yakushev, E. V.; Sabater, S.; Vicent, T.; Caminal Glòria; Younos, T.; Grady, C. A.; Viana, M. *The handbook of environmental chemistry. Environmental effects of marine finfish aquaculture*; Springer: Berlin, 1980.

(52) Harrison, R. M.; DeMora, S. J. *Introductory chemistry for the environmental sciences*; Cambridge Univ. Press: Cambridge, 2001.

(53) Kroeker, K. J.; Kordas, R. L.; Crim, R.; Hendriks, I. E.; Ramajo, L.; Singh, G. S.; Duarte, C. M.; Gattuso, J.-P. Impacts of Ocean Acidification on Marine Organisms: Quantifying Sensitivities and Interaction with Warming. *Global Change Biology* **2013**, *19* (6), 1884–1896.

(54) Pierce, B. A. The Effects of Acid Precipitation on Amphibians. *Ecotoxicology* **1993**, *2* (1), 65–77.

(55) Ocean Acidification. http://theenergygame.blogspot.com/2010/05/ocean-acidification.html (accessed Oct 27, 2019).

(56) Munawer, M. E. Human Health and Environmental Impacts of Coal Combustion and Post-Combustion Wastes. *Journal of Sustainable Mining* **2018**, *17* (2), 87–96.

(57) Wang, H.; Xu, J.; Zhao, W.; Zhang, J. Effects and Risk Evaluation of Oil Spillage in the Sea Areas of Changxing Island. *International Journal of Environmental Research and Public Health* **2014**, *11* (8), 8491–8507.

(58) U.S. Regulation of Oil and Gas Operations. https://www.americangeosciences.org/geoscience-currents/us-regulation-oil-and-gas-operations (accessed Oct 27, 2019).

(59) Bradshaw, M. J. The Geopolitics of Global Energy Security. *Geography Compass* **2009**, *3* (5), 1920–1937.

(60) Brundtland, G. H. *Report of the World Commission on environment and development: "our common future."*; United Nations: New York, 1987.

(61) Jacobson, M. Z.; Delucchi, M. A.; Cameron, M. A.; Frew, B. A. Low-Cost Solution to the Grid Reliability Problem with 100% Penetration of Intermittent Wind, Water, and Solar for All Purposes. *Proceedings of the National Academy of Sciences* **2015**, *112* (49), 15060–15065.

(62) Yilmaz, N. Comparative Analysis of Biodiesel–Ethanol–Diesel and Biodiesel–Methanol–Diesel Blends in a Diesel Engine. *Energy* **2012**, *40* (1), 210–213.

(63) Knothe, G.; Steidley, K. R. A Comparison of Used Cooking Oils: A Very Heterogeneous Feedstock for Biodiesel. *Bioresource Technology* **2009**, *100* (23), 5796–5801.

(64) Knothe, G. Improving Biodiesel Fuel Properties by Modifying Fatty Ester Composition. *Energy & Environmental Science* **2009**, *2* (7), 759.

(65) Mccormick, R. Effects of Biodiesel on NOx Emissions. **2005**.

(66) Kass, M. D.; Lewis, S. A.; Sr.; Swartz, M. M.; Huff, S. P.; Lee, D.-W.; Wagner, R. M.; Storey, J. M. E. Utilizing Water Emulsification to Reduce NOx and Particulate Emissions Associated with Biodiesel. *Transactions of the ASABE* **2009**, *52* (1), 5–13.

(67) Yen, H.-W.; Ho, S.-H.; Chen, C.-Y.; Chang, J.-S. CO2, NOxand SOxremoval from Flue Gas via Microalgae Cultivation: A Critical Review. *Biotechnology Journal* **2015**, *10* (6), 829–839.

(68) Haas, M. J.; Mcaloon, A. J.; Yee, W. C.; Foglia, T. A. A Process Model to Estimate Biodiesel Production Costs. *Bioresource Technology* **2006**, *97* (4), 671–678.

(69) Chiu, C.-W.; Schumacher, L. G.; Suppes, G. J. Impact of Cold Flow Improvers on Soybean Biodiesel Blend. *Biomass and Bioenergy* **2004**, *27* (5), 485–491.

(70) Moser, B. R. Biodiesel Production, Properties, and Feedstocks. *Biofuels* **2010**, 285–347.

(71) Körbitz, W. Biodiesel Production in Europe and North America, an Encouraging Prospect. *Renewable Energy* **1999**, *16* (1-4), 1078–1083.

(72) French, R.; Czernik, S. Catalytic Pyrolysis of Biomass for Biofuels Production. *Fuel Processing Technology* **2010**, *91* (1), 25–32.

(73) Mettler, M. S.; Vlachos, D. G.; Dauenhauer, P. J. Top Ten Fundamental Challenges of Biomass Pyrolysis for Biofuels. *Energy & Environmental Science* **2012**, *5* (7), 7797.

(74) Demirbas, M. F. Biorefineries for Biofuel Upgrading: A Critical Review. *Applied Energy* **2009**, *86*.

(75) Lin, R.; Zhu, Y.; Tavlarides, L. L. Mechanism and Kinetics of Thermal Decomposition of Biodiesel Fuel. *Fuel* **2013**, *106*, 593–604.

(76) Lin, R.; Zhu, Y.; Tavlarides, L. L. Effect of Thermal Decomposition on Biodiesel Viscosity and Cold Flow Property. *Fuel* **2014**, *117*, 981–988.

(77) Alhroub, I.; Shen, W.; Yan, J.; Sulkes, M. Thermal Cracking of Triacylglycerols: Molecular Beam Studies. *Journal of Analytical and Applied Pyrolysis* **2015**, *115*, 24–36.

(78) Omidghane, M.; Jenab, E.; Chae, M.; Bressler, D. C. Production of Renewable Hydrocarbons by Thermal Cracking of Oleic Acid in the Presence of Water. *Energy & Fuels* **2017**, *31* (9), 9446–9454.

(79) Stamenković, O. S.; Veličković, A. V.; Veljković, V. B. The Production of Biodiesel from Vegetable Oils by Ethanolysis: Current State and Perspectives. *Fuel* **2011**, *90* (11), 3141–3155.

(80) Huynh, L. K.; Violi, A. Thermal Decomposition of Methyl Butanoate: Ab Initio Study of a Biodiesel Fuel Surrogate. *The Journal of Organic Chemistry* **2008**, *73* (1), 94–101.

(81) Lu, M.; Chai, M. Experimental Investigation of the Oxidation of Methyl Oleate: One of the Major Biodiesel Fuel Components. *ACS Symposium Series Synthetic Liquids Production and Refining* **2011**, 289–312.

(82) Czajczyńska, D.; Nannou, T.; Anguilano, L.; Krzyżyńska, R.; Ghazal, H.; Spencer, N.; Jouhara, H. Potentials of Pyrolysis Processes in the Waste Management Sector. *Energy Procedia* **2017**, *123*, 387–394.

(83) Schwab, A. W.; Dykstra, G. J.; Selke, E.; Sorenson, S. C.; Pryde, E. H. Diesel Fuel from Thermal Decomposition of Soybean Oil. *Journal of the American Oil Chemists Society* **1988**, *65* (11), 1781–1786.

(84) Demirbas, A. Importance of Biodiesel as Transportation Fuel. *Energy Policy* **2007**, *35* (9), 4661–4670.

(85) Lappi, H.; Alén, R. Pyrolysis of Vegetable Oil Soaps—Palm, Olive, Rapeseed and Castor Oils. *Journal of Analytical and Applied Pyrolysis* **2011**, *91* (1), 154–158.

(86) Lappi, H.; Alén, R. Production of Vegetable Oil-Based Biofuels—Thermochemical Behavior of Fatty Acid Sodium Salts during Pyrolysis. *Journal of Analytical and Applied Pyrolysis* **2009**, *86* (2), 274–280.

(87) Asomaning, J.; Mussone, P.; Bressler, D. C. Thermal Deoxygenation and Pyrolysis of Oleic Acid. *Journal of Analytical and Applied Pyrolysis* **2014**, *105*, 1–7.

(88) Kubátová, A.; Šťávová, J.; Seames, W. S.; Luo, Y.; Sadrameli, S. M.; Linnen, M. J.; Baglayeva, G. V.; Smoliakova, I. P.; Kozliak, E. I. Triacylglyceride Thermal Cracking: Pathways to Cyclic Hydrocarbons. *Energy & Fuels* **2011**, *26* (1), 672–685.

(89) Li, X.; Xu, X.; You, X.; Truhlar, D. G. Benchmark Calculations for Bond Dissociation Enthalpies of Unsaturated Methyl Esters and the Bond Dissociation Enthalpies of Methyl Linolenate. *The Journal of Physical Chemistry A* **2016**, *120* (23), 4025–4036.

(90) Singer, S. D.; Weselake, R. J. Production of Biodiesel from Plant Oils. *Plant Bioproducts* **2018**, 41–58.

(91) Poutsma, M. L. Free-Radical Thermolysis and Hydrogenolysis of Model Hydrocarbons Relevant to Processing of Coal. *Energy & Fuels* **1990**, *4* (2), 113–131.

(92) Cosgrove, J. P.; Church, D. F.; Pryor, W. A. The Kinetics of the Autoxidation of Polyunsaturated Fatty Acids. *Lipids* **1987**, *22* (5), 299–304.

(93) Imahara, H.; Minami, E.; Hari, S.; Saka, S. Thermal Stability of Biodiesel in Supercritical Methanol. *Fuel* **2008**, *87* (1), 1–6.

(94) Niehaus, R. A.; Goering, C. E.; Savage, L. D.; Jr.; Sorenson, S. C. Cracked Soybean Oil as a Fuel for a Diesel Engine. *Transactions of the ASAE* **1986**, *29* (3), 0683–0689.

(95) Kubátová, A.; Šťávová, J.; Seames, W. S.; Luo, Y.; Sadrameli, S. M.; Linnen, M. J.; Baglayeva, G. V.; Smoliakova, I. P.; Kozliak, E. I. Triacylglyceride Thermal Cracking: Pathways to Cyclic Hydrocarbons. *Energy & Fuels* **2011**, *26* (1), 672–685.

(96) Savage, P. E. ChemInform Abstract: Mechanisms and Kinetics Models for Hydrocarbon Pyrolysis. *ChemInform* **2010**, *31* (25).

(97) 98/03880 Carbon Cycle for Rapeseed Oil Biodiesel Fuels. *Fuel and Energy Abstracts* **1998**, *39* (5), 363.

(98) Knothe, G. Dependence of Biodiesel Fuel Properties on the Structure of Fatty Acid Alkyl Esters. *Fuel Processing Technology* **2005**, *86* (10), 1059–1070.

(99) Malpathak, S.; Ma, X.; Hase, W. L. Addressing an Instability in Unrestricted Density Functional Theory Direct Dynamics Simulations. *Journal of Computational Chemistry* **2018**, *40* (8), 933–936.

(100) Lakshmanan, S.; Pratihar, S.; Hase, W. L. Direct Dynamics Simulations of the CH2 O2 Reaction on the Ground- and Excited-State Singlet Surfaces. *The Journal of Physical Chemistry A* **2019**, *123* (20), 4360–4369.

(101) Ventura, O. N.; Kieninger, M.; Irving, K. Density Functional Theory: A Useful Tool for the Study of Free Radicals. *Advances in Quantum Chemistry* **1997**, 293–309.

(102) Zhao, Y.; Truhlar, D. G. The M06 Suite of Density Functionals for Main Group Thermochemistry, Thermochemical Kinetics, Noncovalent Interactions, Excited States, and Transition Elements: Two New Functionals and Systematic Testing of Four M06-Class Functionals and 12 Other Functionals. *Theoretical Chemistry Accounts* **2007**, *120* (1-3), 215–241.

(103) Cohen, A. J.; Mori-Sánchez, P.; Yang, W. Challenges for Density Functional Theory. *Chemical Reviews* **2011**, *112* (1), 289–320.

(104) Wang, Y.; Ma, S.; Zhao, M.; Kuang, L.; Nie, J.; Riley, W. W. Improving the Cold Flow Properties of Biodiesel from Waste Cooking Oil by Surfactants and Detergent Fractionation. *Fuel* **2011**, *90* (3), 1036–1040.

(105) Knothe, G. Dependence of Biodiesel Fuel Properties on the Structure of Fatty Acid Alkyl Esters. *Fuel Processing Technology* **2005**, *86* (10), 1059–1070.

(106) Kubátová, A.; Luo, Y.; Šťávová, J.; Sadrameli, S.; Aulich, T.; Kozliak, E.; Seames, W. New Path in the Thermal Cracking of Triacylglycerols (Canola and Soybean Oil). *Fuel* **2011**, *90* (8), 2598–2608.

(107) Abdel-Shafy, H. I.; Mansour, M. S. A Review on Polycyclic Aromatic Hydrocarbons: Source, Environmental Impact, Effect on Human Health and Remediation. *Egyptian Journal of Petroleum* **2016**, *25* (1), 107–123.

(108) Billaud, F.; Dominguez, V.; Broutin, P.; Busson, C. Production of Hydrocarbons by Pyrolysis of Methyl Esters from Rapeseed Oil. *Journal of the American Oil Chemists Society* **1995**, *72* (10), 1149–1154.

(109) Cramer, C. J. *Essentials of computational chemistry*; Wiley: Chichester, 2004.

(110) Young, D. C. *Computational chemistry: a practical guide for applying techniques to real world problems*; Wiley-Blackwell: Oxford, 2011.

(111) Uzer, T.; Miller, W. Theories of Intramolecular Vibrational Energy Transfer. *Physics Reports* **1991**, *199* (2), 73–146.

(112) Nesbitt, D. J.; Field, R. W. Vibrational Energy Flow in Highly Excited Molecules: Role of Intramolecular Vibrational Redistribution. *The Journal of Physical Chemistry* **1996**, *100* (31), 12735–12756.

(113) Intramolecular Vibrational Redistribution. *Energy Dissipation in Molecular Systems* 43–72.

(114) Felker, P. M.; Zewail, A. H. Dynamics of Intramolecular Vibrational-Energy Redistribution (IVR). II. Excess Energy Dependence. *The Journal of Chemical Physics* **1985**, *82* (7), 2975–2993.

(115) Smith, S. Unimolecular Reaction Dynamics: Theory and Experiments (Baer, Tomas; Hase, William L.). *Journal of Chemical Education* **1998**, *75* (9), 1098.

(116) Zhao, Y.; Schultz, N. E.; Truhlar, D. G. Exchange-Correlation Functional with Broad Accuracy for Metallic and Nonmetallic Compounds, Kinetics, and Noncovalent Interactions. *The Journal of Chemical Physics* **2005**, *123* (16), 161103.

(117) Zhao, Y.; Truhlar, D. G. A New Local Density Functional for Main-Group Thermochemistry, Transition Metal Bonding, Thermochemical Kinetics, and Noncovalent Interactions. *The Journal of Chemical Physics* **2006**, *125* (19), 194101.

(118) Hohenstein, E. G.; Chill, S. T.; Sherrill, C. D. Assessment of the Performance of the M05−2X and M06−2X Exchange-Correlation Functionals for Noncovalent Interactions in Biomolecules. *Journal of Chemical Theory and Computation* **2008**, *4* (12), 1996–2000.

(119) Gunsteren, W. F. V.; Berendsen, H. J. C. Computer Simulation of Molecular Dynamics: Methodology, Applications, and Perspectives in Chemistry. *Angewandte Chemie International Edition in English* **1990**, *29* (9), 992–1023.

(120) Almas, Q. L.; Keefe, B. L.; Profitt, T.; Pearson, J. K. Choosing an Appropriate Model Chemistry in a Big Data Context: Application to Dative Bonding. *Computational and Theoretical Chemistry* **2016**, *1085*, 46–55.

(121) Kruse, H.; Goerigk, L.; Grimme, S. Why the Standard B3LYP/6-31G* Model Chemistry Should Not Be Used in DFT Calculations of Molecular Thermochemistry: Understanding and Correcting the Problem. *The Journal of Organic Chemistry* **2012**, *77* (23), 10824–10834.

(122) VI. Scientific Methods. *Hippocratic Medicine* **1941**, 57–116.

(123) Becke, A. D. Perspective: Fifty Years of Density-Functional Theory in Chemical Physics. *The Journal of Chemical Physics* **2014**, *140* (18).

(124) Moreira, I. D. P. R. Performance of Simplified G2 Model Chemistry Approaches in the Study of Unimolecular Mechanisms: Thermal Decomposition of Acetic Acid in Gas Phase. *Journal of Molecular Structure: THEOCHEM* **1999**, *466* (1-3), 119–126.

(125) Ochterski, J. W.; Petersson, G. A.; Montgomery, J. A. A Complete Basis Set Model Chemistry. V. Extensions to Six or More Heavy Atoms. *The Journal of Chemical Physics* **1996**, *104* (7), 2598–2619.

(126) Bircher, M. P.; López-Tarifa, P.; Rothlisberger, U. Shedding Light on the Basis Set Dependence of the Minnesota Functionals: Differences Between Plane Waves, Slater Functions, and Gaussians. *Journal of Chemical Theory and Computation* **2018**, *15* (1), 557–571.

(127) Bogojeski, M.; Vogt-Maranto, L.; Tuckerman, M. E.; Mueller, K.-R.; Burke, K. Density Functionals with Quantum Chemical Accuracy: From Machine Learning to Molecular Dynamics. **2019**.

(128) Fujisaki, H.; Moritsugu, K.; Matsunaga, Y.; Morishita, T.; Maragliano, L. Extended Phase-Space Methods for Enhanced Sampling in Molecular Simulations: A Review. *Frontiers in Bioengineering and Biotechnology* **2015**, *3*.

(129) Hu, Y.; Hong, W.; Shi, Y.; Liu, H. Temperature-Accelerated Sampling and Amplified Collective Motion with Adiabatic Reweighting to Obtain Canonical Distributions and Ensemble Averages. *Journal of Chemical Theory and Computation* **2012**, *8* (10), 3777–3792.

(130) Abrams, C. F.; Vanden-Eijnden, E. On-the-Fly Free Energy Parameterization via Temperature Accelerated Molecular Dynamics. *Chemical Physics Letters* **2012**, *547*, 114–119.

(131) Miron, R. A.; Fichthorn, K. A. Accelerated Molecular Dynamics with the Bond-Boost Method. *The Journal of Chemical Physics* **2003**, *119* (12), 6210–6216.

(132) Abrams, C.; Bussi, G. Enhanced Sampling in Molecular Dynamics Using Metadynamics, Replica-Exchange, and Temperature-Acceleration. *Entropy* **2013**, *16* (1), 163–199.

(133) Sorensen, M. R.; Voter, A. F. Temperature-Accelerated Dynamics for Simulation of Infrequent Events. *The Journal of Chemical Physics* **2000**, *112* (21), 9599–9606.

(134) Agrawal, P. M.; Malshe, M.; Narulkar, R.; Raff, L. M.; Hagan, M.; Bukkapatnum, S.; Komanduri, R. A Self-Starting Method for Obtaining Analytic Potential-Energy Surfaces from Ab Initio Electronic Structure Calculations. *The Journal of Physical Chemistry A* **2009**, *113* (5), 869–877.

(135) Maher, K. D.; Kirkwood, K. M.; Gray, M. R.; Bressler, D. C. Pyrolytic Decarboxylation and Cracking of Stearic Acid. *Industrial & Engineering Chemistry Research* **2008**, *47* (15), 5328–5336.

(136) Hermida, L.; Abdullah, A. Z.; Mohamed, A. R. Deoxygenation of Fatty Acid to Produce Diesel-like Hydrocarbons: A Review of Process Conditions, Reaction Kinetics and Mechanism. *Renewable and Sustainable Energy Reviews* **2015**, *42*, 1223–1233.

(137) Corminboeuf, C.; Tran, F.; Weber, J. The Role of Density Functional Theory in Chemistry: Some Historical Landmarks and Applications to Zeolites. *Journal of Molecular Structure: THEOCHEM* **2006**, *762* (1-3), 1–7.

(138) Zangwill, A. A Half Century of Density Functional Theory. *Physics Today* **2015**, *68* (7), 34–39.

(139) Almas, Q. L.; Keefe, B. L.; Profitt, T.; Pearson, J. K. Choosing an Appropriate Model Chemistry in a Big Data Context: Application to Dative Bonding. *Computational and Theoretical Chemistry* **2016**, *1085*, 46–55.

(140) Young, D. C. *Computational chemistry: a practical guide for applying techniques to real world problems*; Wiley-Blackwell: Oxford, 2011.

(141) Brenner, A. E. More on Moore's Law. *Physics Today* **2001**, *54* (7), 84–84.

(142) Schaller, R. Moores Law: Past, Present and Future. *IEEE Spectrum* **1997**, *34* (6), 52–59.

(143) Xu, R.; Ferrante, L.; Briens, C.; Berruti, F. Flash Pyrolysis of Grape Residues into Biofuel in a Bubbling Fluid Bed. *Journal of Analytical and Applied Pyrolysis* **2009**, *86* (1), 58–65.

(144) Hinchliffe, A. *Molecular modelling for beginners*; Wiley-Blackwell: Oxford, 2008.

(145) Honeycutt, J. D.; Thirumalai, D. Proceedings of the National Academy of Sciences 1990, 87 (9), 3526–3529.

(146) Lewars, E. G. Computational Chemistry Introduction to the Theory and Applications of Molecular and Quantum Mechanics; Springer International Publishing: Cham, 2018.

(147) Ramachandran, K. I.; Deepa, G.; Namboori, K. Computational chemistry and molecular modeling: principles and applications; Springer: Berlin, 2010.

(148) Schlegel, H. B. Journal of Computational Chemistry 2003, 24 (12), 1514–1527.

(149) Cook, D. B. Handbook of computational quantum chemistry; Dover Publications: Mineola, NY, 2005.

(150) Cranford, S. W. Thermal Stability of Idealized Folded Carbyne Loops. *Nanoscale Research Letters* **2013**, *8* (1).

(151) Liu, L.; Liu, Y.; Zybin, S. V.; Sun, H.; Goddard, W. A. ReaxFF-Lg: Correction of the ReaxFF Reactive Force Field for London Dispersion, with Applications to the Equations of State for Energetic Materials. *The Journal of Physical Chemistry A* **2011**, *115* (40), 11016–11022.

(152) Zheng, M.; Li, X.; Liu, J.; Guo, L. Initial Chemical Reaction Simulation of Coal Pyrolysis via ReaxFF Molecular Dynamics. *Energy & Fuels* **2013**, *27* (6), 2942–2951.

(153) Senn, H. M.; Thiel, W. QM/MM Studies of Enzymes. *Current Opinion in Chemical Biology* **2007**, *11* (2), 182–187.

(154) Senn, H. M.; Thiel, W. QM/MM Methods for Biological Systems. *Atomistic Approaches in Modern Biology Topics in Current Chemistry* 173–290.

(155) Müller-Kirsten, H. J. W. Introduction to Quantum Mechanics. **2012**.

(156) The Quantum Mechanical Three-Body Problem. **1974**.

(157) Fischer, C. F. General Hartree-Fock Program. *Computer Physics Communications* **1987**, *43* (3), 355–365.

(158) Jones, H. W.; Etemadi, B. Accurate Ground-State Calculations ofH2 Using Basis Sets of Atom-Centered Slater-Type Orbitals. *Physical Review A* **1993**, *47* (4), 3430–3432.

(159) Approximation Methods for Many-Body Systems. *Physics Subject Headings (PhySH)*.

(160) Ayala, P. Y.; Scuseria, G. E. Linear Scaling Second-Order Moller–Plesset Theory in the Atomic Orbital Basis for Large Molecular Systems. *The Journal of Chemical Physics* **1999**, *110* (8), 3660–3671.

(161) Banks, S.; Bridgwater, A. Catalytic Fast Pyrolysis for Improved Liquid Quality. *Handbook of Biofuels Production* **2016**, 391–429.

(162) Jones, R. O. Density Functional Theory: Its Origins, Rise to Prominence, and Future. *Reviews of Modern Physics* **2015**, *87* (3), 897–923.

(163) Wood, W. W.; Erpenbeck, J. J.; Baker, G. A.; Johnson, J. D. Molecular Dynamics Ensemble, Equation of State, and Ergodicity. *Physical Review E* **2000**, *63* (1).

(164) Mountain, R. D.; Thirumalai, D. Measures of Effective Ergodic Convergence in Liquids. *The Journal of Physical Chemistry* **1989**, *93* (19), 6975–6979.

(165) Frisch, M. J.; Trucks, G. W.; Schlegel, H. B.; Scuseria, G. E.; Robb, M. A.; Cheeseman, J. R.; Scalmani, G.; Barone, V.; Mennucci, B.; Petersson, G. A.; Nakatsuji, H.; Caricato, M.; Li, X.; Hratchian, H. P.; Izmaylov, A. F.; Bloino, J.; Zheng, G.; Sonnenberg, J. L.; Hada, M.; Ehara, M.; Toyota, K.; Fukuda, R.; Hasegawa, J.; Ishida, M.; Nakajima, T.; Honda, Y.; Kitao, O.; Nakai, H.; Vreven, T.; Montgomery Jr., J. A.; Peralta, J. E.; Ogliaro, F. o.; Bearpark, M. J.; Heyd, J.; Brothers, E. N.; Kudin, K. N.; Staroverov, V. N.; Kobayashi, R.; Normand, J.; Raghavachari, K.; Rendell, A. P.; Burant, J. C.; Iyengar, S. S.; Tomasi, J.; Cossi, M.; Rega, N.; Millam, N. J.; Klene, M.; Knox, J. E.; Cross, J. B.; Bakken, V.; Adamo, C.; Jaramillo, J.; Gomperts, R.; Stratmann, R. E.; Yazyev, O.; Austin, A. J.; Cammi, R.; Pomelli, C.; Ochterski, J. W.; Martin, R. L.; Morokuma, K.; Zakrzewski, V. G.; Voth, G. A.; Salvador, P.; Dannenberg, J. J.; Dapprich, S.; Daniels, A. D.; Farkas, Ã. d. n.; Foresman, J. B.; Ortiz, J. V.; Cioslowski, J.; Fox, D. J. In *Gaussian 09*; Gaussian, Inc., Wallingford, CT, USA, 2009.

(166) Monk, P. M. S. *Physical chemistry: understanding our chemical world*; Wiley: Chichester, 2007.

(167) Myers, R. T. *Holt chemistry*; Holt, Rinehart and Winston: Orlando, FL, 2007.

(168) Bondi, A. Van Der Waals Volumes and Radii. *The Journal of Physical Chemistry* **1964**, *68* (3), 441–451.

(169) Chai, M.; Tu, Q.; Lu, M.; Yang, Y. J. Esterification Pretreatment of Free Fatty Acid in Biodiesel Production, from Laboratory to Industry. *Fuel Processing Technology* **2014**, *125*, 106–113.

(170) Karplus, M. Three-Dimensional "Pople Diagram". *The Journal of Physical Chemistry* **1990**, *94* (14), 5435–5436.

(171) Ganazzoli. Conformations And Dynamics Of Stars And Dendrimers: The Gaussian Self-Consistent Approach. *Condensed Matter Physics* **2002**, *5* (1), 37.

(172) Schlegel, H. B. In Modern Electronic Structure Theory; Yarkony, D. R., Ed.; World Scientific Publishing: Singapore, 1995, p. 459.

(173) Boer, K. D.; Bahri, P. A. Supercritical Methanol for Fatty Acid Methyl Ester Production: A Review. *Biomass and Bioenergy* **2011**, *35* (3), 983–991.

(174) Boer, K. D.; Bahri, P. A. Supercritical Methanol for Fatty Acid Methyl Ester Production: A Review. *Biomass and Bioenergy* **2011**, *35* (3), 983–991.

(175) Krueger, S.; Gaich, T. ChemInform Abstract: Recent Applications of the Divinylcyclopropane-Cycloheptadiene Rearrangement in Organic Synthesis. *ChemInform* **2014**, *45* (30).

APPENDICES

Appendix A. Complete Ensemble

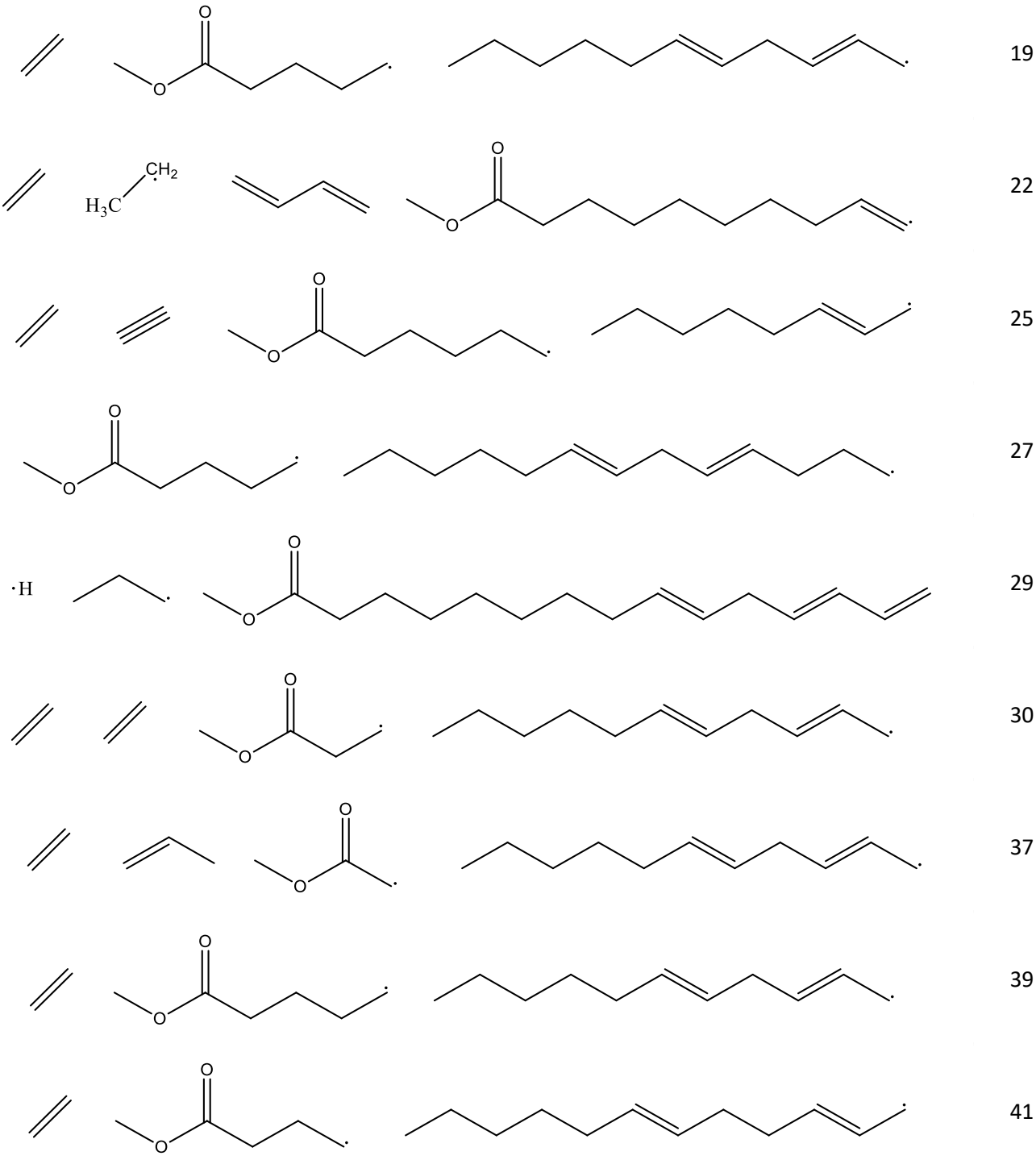

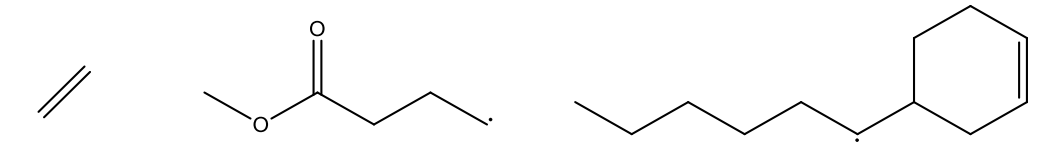

42

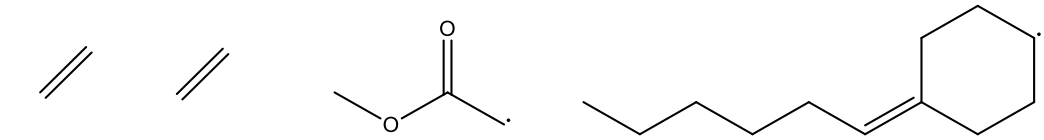

43

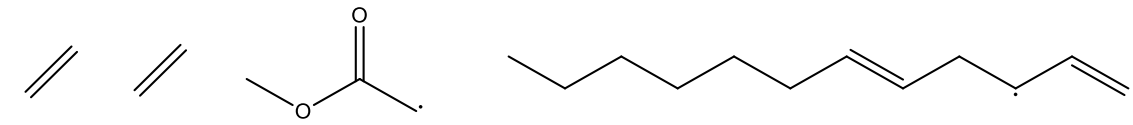

44

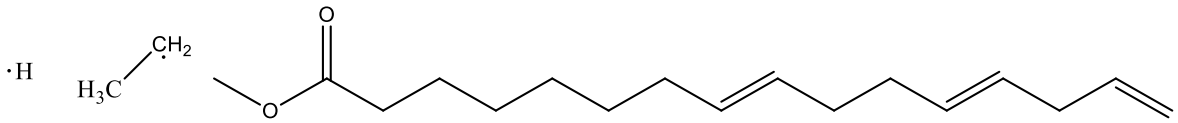

45

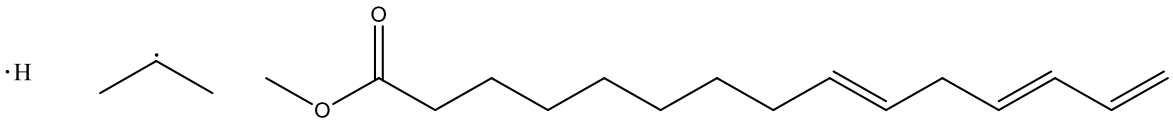

48

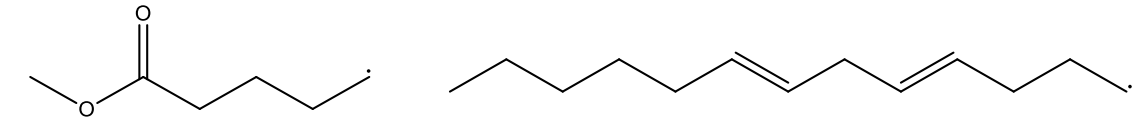

51

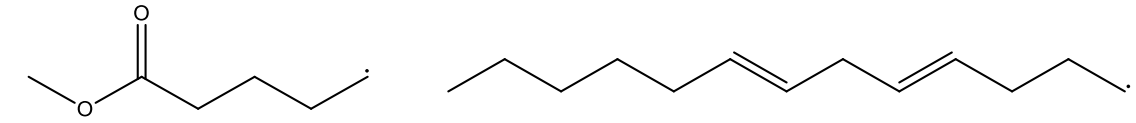

55

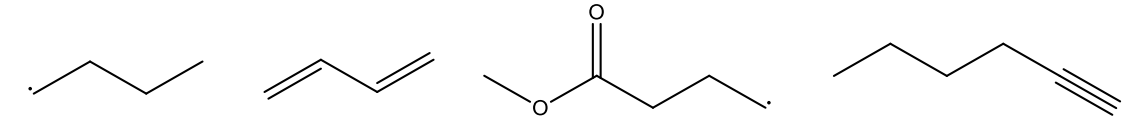

62

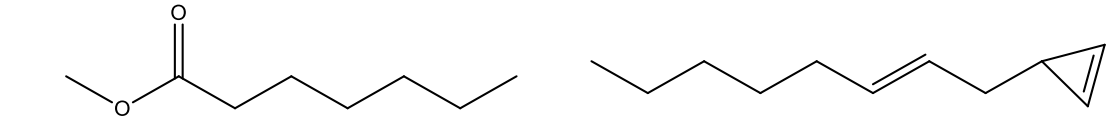

75

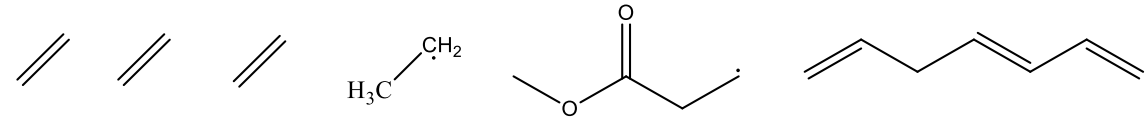

76

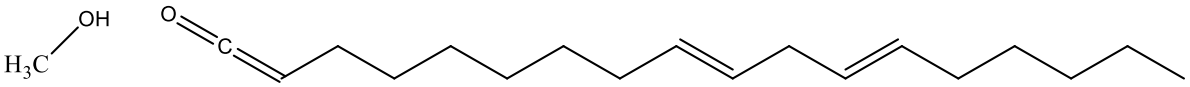

78

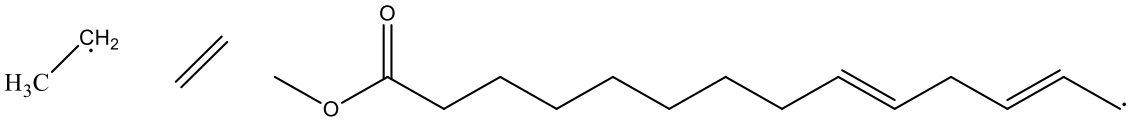

80

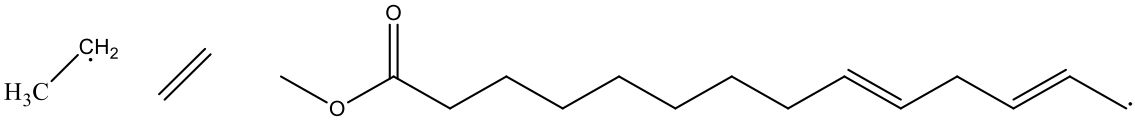

88

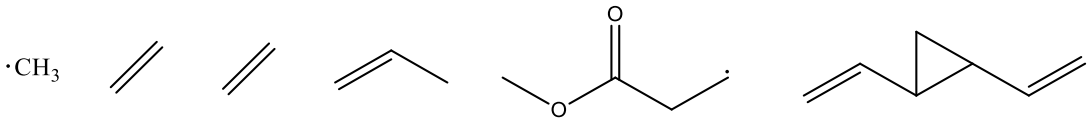

93

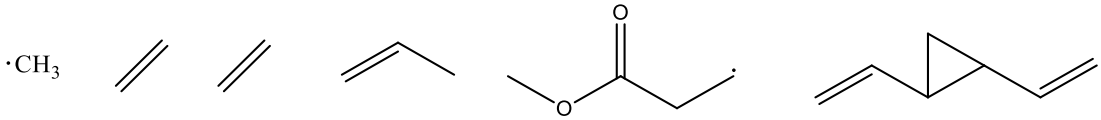

94

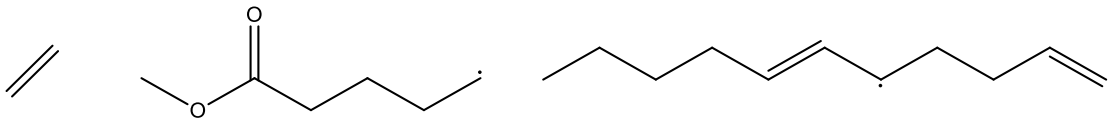

98

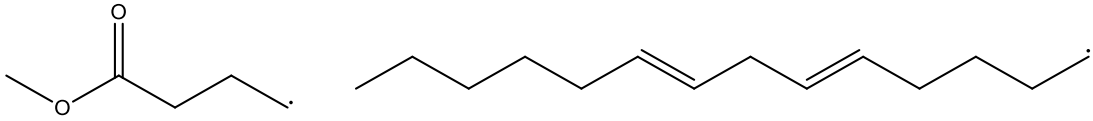

100

112

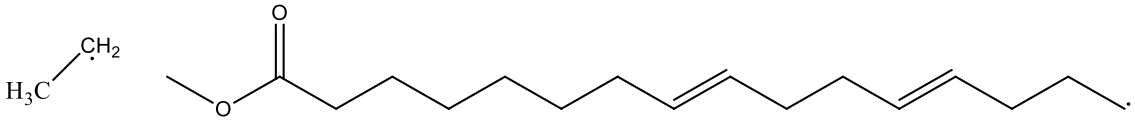

114

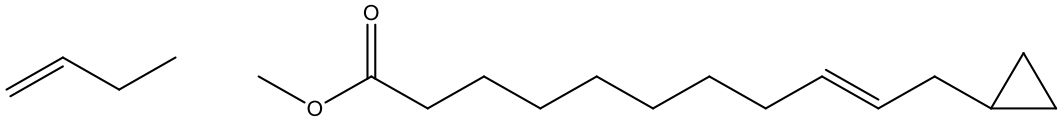

120

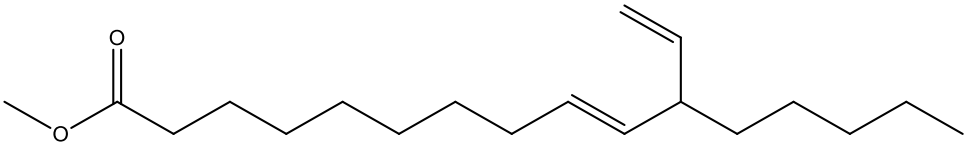

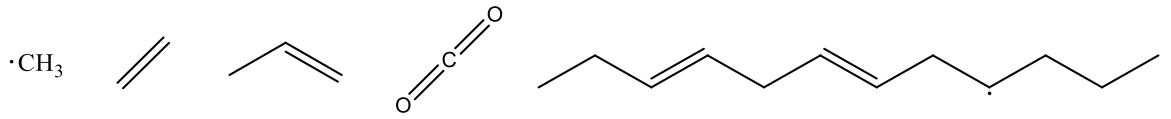

123

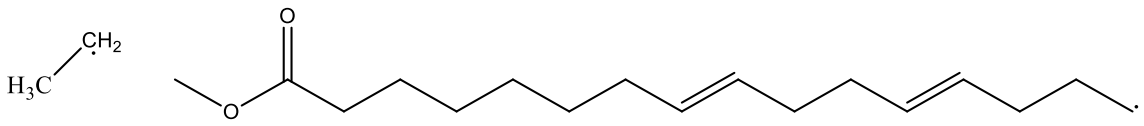

125

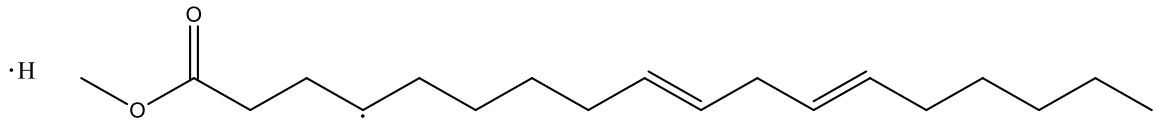

130

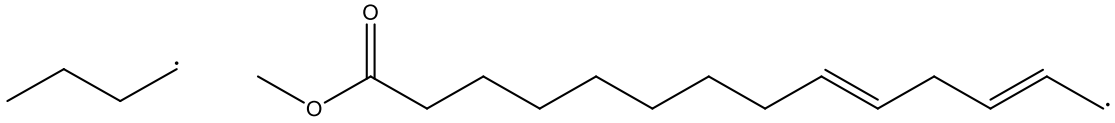

134

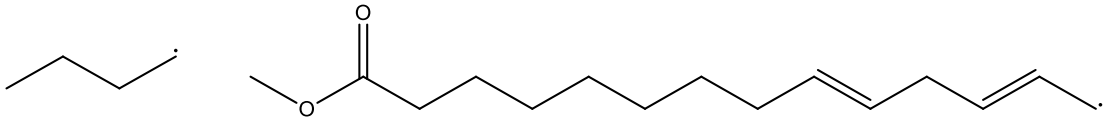

135

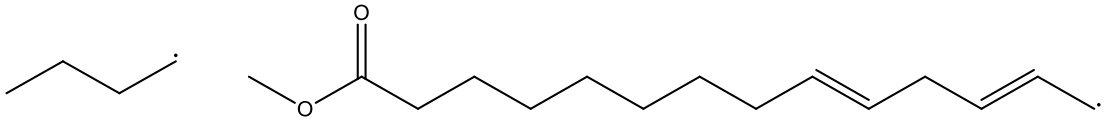

136

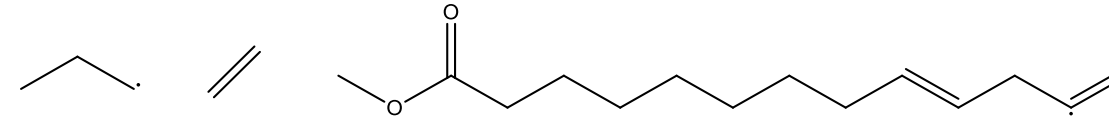

138

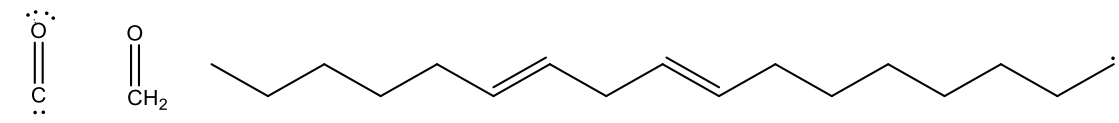

139

141

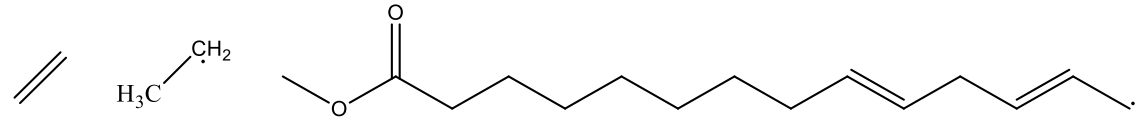

142

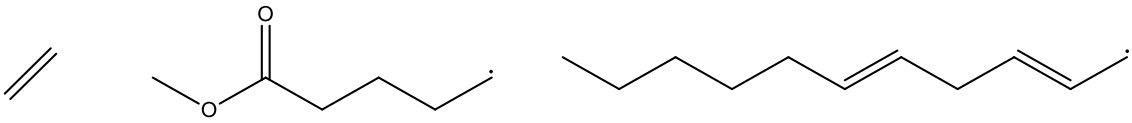

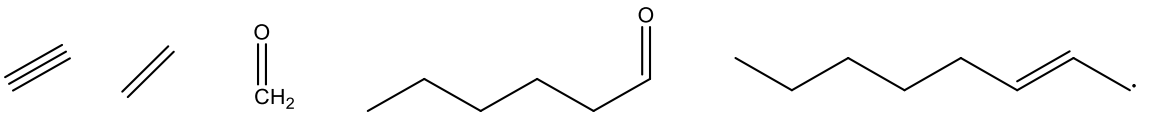

146

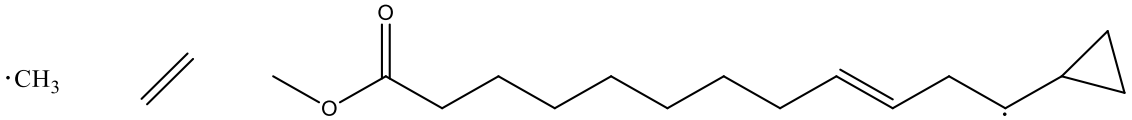

147

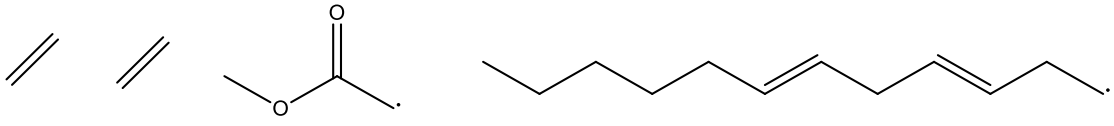

148

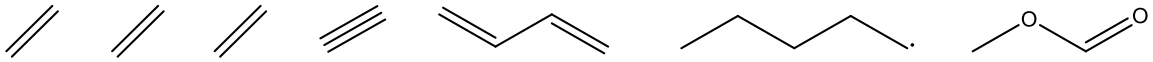

151

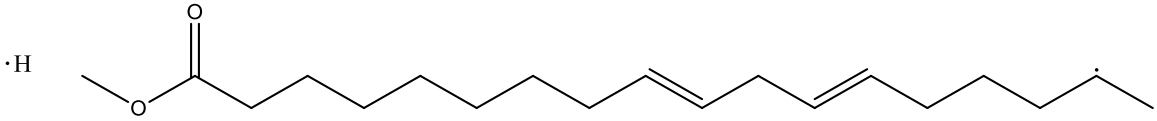

152

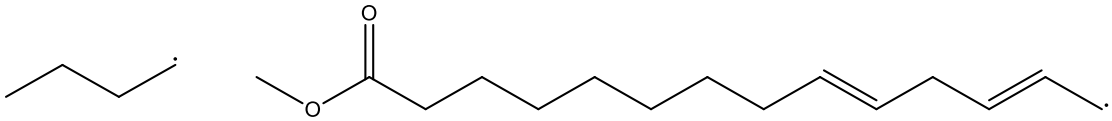

153

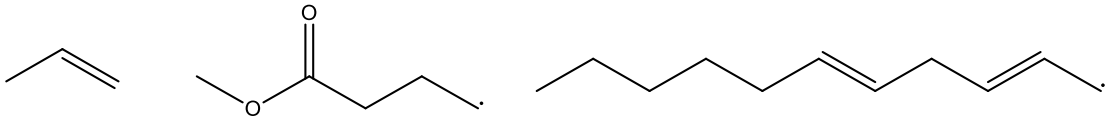

154

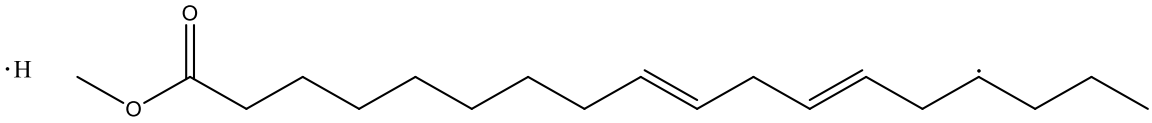

155

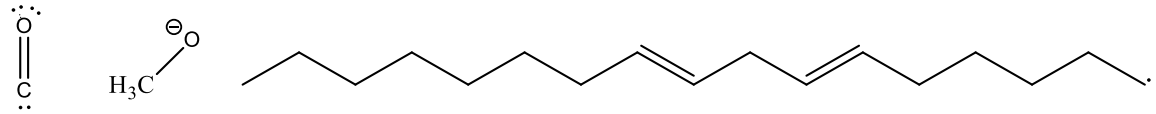

158

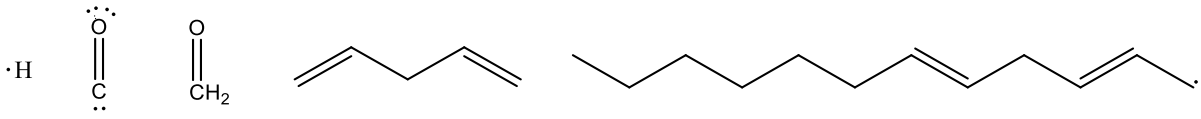

164

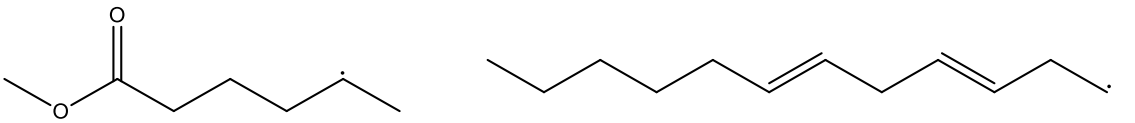

167

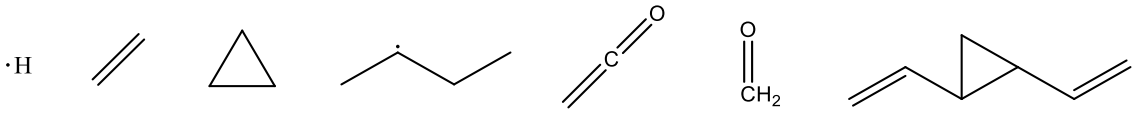

168

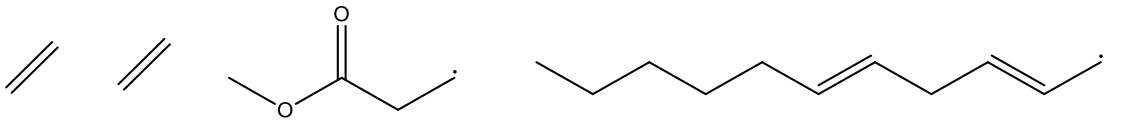

178

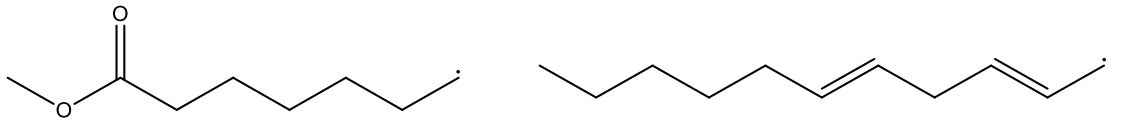

187

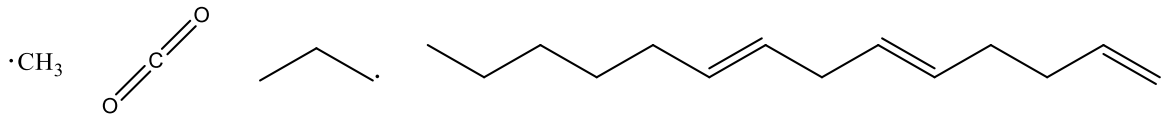

192

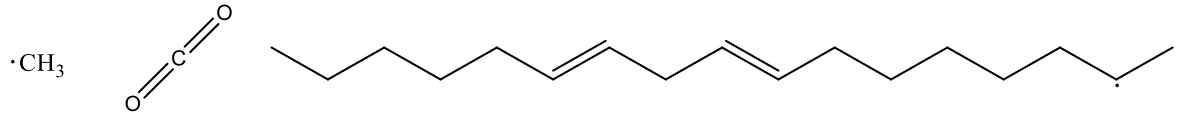

193

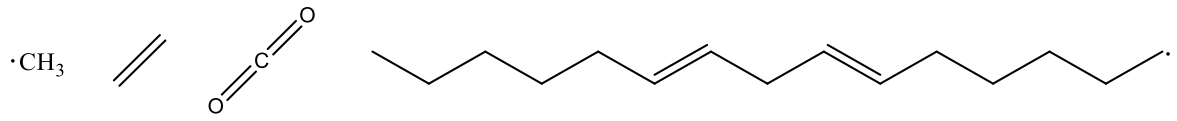

195

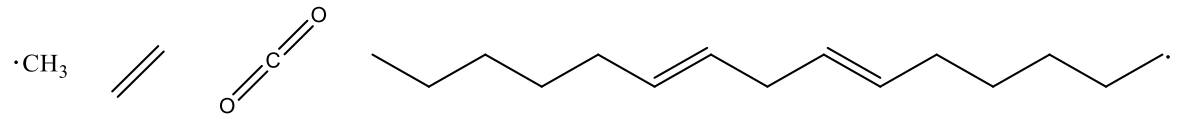

202

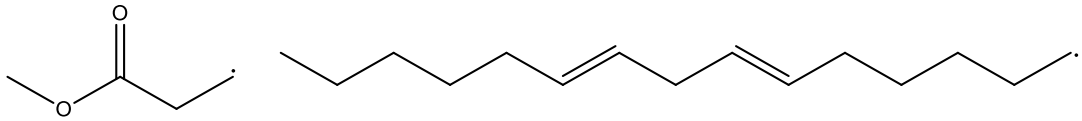

204

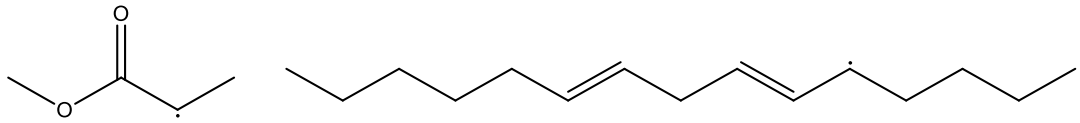

205

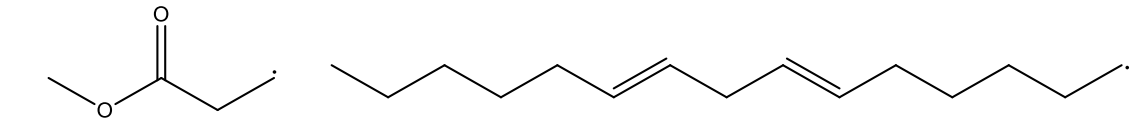

206

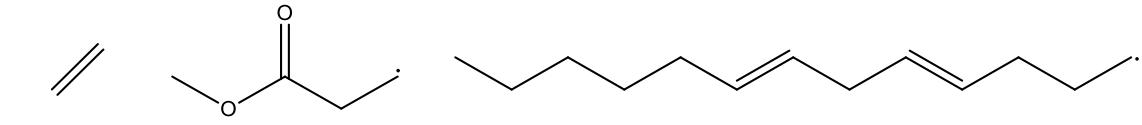

207

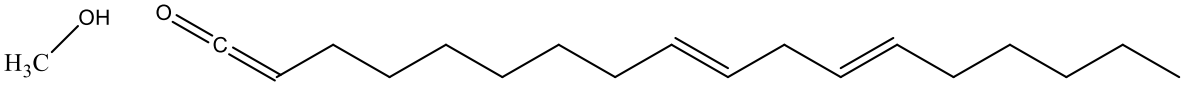

211

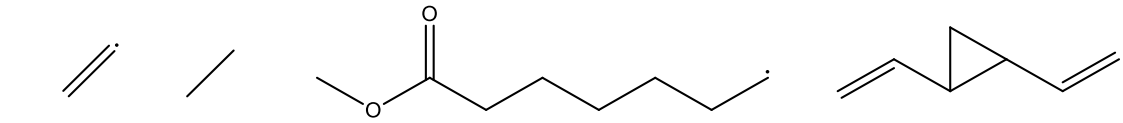

216

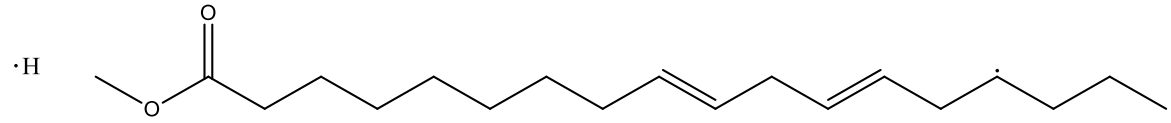

220

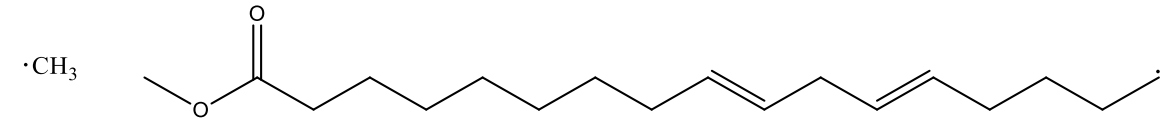

223

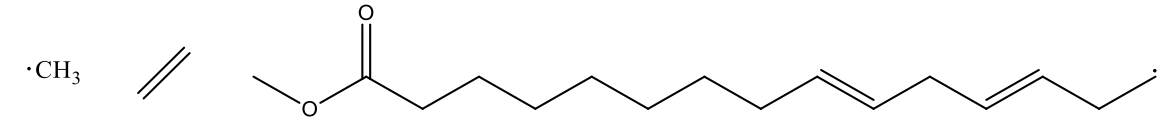

225

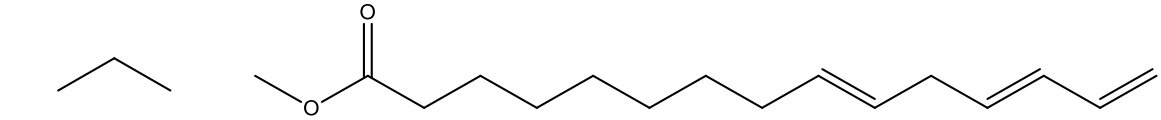

229

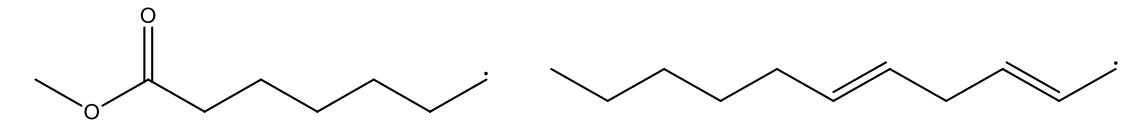

230

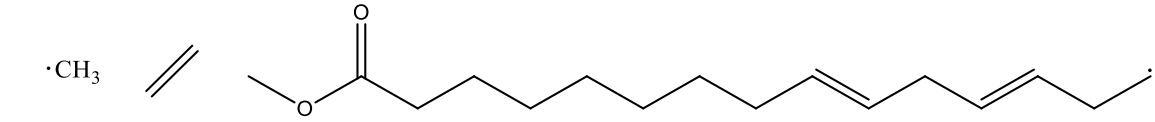

231

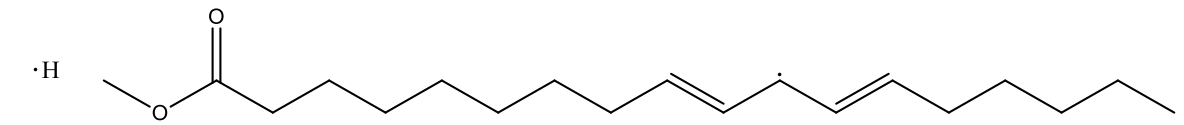

236

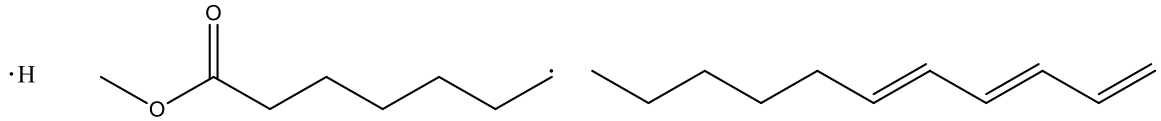

237

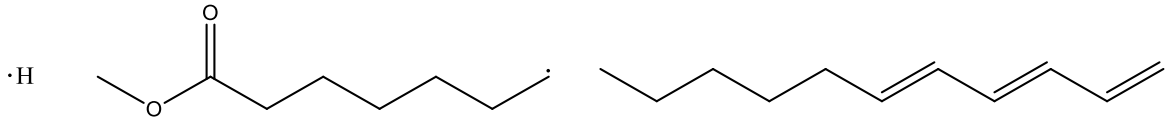

238

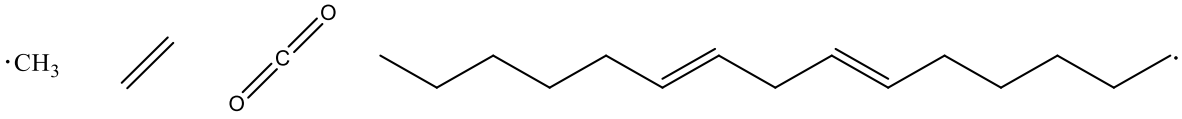

240

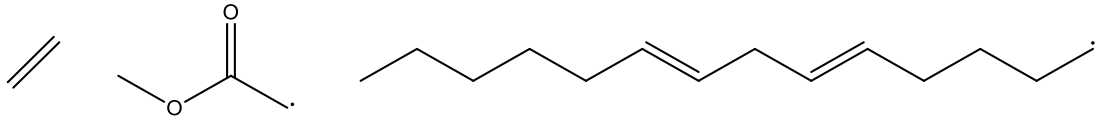

242

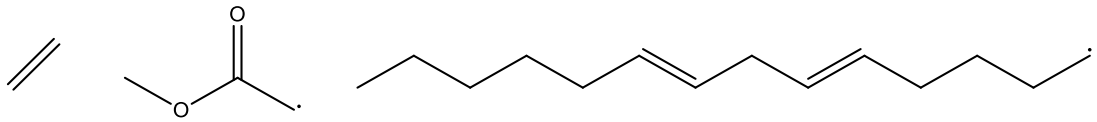

243

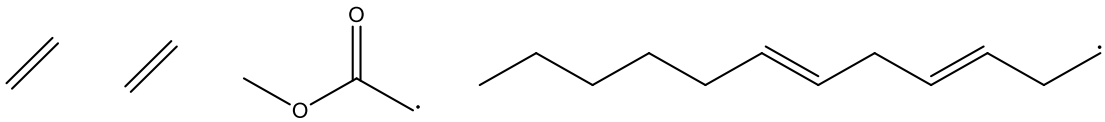

244

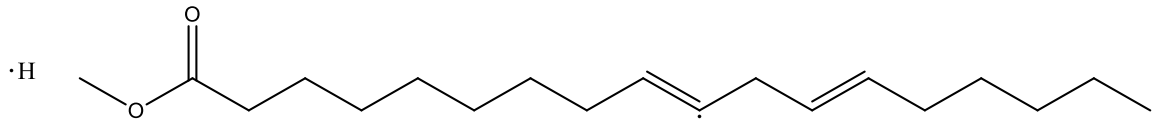

246

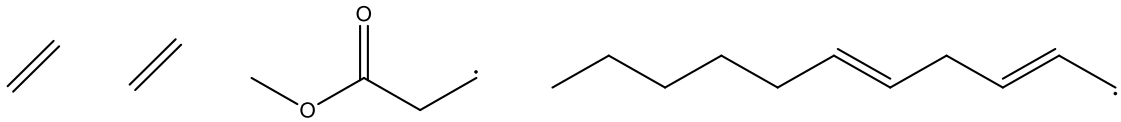

249

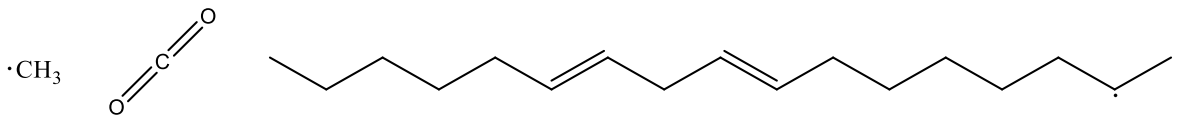

251

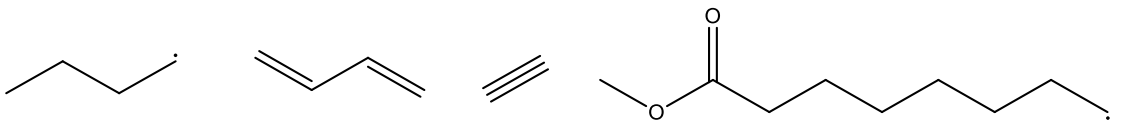

252

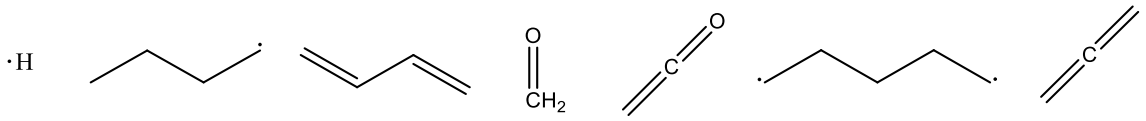

255

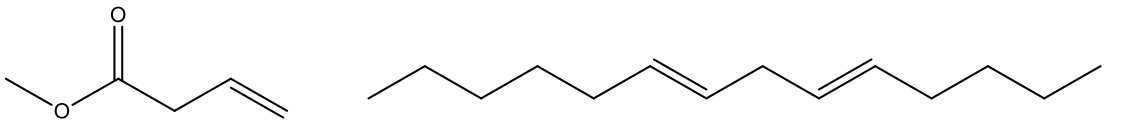

257

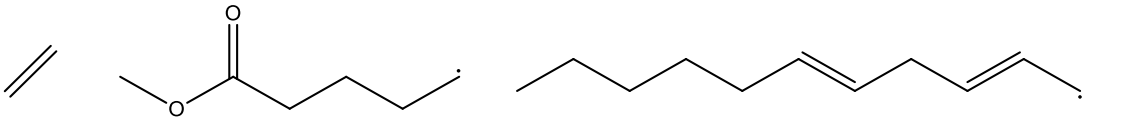

262

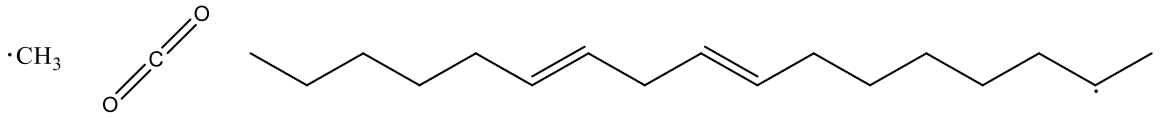

264

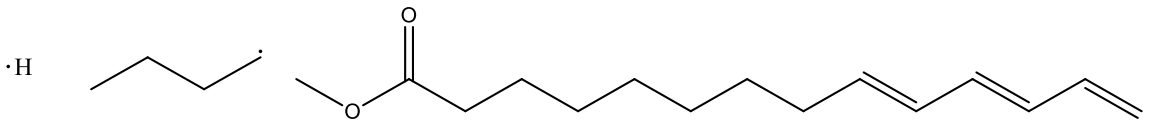

267

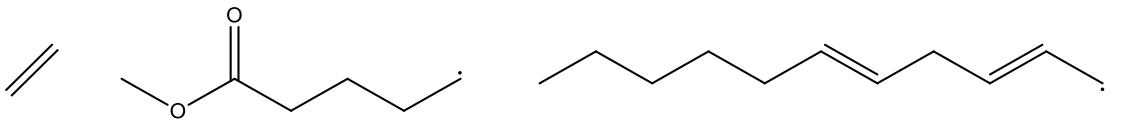

268

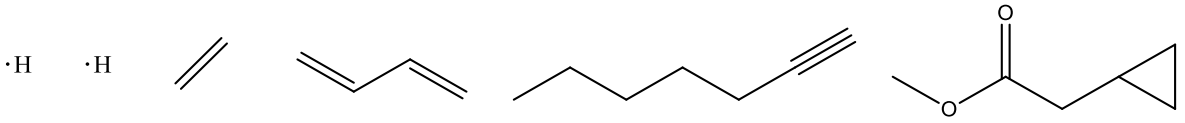

270

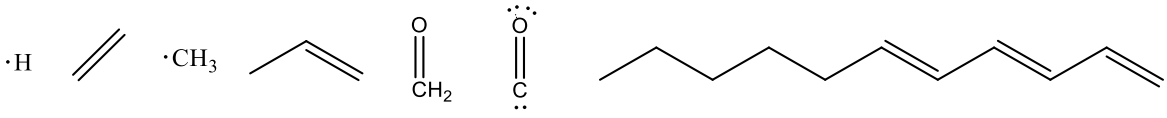

272

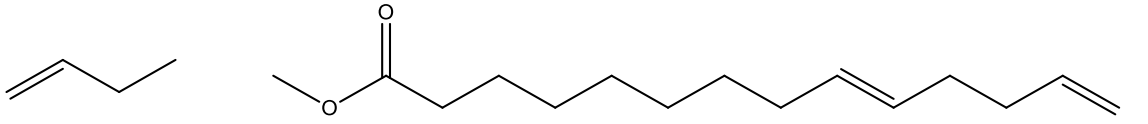

275

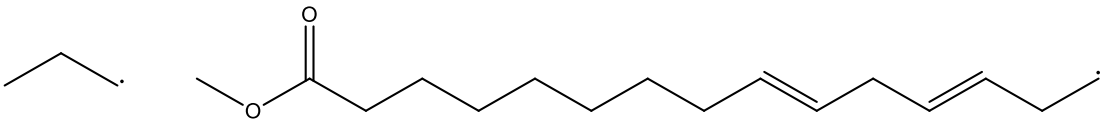
277

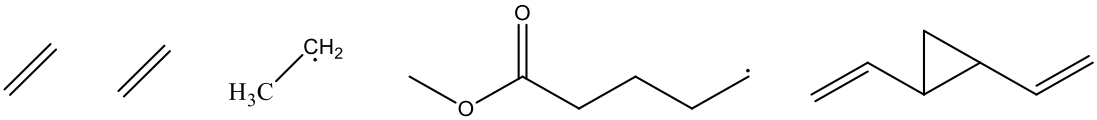
278

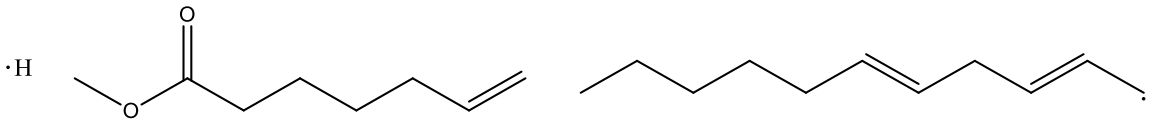
283

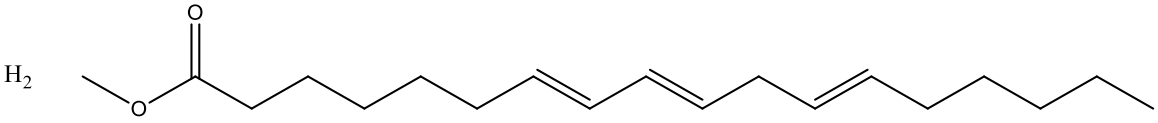
284

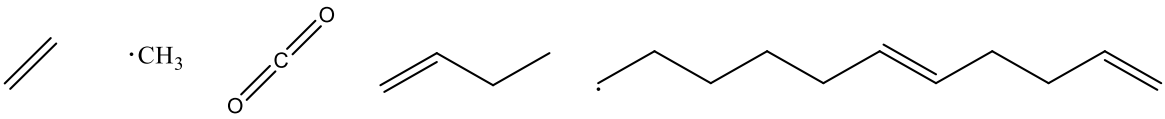
297

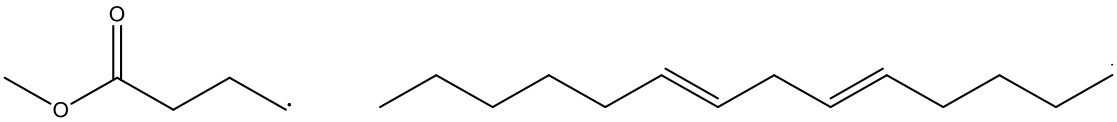
301

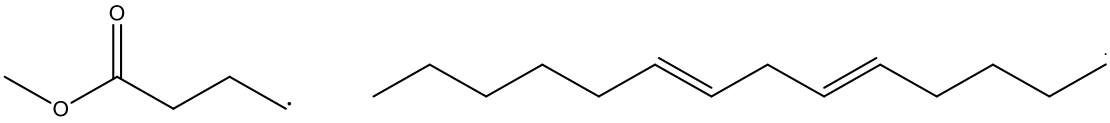
302

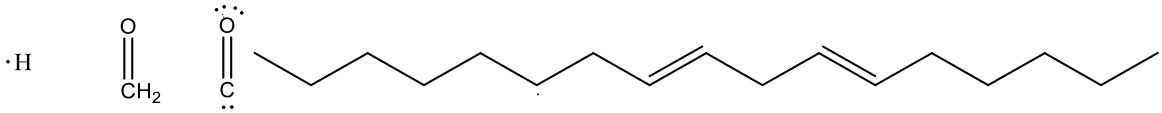
306

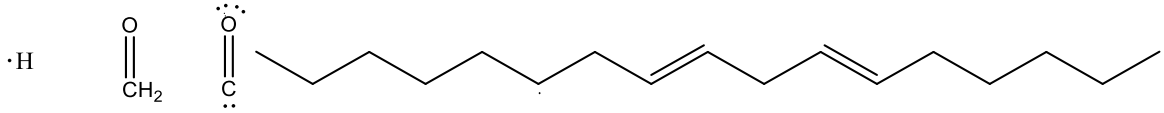
307

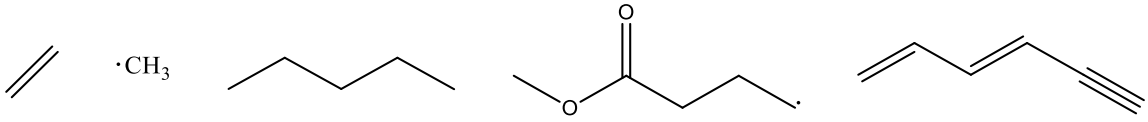
317

Appendix B. Latter BDE Ensemble Analysis

Compilation of trajectory jobs obtained with the derived BDE values (in Hartrees). The far-right column shows a color-coded difference between the starting state and dissociated state. Blue shaded data points represent little or no deviation, and red shaded represents extreme change.

Job	Dissociation	Difference
19	3	-0.18
22	4	-0.24
25	4	-0.23
27	2	-0.16
29	3	-0.19
30	4	-0.22
37	4	-0.20
39	3	-0.18
41	3	-0.17
42	3	-0.15
43	4	-0.18
44	4	-0.22
45	3	-0.20
48	3	-0.18
51	2	-0.16
55	2	-0.16
62	4	-0.24
75	2	-0.08
76	6	-0.31
78	2	-0.07
80	3	-0.16
88	3	-0.16
93	6	-0.32
94	6	-0.32
98	3	-0.18
100	2	-0.15
112	2	-0.14
114	2	-0.04
120	1	0.00
123	5	-0.20
125	2	-0.14
130	2	-0.16
134	2	-0.12
135	2	-0.12
136	2	-0.12

138	3	-0.20
139	4	-0.21
141	3	-0.16
142	3	-0.18
146	5	-0.27
147	3	-0.19
148	4	-0.23
151	7	-0.39
152	2	-0.16
153	2	-0.12
154	3	-0.17
155	2	-0.15
158	3	-0.18
164	5	-0.26
167	2	-0.14
168	7	-0.38
178	4	-0.22
187	2	-0.14
192	4	-0.17
193	3	-0.12
195	4	-0.17
202	4	-0.17
204	2	-0.16
205	2	-0.13
206	2	-0.15
207	3	-0.20
211	2	-0.07
216	4	-0.57
220	2	-0.15
223	2	-0.16
225	3	-0.20
229	2	-0.03
230	2	-0.14
231	3	-0.20
236	2	
237	3	-0.21
238	3	-0.21
240	4	-0.16
242	3	-0.18
243	3	-0.18
244	4	-0.23
246	2	-0.16
249	4	-0.22
251	3	-0.12
252	4	

255	7	-1.53
257	2	-0.04
262	3	-0.18
264	3	-0.12
267	3	-0.20
268	3	-0.18
270	6	
272	7	-0.34
275	2	-0.04
277	2	-0.16
278	5	-0.28
283	3	-0.17
284	2	-0.03
297	5	-0.20
301	2	-0.15
302	2	-0.15
306	4	-0.21
307	4	-0.21
317	5	-0.28

Appendix C. Homology Distributions

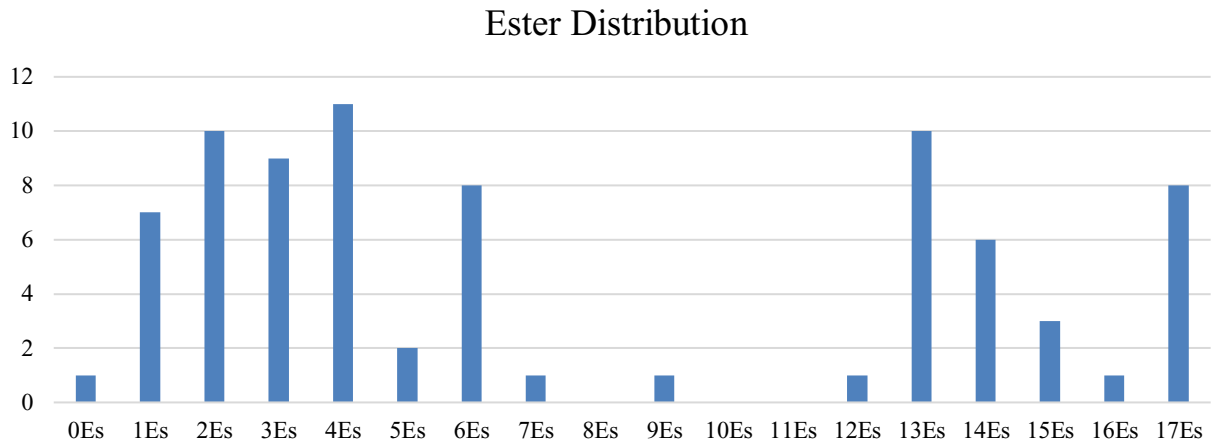

Homology distribution of theoretically obtained esters (non-deoxygenated products). Notable is a significant lack of 7 – 12 C esters, indicative of the unsaturation influence in the dissociation pathway.

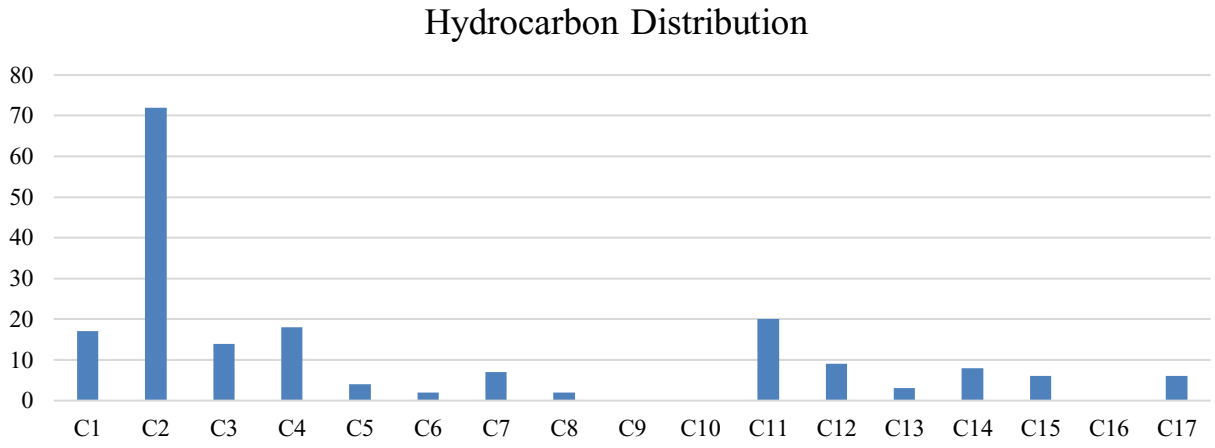

Homology analysis of observed hydrocarbon products from pyrolysis of methyl linoleate. In tandem with the ester analysis, there is a significant dip in production of products of 8 – 10 C length (deviation of note as well).

Appendix D. Python Program for Further Dissociations

```
# Ask for the Job Name to get File Location
Job = input("Enter Job Number (NNN): ")
FileName = "MB-P02-J" + Job + ".log"

# Define variable lines and files with lines from file
lines = []
contents = open(FileName, "rt")
with open(FileName, "rt") as LogFile:
for line in contents:
lines.append(line)

# search for a key phrase within the Log File to find the end
KeyPhrase = 'Final analysis for traj'
with open(FileName) as myFile:
for num, line in enumerate(myFile, 1):
if KeyPhrase in line:
Finish = num - 3

# search for another key phrase within the Log File to find the start
KeyPhrase = 'Summary information for step   2000'
with open(FileName) as myFile:
        for num, line in enumerate(myFile, 1):
                if KeyPhrase in line:
                        Start = num + 19

# extract a list of the content between the lines within Start and Finish
i = Start
Extracted = ""
for i in range(Start, Finish):
Extracted += lines[i]
i += 1

# separate the extracted Log File data into an array
Split = Extracted.split()

# delete Molecular Velocity MW:
del Split[440]
del Split[441]
del Split[442]

# calculate the total number of atoms involved in the system
TotalAtoms = int(len(Split)/16)

Loc_a = [0 for x in range(TotalAtoms)]
```

```
Loc_x = [0 for x in range(TotalAtoms)]
Loc_y = [0 for x in range(TotalAtoms)]
Loc_z = [0 for x in range(TotalAtoms)]
Vel_a = [0 for x in range(TotalAtoms)]
Vel_x = [0 for x in range(TotalAtoms)]
Vel_y = [0 for x in range(TotalAtoms)]
Vel_z = [0 for x in range(TotalAtoms)]

x = 0
for x in range(0,TotalAtoms):
Loc_x[x] = Split[8*x+3]
Loc_y[x] = Split[8*x+5]
Loc_z[x] = Split[8*x+7]
Vel_x[x] = Split[8*(x+TotalAtoms)+3]
Vel_y[x] = Split[8*(x+TotalAtoms)+5]
Vel_z[x] = Split[8*(x+TotalAtoms)+7]

# search for another key phrase within the Log File to find the start for an elements list
KeyPhrase = 'Charge =  0 Multiplicity = 1'
with open(FileName) as myFile:
        for num, line in enumerate(myFile, 1):
                if KeyPhrase in line:
                        Start = num

# search for another key phrase within the Log File to find the end for an elements list
KeyPhrase = 'INPUT DATA FOR L121'
with open(FileName) as myFile:
        for num, line in enumerate(myFile, 1):
                if KeyPhrase in line:
                        Finish = num - 4

# extracts data from elements list into a new data array
i = Start
Extracted = ""
for i in range(Start, Finish):
Extracted += lines[i]
i += 1

# separate the extracted Elements File data into an array
Split = Extracted.split()

# adds atoms to the Matrices
i = 0
for i in range(0, TotalAtoms):
Loc_a[i] = Split[4*i]
Vel_a[i] = Split[4*i]
```

```
i = 0

for i in range(0,TotalAtoms):
value = Loc_x[i].replace('D','e')
Loc_x[i] = float(value)
value = Loc_y[i].replace('D','e')
Loc_y[i] = float(value)
value = Loc_z[i].replace('D','e')
Loc_z[i] = float(value)
value = Vel_x[i].replace('D','e')
Vel_x[i] = float(value)
value = Vel_y[i].replace('D','e')
Vel_y[i] = float(value)
value = Vel_z[i].replace('D','e')
Vel_z[i] = float(value)


StringJob = ""
i = 0

# ask user what atoms to include and put it into an array
Atoms=[]
newAtom = input('Enter Atom Numbers: ')
Atoms = list(map(int, newAtom.split()))

NewAtoms = int(len(Atoms))

for i in range(0,NewAtoms):
StringJob += Loc_a[Atoms[i] - 1]
StringJob += "        "
StringJob += str(Loc_x[Atoms[i] - 1])
StringJob += " "
StringJob += str(Loc_y[Atoms[i] - 1])
StringJob += " "
StringJob += str(Loc_z[Atoms[i] - 1])
StringJob += '\n'

StringJob += '\n'

i = 0
for i in range(0,NewAtoms):
StringJob += str(Vel_x[Atoms[i] - 1])
StringJob += " "
StringJob += str(Vel_y[Atoms[i] - 1])
```

```
StringJob += " "
StringJob += str(Vel_z[Atoms[i] - 1])
StringJob += '\n'
StringJob += '\n'
StringJob += '\n'

newAtom = input('File Name: ')

results = open("traj_" + newAtom + ".txt",'w')
results.write(StringJob)
results.close()
```